การออกแบบ, การสังเคราะห์และการประเมินผลทางชีววิทยาเพื่อยังยั้ง FIV และ HIV

DESIGN, SYNTHESIS AND BIOLOGICAL EVALUATION OF FELINE AND HUMAN IMMUNODEFICIENCY VIRUS INHIBITORS

พณิชา ธรรมจง

PHANICHA THAMMAJONG

วิทยานิพนธ์นี้เป็นส่วนหนึ่งของการศึกษาตามหลักสูตรปริญญาวิศวกรรมศาสตร์มหาบัณฑิต

สาขาวิชาวิศวกรรมชีวการแพทย์

คณะวิศวกรรมศาสตร์

สถาบันเทคโนโลยีพระจอมเกล้าเจ้าคุณทหารลาดกระบัง

พ.ศ.2567

KMITL-2024-EN-M-317-300

DESIGN, SYNTHESIS AND BIOLOGICAL EVALUATION OF FELINE AND HUMAN IMMUNODEFICIENCY VIRUS INHIBITORS

PHANICHA THAMMAJONG

A THESIS SUBMITTED IN PARTIAL FULFILLMENT
OF THE REQUIREMENTS FOR DEGREE OF
MASTER OF ENGINEERING IN BIOMEDICAL ENGINEERING
SCHOOL OF ENGINEERING
KING MONGKUT'S INSTITUTE OF TECHNOLOGY LADKRABANG
2024

KMITL-2024-EN-M-317-300

หัวข้อวิทยานิพนธ์	การออกแบบ, การสังเคราะห์และการประเมินผลทางชีววิทยาเพื่อยังยั้ง FIV และ HIV
นักศึกษา	นางสาว พณิชา ธรรมจง
รหัสประจำตัว	64601095
ปริญญา	วิศวกรรมศาสตร์มหาบัณฑิต
สาขาวิชา	วิศวกรรมชีวการแพทย์
พ.ศ.	2567
อาจารย์ที่ปรึกษาวิทยานิพนธ์	รศ.ดร.แมทธิว พอล กลีสัน

บทคัดย่อ

ไวรัสภูมิคุ้มกันบกพร่องในแมว (FIV) เป็นการติดเชื้อที่พบได้ทั่วไปในแมวบ้านและแมวป่าทั่วโลก แม้จะมีความเข้าใจเชิงบำบัดเกี่ยวกับโรคนี้ในมนุษย์อย่างมากมาย แต่ข้อมูลเกี่ยวกับการรักษาโรคนี้ในแมวยังมีอยู่อย่างจำกัด ซึ่งการรักษาในปัจจุบันอาศัยยาที่พัฒนาขึ้นสำหรับเชื้อไวรัสภูมิคุ้มกันบกพร่องในมนุษย์ (HIV) และกลุ่มยาที่นิยมใช้คือ non-nucleotide reverse transcriptase inhibitors (NNRTIs) โดย FIV-RT มีความคล้ายคลึงกับ HIV-1 RT 67% ในระดับเอนไซม์ และ 88% ใน allosteric pocket targeted ที่เป็นเป้าหมายของ NNRTIs งานวิจัยนี้มีวัตถุประสงค์เพื่อพยายามขยายและเพิ่มความรู้ทางเภสัชวิทยาเกี่ยวกับการรักษาทั้ง HIV และ FIV โดยเราได้นำเสนอวิธีการสังเคราะห์ และการตรวจสอบเอกลักษณ์ของสารยับยั้งรวบทั้งหมด 22 โครงสร้าง ซึ่งการปรับปรุงโครงสร้างอนุพันธ์ของ 2,4-dichloropyrimidine เพื่อเพิ่มประสิทธิภาพการยับยั้งต่อ HIV และ FIV และการละลาย โดยงานวิจัยนี้ได้มีการจำลองรูปแบบการจับ (Binding mode) ระหว่างสารยับยั้งกับ HIV และ FIV โดยใช้วิธีการจำลอง Docking และ วิธีทางกลศาสตร์ควอนตัม (Quantum Mechanics, QM) พบว่าสารประกอบ **19** และ **27** เป็นสารยับยั้งที่มีความสมดุลที่ดีเมื่อเทียบกับยาต้าน HIV สารประกอบ**19** แสดงค่าการยับยั้ง HIV ที่ 77.19%, การยับยั้ง FIV ที่ 76.92% และค่าการละลายที่ 313 µg/ml ส่วนสารประกอบที่ **27** แสดงค่าการยับยั้ง HIV ที่ 92.56%, การยับยั้ง FIV ที่ 97.42% และค่าการละลายที่ 9.52 µg/ml โดยยาต้านที่ใช้ในการเปรียบเทียบได้แก่ Rilpivirine, Efavirenz และ Nevirapine ซึ่งแสดงค่าการยับยั้ง HIV ที่ 90.47%, 85.73% และ 79.72%, การยับยั้ง FIV ที่ 70.41%, 80.46% และ 65.27% และค่าการละลายที่ 1.19 µg/ml, 69.60 µg/ml และ 610 µg/ml ตามลำดับ

Thesis	Design, Synthesis and Biological Evaluation of Feline and Human immunodeficiency virus Inhibitors
Student	Ms. Phanicha Thammajong
Student ID.	64601095
Degree	Master of Engineering
Program	Biomedical Engineering
Year	2024
Thesis Advisor	Assoc. Prof. Dr. Matthew Paul Gleeson

Abstract

Feline immunodeficiency virus (FIV) is a common infection found in domesticated and wild cats worldwide. Despite the wealth of therapeutic understanding of the disease in humans, considerably less information exists regarding the treatment of the disease in felines. Current treatment relies on drugs developed for the related human immunodeficiency virus (HIV) and includes compounds of the popular non-nucleotide reverse transcriptase (NNRTI) class. This is despite FIV-RT being only 67% similar to HIV-1 RT at the enzyme level, increasing to 88% for the allosteric pocket targeted by NNRTIs. The goal of this project was to try to quantify how well the more extensive pharmacological knowledge available for human disease translates to felines. We report the synthesis and characterization of 22 new inhibitors of FIV and HIV. Structure-based design was employed to modify from drug reference that Rilpivirine and Etravirine. Modification includes scaffold hopping to 2,4-dichloropyrimidine core as well as incorporation of ionizable groups to improve both activity and solubility. The prospective binding mode of the compounds was determined using HIV and FIV docking and QM methods to inhibitors of known how their bind. Chemical modifications were then designed to both increase efficiency and solubility as well as validate the binding mode prediction. We identified compounds **19** and **27** as well-balanced inhibitors with favorable inhibition percentages for both HIV and FIV, along with good solubility. Specifically,

compound **19** demonstrated 77.19% inhibition of HIV, 76.92% inhibition of FIV, and solubility of 313 µg/ml, while compound **27** showed 92.56% inhibition of HIV, 97.42% inhibition of FIV, and solubility of 9.52 µg/ml. In comparison, the known anti-HIV-1 reverse transcriptase drugs Rilpivirine, Efavirenz, and Nevirapine showed HIV inhibition rates of 90.47%, 85.73%, and 79.72%, FIV inhibition rates of 70.41%, 80.46%, and 65.27%, and solubility values of 1.19 µg/ml, 69.60 µg/ml, and 610 µg/ml, respectively

Table of Contents

List of Tables

page

List of schemes

List of Figures

page

List of Abbreviations

mL	=	milliliter
mg	=	milligram
µM	=	micro molar
nM	=	nano molar
nm	=	nanometer
ns	=	nanosecond
ppm	=	part per million
SD	=	Standard deviation
NMR	=	Nuclear Magnetic Resonance
HPLC	=	High Performance Liquid Chromatography
TLC	=	Thin layer chromatography
MS	=	Mass Spectroscopy
PBS	=	Phosphate Buffer Solution
PDB	=	Protein Data Bank
H_2	=	Hydrogen
N_2	=	Nitrogen
Pd/C	=	Palladium on activated carbon
SAR	=	Structure Activity Relationships
TEA	=	Triethylamine
TFA	=	Trifluoroacetic acid
THF	=	Tetrahydrofuran
MeOH	=	Methanol
DIPEA	=	N, N-Diisopropylethylamine
EtOAc	=	Ethylacetate
pTSA	=	para-toluene sulfonic acid
DMSO	=	Dimethyl sulfoxide
MD	=	Molecular Dynamic
DCM	=	Dichloromethane

QM	=	Quantum Mechanic
CONF	=	Conformation
HB	=	Hydrogen Bond
%I	=	%Inhibition
IC_{50}	=	half-maximal inhibitory concentration

ACKNOWLEDGMENTS

Firstly, I would like to grateful thank Assoc. Prof. Dr. Matthew Paul Gleeson, my thesis advisor for suggestion and inspiration this work, valuable suggestion to solve many unexpected problems and give a chance to me study this interesting topic. I really appreciate his spirit as a teacher who has given me lessons in both academic and work aspects. He not only taught me work procedure, principles, and excellent qualities, but also genuinely gave me advice and support to achieve a work-life balance. With this precious opportunity, I have gained invaluable experience and knowledge that will be useful to me in my future career.

Secondly, I would like to extend my acknowledgement to my friends in CMCL group for their friendship, support, and sincere interest towards my study during all these years. Thank you, all my friends, in my life who help me, and always stay by my side. And all my stars who heal me when I'm deepest in my life.

Finally, an honorable mention goes to my family (my dad, mom, sister, brothers, aunts and grandpa) for their support, love and always encourage me to get through challenging time.

Phanicha Thammajong

Chapter 1

Introduction

The Human Immunodeficiency Virus (HIV) and the Feline Immunodeficiency Virus (FIV) represent two of the most critical viral pathogens affecting humans and animals, respectively. Both viruses belong to the Lentivirus genus, within the Retroviridae family, and share many structural and functional similarities. However, they infect different hosts HIV primarily infects humans, while FIV targets domestic cats. Understanding these viruses, their impact, and the current state of antiviral treatments is essential for advancing therapeutic strategies.

Feline immunodeficiency virus is a lentivirus subfamily of *retroviridae* which infects domestic cats and wild feline species [1-3]. FIV causes immune dysfunction resulting in depletion of CD4+ cells, an increase in CD8+ peripheral blood lymphocyte counts, increasing the susceptibility of the animal to opportunistic infections, and often death [2, 4]. The final stage in felines infected with FIV is characterized by the development of acquired immunodeficiency syndrome (AIDS) like symptoms [5] comparable to that caused in humans by human HIV [6].

Initial efforts to treat FIV have focused on repurposing marketed human drugs, particularly those targeting reverse transcriptase [7-10]. FIV-RT and HIV-1 RT are both heterodimeric enzymes made up of two subunits, p51 and p66 whose role is to perform RNA transcription during virus replication. Amino acid sequence analysis shows the two enzymes share 48% identity and 67% similarity [11, 12]. This led to the discovery that human nucleoside reverse transcriptase inhibitors (NRTIs), such as Zidovudine and Lamivudine, were also able to bind to FIV-RT.

Clinical studies identified that NRTIs can result in undesirable side effects in felines infected with FIV [1, 7, 13-16]. This prompted greater interest in later generation NNRTIs which make use of an allosteric pocket adjacent to the nucleotide binding site [17-19]. The NNRTIs (**Figure 1**) include 1st generation drug Nevirapine, 2nd generation Delaviridine, 3rd generation Efavirenz and 4th generation Rilpivirine. Further chemical classes [20, 21] in development include TNK651 and CHEMBL1923492 [17, 22-24].

While the repurposing of known human inhibitors for use in felines has proved useful, the strategy has not been entirely successful due to sub-optimal potency they are reported to display against FIV-RT [25-30]. This suggests a need to identify specific molecules with optimal activity in this species directly. Efforts to develop specific inhibitors against FIV-RT were aided by Galilee *et al* [10] who reported the 1st X-ray crystal structure of the enzyme.

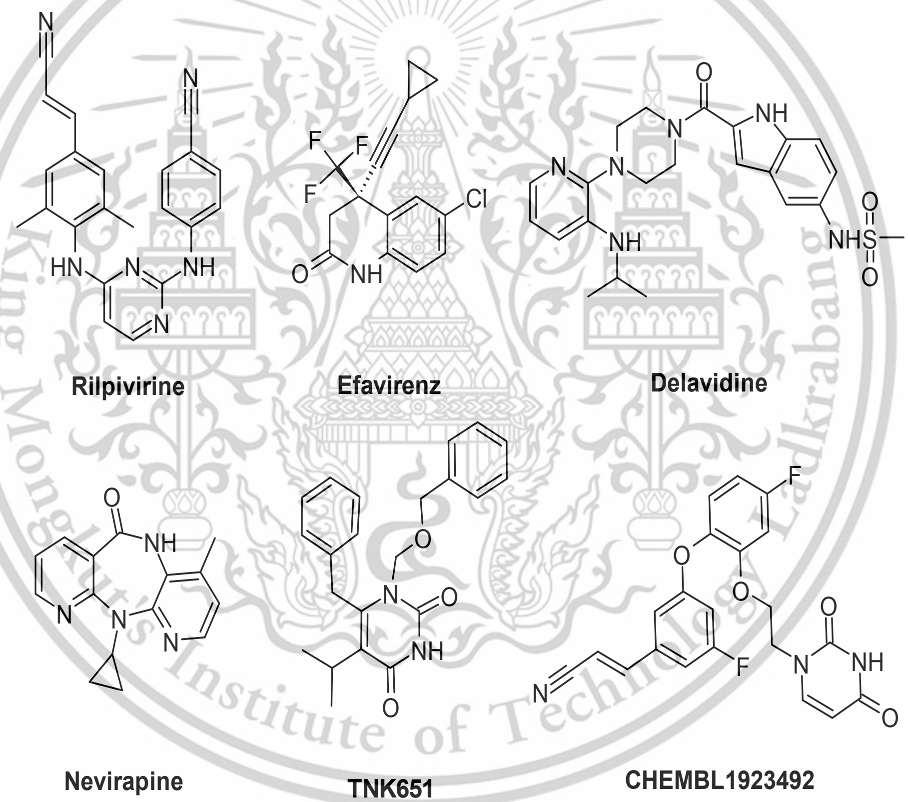

Figure 1 Chemical structures of marketed anti-HIV-1 RT drugs, Rilpivirine, Efavirenz**,** Delavirdine, Nevirapine, and development compounds, TNK651 and CHEMBL1923492.

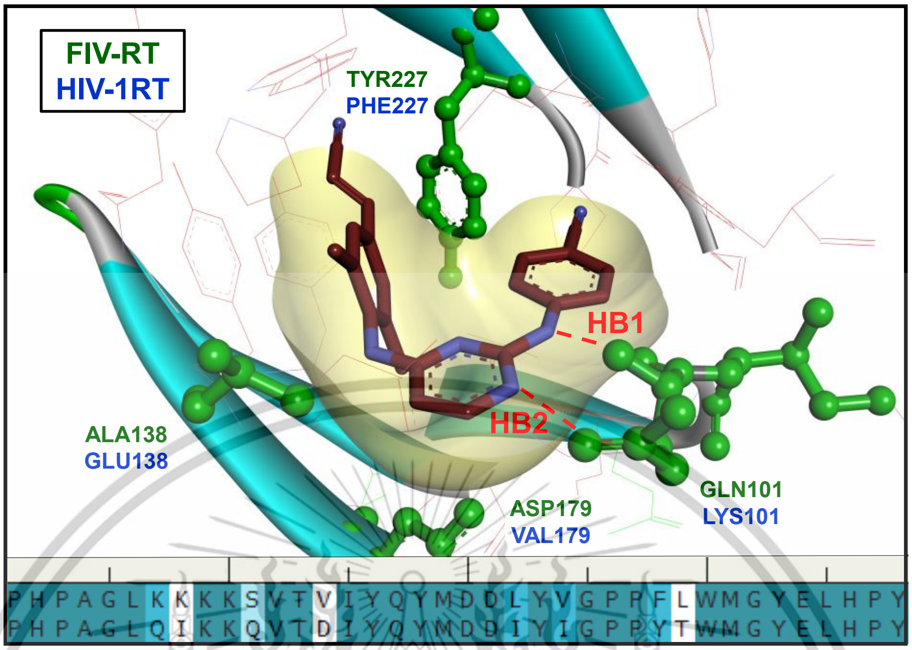

Figure 2 Active site amino acid differences between HIV-1 RT (red, PDB ID: 2ZD1) versus FIV-RT [10] (2ZD1-based homology model, green). The 4 key residues surrounding the NNRTI binding site of Rilpivirine are highlighted.

They compared FIV-RT to HIV-1 RT and noted that efforts to use HIV therapeutic treatments for felines are challenging, particularly for next generation NNRTIs due to profound differences in protein flexibility coupled with key active site residues differences. Unfortunately, the apo structure lacked the allosteric site targeted by the more effective NNRTIs, meaning it had limited utility for structure-based design efforts.

In this work we report the 1st SAR investigation on FIV using a set of diverse molecules targeting the NNRTI binding site. We began by employing a computational protocol to select NNRTI-like molecules previously from those prepared in our group for both RT-related and unrelated targets. We were interested in using these molecules to probe the differences between FIV-RT and HIV-1 RT using a combination of biochemical screening and cheminformatics methods. The goal of the analysis was to confirm we had selected a set of structurally diverse NNRTI-like molecules to help us explore the SAR differences between FIV and HIV.

Our main goal was to use the data generated in this chemo-centric approach to (a) assess the degree of similarity between the two related RT targets based on the observed experimental inhibition values, (b) to identify molecules with FIV activities better than current HIV-1RT repurposed drugs and (c) analyze the experimental data to try and better understand the structure-activity relationships (SAR) of FIV and how the differ from FIV. Critically, such data could allow us to develop more effective feline-targeted inhibitors in the future.

1.1. Understanding HIV and FIV

HIV is the causative agent of acquired immunodeficiency syndrome (AIDS), a condition characterized by the progressive failure of the immune system, leading to life-threatening opportunistic infections and cancers. Since its discovery in the early 1980s, HIV has become a global pandemic, with over 38 million people currently living with the virus worldwide. HIV primarily infects CD4+ T cells, macrophages, and dendritic cells, leading to the depletion of these critical components of the immune system. The virus integrates its genetic material into the host genome, establishing a persistent infection that is difficult to eradicate.

FIV, discovered in 1986, is a significant pathogen in domestic cats, causing an AIDS-like syndrome. FIV infection leads to a progressive immunodeficiency similar to HIV in humans, making cats more susceptible to various infections and diseases. FIV primarily infects CD4+ T cells and other immune cells, causing a decline in immune function over time. The natural history of FIV infection in cats closely parallels that of HIV in humans, making FIV an invaluable model for studying lentiviral infections and testing antiviral therapies.

1.2. The Global Challenge of HIV and FIV

The global impact of HIV is profound, with millions of new infections and AIDS-related deaths each year. Despite significant advancements in antiretroviral therapy (ART), which can suppress viral replication and improve the quality of life for infected individuals, HIV remains a leading cause of death in many parts of the world. ART typically involves a combination of drugs targeting different stages of the HIV life cycle, including reverse transcriptase inhibitors, protease inhibitors, integrase inhibitors, and entry inhibitors. While these drugs can effectively control the virus, they do not cure the infection, and patients must adhere to lifelong treatment regimens. This long-term treatment is associated with numerous challenges, including drug resistance, side effects, high costs, and difficulties in ensuring consistent access to medications, particularly in resource-limited settings.

FIV presents a parallel challenge in veterinary medicine. While less is known about FIV's global prevalence, it is a significant concern for cat populations, particularly in multi-cat households, shelters, and feral cat communities. Current treatments for FIV are limited and primarily supportive, aiming to manage symptoms and secondary infections rather than directly targeting the virus. No specific antiviral drugs have been approved for FIV, though some human HIV medications have been used off-label with varying degrees of success. The need for effective, safe, and accessible antiviral therapies for FIV is critical, as infected cats often face a poor prognosis and reduced quality of life.

1.3. Differences Between HIV and FIV

While HIV and FIV share many similarities in terms of their structure, replication mechanisms, and pathogenic effects, several key differences distinguish these viruses. Understanding these differences is crucial for developing targeted therapies and leveraging research across species. Firstly, the host range is a fundamental difference. HIV exclusively infects humans, whereas FIV infects cats. This difference in host specificity is due to variations in the viral envelope proteins and the receptors they target on host cells. HIV primarily uses the CD4 receptor and either CCR5 or CXCR4 co-receptors to enter human cells. In contrast, FIV uses a different set of receptors to infect feline cells. Secondly, the clinical course of infection varies between the two viruses. HIV infection in humans progresses through several stages: acute infection, clinical latency, and AIDS. Without treatment, most individuals progress to AIDS within 10-15 years, although this can vary widely. FIV infection in cats also progresses through similar stages, but the timeline can be different, with some cats remaining asymptomatic for many years before developing immunodeficiency. Thirdly, the genetic diversity and mutation rates of the viruses can differ. HIV is notorious for its high mutation rate, which complicates vaccine development and leads to the rapid emergence of drug-resistant strains. FIV also exhibits genetic diversity, but the implications of this diversity for disease progression and treatment are less well understood. Despite these differences, the similarities between HIV and FIV make them valuable models for comparative research. Both viruses cause chronic, lifelong infections that progressively weaken the immune system. Studying these viruses together can provide insights into common mechanisms of lentiviral pathogenesis and identify potential therapeutic targets. So, the need for novel antiviral therapies for HIV and FIV is clear. Current treatments, while effective at controlling viral replication, do not cure the infections and are associated with numerous challenges. Developing new drugs that can overcome resistance, have fewer side effects, and are accessible to patients worldwide is imperative. Furthermore, leveraging the similarities and differences between HIV and FIV can enhance our understanding of lentiviral infections and lead to breakthroughs in both human and veterinary medicine. This research aims to design, synthesize, and biologically evaluate new compounds with potential antiviral activity against both HIV and FIV, contributing to the development of more effective treatments and improving the quality of life for those affected by these viruses.

1.4 Goal and Objective

We are going to merge features of FIV and HIV inhibitor and known HIV drug Rilpivirine and Etravirine, especial ring, hydrophobic region modification and apply basic center to tightly bind in active site of protein target and solubility improvement, then synthesized the series of 22 compounds and assessed within biochemical and biological assays by our established academic collaborators.

1. To get better understanding about Structure Activity Relation (SAR) and design FIV and HIV inhibitors using structure-based method.

2. To Synthesize 22 novel compounds based on 2,4-dichloropyrimidine scaffold as inhibitors to inhibit virus.

3. To discover the new route of synthesis to make the compounds associated with FIV and HIV inhibitors.

4. To evaluate biological activity, selectivity, potency of FIV and HIV inhibitors that we have synthesized, assay toxicity and solubility of compounds.

1.5 Scope of the study

The research involves a multi-disciplinary study effort covering. (a) computational inhibitors target analysis, (b) 2,4-dichloropyrimidine based compounds synthesis and characterization and (c) biological assay being performed by established our collaborator in Thailand.

Chapter 2

Theory and Literature Reviews

1. Overview of FIV and HIV

1.1 Feline Immunodeficiency Virus (FIV)

Feline Immunodeficiency Virus (FIV) is a lentivirus that affects domestic cats, leading to a progressive immunodeficiency syndrome similar to AIDS in humans. FIV was first identified in the 1980s and has since been recognized as a significant cause of illness in cats [31]. The virus targets CD4+ T cells, leading to a gradual decline in immune function and increased susceptibility to opportunistic infections and neoplasms. FIV infection typically progresses through three stages: acute, asymptomatic, and terminal [32].

Research has shown that FIV is highly similar to HIV in terms of its structure and replication mechanisms. Both viruses belong to the Retroviridae family and have similar life cycles, including reverse transcription, integration into the host genome, and the production of new viral particles. This similarity makes FIV an invaluable model for studying lentiviral infections and testing antiviral therapies.

1.2 Human Immunodeficiency Virus (HIV)

Human Immunodeficiency Virus (HIV) is the causative agent of acquired immunodeficiency syndrome (AIDS), a condition characterized by a progressive failure of the immune system. Since its discovery in the early 1980s, HIV has become a global pandemic, with over 38 million people living with the virus worldwide (WHO, 2021). HIV primarily infects CD4+ T cells, macrophages, and dendritic cells, leading to a gradual decline in immune function and increased susceptibility to opportunistic infections and cancers [33].

HIV infection progresses through several stages: acute infection, clinical latency, and AIDS. Without treatment, most individuals progress to AIDS within 10-15 years, although this timeline can vary [34]. The virus integrates its genetic material into the host genome, establishing a persistent infection that is difficult to eradicate. Current treatments aim to suppress viral replication but do not cure the infection.

2. Current Antiviral Treatments for HIV and FIV

2.1 HIV Antiviral Treatments

Antiretroviral therapy (ART) has transformed the management of HIV from a fatal disease to a manageable chronic condition. ART typically involves a combination of drugs targeting different stages of the HIV life cycle:

Reverse Transcriptase Inhibitors (RTIs)

Reverse transcriptase (RT) is a key enzyme in the lifecycle of retroviruses such as HIV-1 and Feline Immunodeficiency Virus (FIV). It catalyzes the conversion of viral RNA into complementary DNA (cDNA), which is subsequently integrated into the host genome, allowing the virus to hijack the host cell's machinery for replication. Targeting RT has been one of the most successful strategies in the development of antiviral therapies, particularly for HIV-1. By inhibiting the RT enzyme, reverse transcriptase inhibitors (RTIs) block the viral replication process, preventing the spread of the virus within the host [35].

RTIs are classified into two major types: nucleoside/nucleotide reverse transcriptase inhibitors (NRTIs) and non-nucleoside reverse transcriptase inhibitors (NNRTIs). Each class inhibits RT through distinct mechanisms, and both have been central to the treatment of HIV-1 infection since the advent of antiretroviral therapy (ART).

Nucleoside/Nucleotide Reverse Transcriptase Inhibitors (NRTIs)

NRTIs were the first class of antiretroviral drugs developed for HIV treatment. Structurally, they mimic the natural nucleosides (the building blocks of DNA) and compete with them for incorporation into the growing DNA strand synthesized by reverse transcriptase. Once an NRTI is incorporated into the viral DNA, it causes chain termination because these molecules lack the necessary 3'-

hydroxyl group required for the attachment of the next nucleotide. This halts the DNA elongation process and prevents further viral replication [36].

Common NRTIs include:

- **Zidovudine (AZT)**: The first NRTI approved for HIV treatment, AZT was a major breakthrough in the management of HIV/AIDS. It competes with the natural nucleoside thymidine and interrupts the reverse transcription process [37].
- **Lamivudine (3TC)**: Lamivudine, a cytidine analog, is another widely used NRTI with strong activity against HIV and hepatitis B virus (HBV). It's often combined with other antiretroviral agents to improve efficacy and reduce resistance [38].

NRTIs remain central to combination antiretroviral therapy (cART) and are typically administered in fixed-dose regimens alongside NNRTIs or protease inhibitors (PIs) to enhance efficacy and minimize drug resistance.

Non-Nucleoside Reverse Transcriptase Inhibitors (NNRTIs)

Unlike NRTIs, NNRTIs bind to a hydrophobic pocket near the active site of RT, inducing a conformational change that disrupts its enzymatic activity. NNRTIs are non-competitive inhibitors, meaning they do not compete with natural nucleotides for incorporation into the growing DNA strand. Instead, their binding alters the structure of RT, preventing it from catalyzing the conversion of viral RNA to DNA [39].

Mechanism of Action

The NNRTI binding pocket is highly specific and is located approximately 10 Å away from the active site where DNA synthesis occurs. When an NNRTI binds to this pocket, it induces a conformational change in RT that renders the enzyme catalytically inactive. This prevents the enzyme from binding to its natural nucleotides, effectively halting reverse transcription [39]. The binding of NNRTIs does not require phosphorylation (unlike NRTIs), which gives them distinct pharmacokinetic properties.

Key NNRTIs in HIV Therapy

1. **Nevirapine (NVP)**: Nevirapine was the first NNRTI approved for clinical use in HIV treatment. It has been widely used due to its potency and affordability, particularly in low-income settings. However, the rapid emergence of resistance to nevirapine limits its long-term efficacy in mono-therapy [40].

2. **Efavirenz (EFV)**: Efavirenz is one of the most commonly used NNRTIs and is part of several first-line HIV treatment regimens. It has a strong inhibitory effect on RT but can be associated with neuropsychiatric side effects [41].

3. **Etravirine (ETR)**: Etravirine is a second-generation NNRTI designed to overcome resistance to first-generation NNRTIs like efavirenz and nevirapine. It exhibits flexibility in binding, allowing it to maintain efficacy even against RT mutants that are resistant to earlier NNRTIs [42].

4. **Rilpivirine (RPV)**: Rilpivirine is another second-generation NNRTI with a favorable safety profile. It is used in combination therapies for treatment-naïve HIV patients and is characterized by fewer neuropsychiatric side effects compared to efavirenz. RPV's smaller molecular size and flexible structure allow it to bind to mutant forms of HIV-1 RT [43].

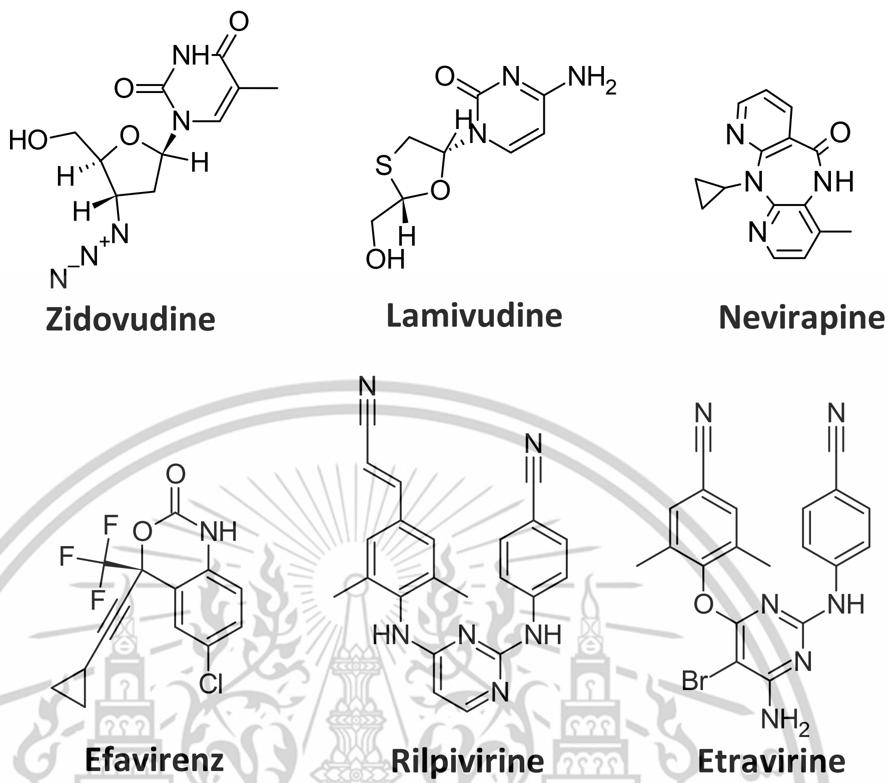

Figure 3 NRTIs and NNRTIs of HIV-1 RT drugs.

Protease Inhibitors (PIs)

These drugs inhibit the protease enzyme, which is essential for the maturation of viral particles [44]. PIs have been shown to significantly improve patient outcomes and reduce the incidence of AIDS-related complications.

Integrase Inhibitors

These drugs inhibit the integrase enzyme, which integrates viral DNA into the host genome [45]. Integrase inhibitors have demonstrated high efficacy in reducing viral loads and are associated with fewer side effects compared to older ART classes.

Entry Inhibitors

These drugs prevent the virus from entering host cells [46]. Entry inhibitors are used in combination with other ART drugs to overcome drug resistance and improve treatment outcomes. Despite the effectiveness of ART, challenges remain, including the emergence of drug-resistant strains, side effects, high treatment costs, and difficulties in ensuring consistent access to medications in resource-limited settings [47]. Additionally, ART does not cure HIV, and patients must adhere to lifelong treatment regimens.

2.2 FIV Antiviral Treatments

Treatment options for FIV are more limited compared to HIV. Currently, there are no specific antiviral drugs approved for FIV. Treatment primarily focuses on supportive care, including managing symptoms and secondary infections. However, some human HIV medications have been used off-label to treat FIV with varying degrees of success:

Reverse Transcriptase Inhibitors

Some studies have explored the use of RTIs such as zidovudine for treating FIV, showing modest improvements in clinical outcomes [48]. However, the long-term efficacy and safety of these treatments in cats remain uncertain.

Protease Inhibitors

Ritonavir and other protease inhibitors have been tested in cats with FIV, with mixed results. While some studies have reported improvements in clinical symptoms, the overall effectiveness of these drugs in treating FIV is still under investigation. Given the limitations of current treatments, there is a critical need for the development of effective antiviral agents specifically targeting FIV. Research into novel therapeutic strategies is essential for improving the prognosis and quality of life for infected cats.

3. Design and Synthesis of Novel Antiviral Agents

3.1 Structure-Based Drug Design (SBDD)

Structure-Based Drug Design (SBDD) involves designing drugs based on the three-dimensional structure of viral proteins. Advances in structural biology, including X-ray crystallography and cryo-electron microscopy, have provided detailed insights into the structure of HIV and FIV proteins, enabling the rational design of inhibitors. For example, the development of integrase inhibitors such as Raltegravir was made possible by understanding the structure of the HIV integrase enzyme [49]. SBDD has also been used to design protease inhibitors and reverse transcriptase inhibitors with improved efficacy and reduced resistance.

3.2 High-Throughput Screening (HTS)

High-Throughput Screening (HTS) allows for the rapid screening of large libraries of compounds to identify potential antiviral agents. HTS has been instrumental in discovering several HIV inhibitors, including protease and reverse transcriptase inhibitors. For example, the discovery of the non-nucleoside reverse transcriptase inhibitor (NNRTI) class of drugs was facilitated by HTS, leading to the development of compounds such as efavirenz and nevirapine. HTS is also being applied to identify new inhibitors of FIV, though research in this area is less advanced compared to HIV [50].

3.3 Fragment-Based Drug Design (FBDD)

Fragment-Based Drug Design (FBDD) involves screening small molecular fragments that bind to viral proteins, which are then optimized to develop potent inhibitors. FBDD has led to the development of novel HIV inhibitors with improved efficacy and reduced resistance. For example, the development of the HIV-1 integrase strand transfer inhibitors (INSTIs) involved FBDD approaches that identified key fragment interactions with the integrase enzyme [51]. FBDD is also being explored for FIV, with the aim of identifying novel inhibitors that target conserved viral proteins.

4. Computational chemistry approaches

4.1 Molecular Docking

Molecular docking is a widely used computational technique in drug discovery and design. It simulates the interaction between small molecules (ligands) and their biological targets (typically proteins) to predict the preferred binding orientation and estimate binding affinity. Docking plays a crucial role in the identification and optimization of potential drug candidates by predicting the most favorable conformations of the ligand within the active site of the target protein. This method has been applied extensively in the development of antiviral drugs, particularly for HIV and FIV, to optimize the binding interactions with viral enzymes such as reverse transcriptase (RT) and integrase [52].

A notable study demonstrates the effectiveness of docking in identifying new inhibitors for HIV-1 RT. The research utilized crystal structures of HIV-1 RT and various inhibitors to perform docking studies, which allowed the design of novel non-nucleoside reverse transcriptase inhibitors (NNRTIs) with enhanced binding affinity. Similarly, used docking techniques to explore the binding affinities of various small molecules to HIV-1 integrase, providing insights into the structural requirements for drug binding and resistance mechanisms [53]. In the context of **FIV**, docking studies are also used to understand how inhibitors can target viral proteins effectively, with work focusing on the development of NNRTIs for feline retroviruses [54].

The docking process involves the use of scoring functions that predict binding energies based on different parameters like hydrogen bonding, van der Waals forces, and electrostatic interactions. Studies such as developed the popular docking software the GOLD docking, AutoDock Vina, have revolutionized the efficiency and accuracy of docking predictions, enabling faster screening of large compound libraries [55, 56].

4.2 Quantum Mechanics

Quantum mechanics (QM) methods are often applied to refine the docking results and provide a more accurate prediction of binding affinities by considering electronic properties at the atomic level. QM-based approaches, such as Density Functional Theory (DFT), can calculate molecular orbitals, electron densities, and interaction energies, which are essential for understanding how ligands interact with their targets at a quantum level [57].

Research about highlights the integration of QM with molecular docking to improve the accuracy of binding affinity predictions [58]. Their work demonstrated that QM methods, when combined with Molecular Mechanics/Generalized Born Surface Area

(MM/GBSA), could significantly refine binding energy calculations for enzyme-inhibitor complexes in HIV-1. This method was shown to correct inaccuracies that are often introduced by empirical force fields in conventional docking, especially when ligands contain complex chemical groups such as charged or polar moieties.

Another application of QM in antiviral drug design where quantum mechanical calculations were used to investigate the interactions of HIV protease inhibitors [59]. The use of ab initio and DFT methods provided insights into the electronic structure of inhibitors, enabling a better understanding of how modifications to their chemical structure could improve their potency and reduce resistance.

4.3 logD

logD, or the distribution coefficient, is a critical parameter in drug design that measures the lipophilicity of a compound under specific pH conditions. Unlike logP (which measures partitioning between octanol and water for neutral compounds), logD accounts for ionization states and is more relevant for compounds that exist in charged and uncharged forms at physiological pH values. The lipophilicity, represented by logD, impacts a drug's absorption, distribution, metabolism, and excretion (ADME) properties, and is therefore essential in the design of bioavailable antiviral agents [60, 61].

In the context of HIV and FIV drug development, achieving an optimal logD is crucial for ensuring that the drug has sufficient solubility to be absorbed effectively while retaining enough lipophilicity to pass through cell membranes and reach its target. On the "Rule of Five" emphasizes the importance of balancing lipophilicity and solubility, showing that compounds with excessively high or low logD values often exhibit poor pharmacokinetics [62].

A study about explores how logD is used to optimize drug candidates for oral bioavailability [63]. By adjusting the chemical structure to achieve a favorable logD, antiviral drugs can be designed to exhibit optimal permeability while maintaining sufficient solubility in aqueous environments like blood plasma. For instance, modifications to the methoxy groups in reverse transcriptase inhibitors have been shown to influence their logD, thereby improving their pharmacological profiles.

Moreover, computational tools that predict logD, such as MarvinSketch [64] are now integrated into drug discovery pipelines to screen compounds early in the development process. These predictions help identify candidates with suitable ADME properties before proceeding to more resource-intensive experimental studies.

For many drug candidates, the pH of 7.4 is used as the standard since it approximates physiological conditions in the human body. LogD at pH 7.4 (LogD7.4) indicates how the compound behaves in a biological environment, including its partitioning between cell membranes (lipid) and blood plasma (aqueous) or intracellular fluids. An optimal LogD7.4 value is critical to ensure that a compound is adequately soluble in water for transport and sufficiently lipophilic to penetrate cell membranes, ultimately influencing bioavailability [65].

4.4 Solubility

Solubility is the ability of a substance to dissolve in a solvent, which, in the context of drug development, typically refers to its dissolution in water or biological fluids. Solubility directly affects a compound's absorption and bioavailability, as drugs must dissolve in gastrointestinal fluids to be absorbed into the bloodstream. Poor solubility can limit a drug's effectiveness, even if it exhibits strong binding to its target [66].

Low aqueous solubility is a common challenge in the development of lipophilic drugs like NNRTIs, which are designed to bind to hydrophobic pockets on target proteins. These compounds often have difficulty dissolving in biological fluids, leading to issues with formulation and limited therapeutic potential. To address this, drug design efforts often focus on structural modifications that enhance solubility, such as the introduction of polar functional groups or the use of prodrug strategies [67].

Factors Affecting Solubility

Several factors influence the solubility of a drug candidate, including:

1. **Molecular Size**: Larger molecules tend to have lower solubility, as their larger surface area requires more energy to dissolve. Smaller drug molecules, on the other hand, can dissolve more readily in biological fluids [65].

2. **Polarity and Hydrogen Bonding**: Molecules with polar functional groups (e.g., hydroxyl, carboxyl, or amine groups) are more likely to form hydrogen bonds with water, increasing their solubility. However, excessive polarity can hinder membrane permeability, so an optimal balance must be maintained [68].

3. **Crystallinity**: The physical form of a compound also impacts solubility. Amorphous forms, which lack the ordered structure of crystalline solids, generally exhibit higher solubility because they require less energy to break apart [69].

4. **pH and pKa**: A compound's solubility can vary depending on the pH of the environment, as ionizable groups may gain or lose protons, altering their interaction with the solvent. Compounds with a pKa close to physiological pH (7.4) are often designed to optimize solubility in biological fluids [70].

Chapter 3

Material and Method

3.1 Material

3.1.1 Analytical Instrumentation

All reagents and solvents were obtained from commercial suppliers and used without further purification. Thin-layer chromatography (TLC) was conducted on aluminum-backed silica gel plates (Silicycle UltraPure Silica gels), and compounds were visualized under UV light. Purification of the compounds was carried out using column chromatography with silica gel G60 (60–200 μm).

^{1}H NMR spectra and ^{13}C NMR were recorded on NMR 500 MHz (Brand: Jeol, spectrometer model: ECZ500/S1). The Chemical shifts (*d*) were reported in part per million (ppm) using TMS as the residual solvent line as the internal standard. ^{1}H NMR and ^{13}C NMR use DMSO-d6 as the solvent for measurement the peaks, the solvent peak and water peak are 2.5 ppm and 3.5 ppm. respectively. The coupling constant (*J*) are reported in Hz, and the patterns are designed as singlet (s), doublet (d), doublet of doublet (dd), triplet (t), quartet (q) and multiplet (m), meaning is the measure of the interaction between a pair of protons.

High Performance Liquid Column Chromatography (HPLC) was used for measured >95% purity based on a UV absorbance HPLC chromatogram (Agilent 1100 system and HITACHI/Chromaster, Poroshell 120 EC-C8 2.7 μM column using a mobile phase consisting of (a) 0.1% formic acid in water and (b) acetonitrile: 99:1% to 1:99% gradient run in 5 minutes)

Mass spectra were obtained from an LC-MSD-Trap mass spectrometer, ion source type ESI(+) mode. High-resolution mass spectra (HRMS) were determined on Bruker Daltonics - micrOTOF-Q III in source ESI(+) mode at Faculty of Science, Kasetsart University.

Melting points were determined on a Stuart Digital Melting Point Apparatus (Melting Point SMP10).

3.1.2 Column and Thin Layer Chromatography

Thin Layer Chromatography (TLC) was employed to monitor all reactions, using aluminum-backed silica gel plates. The chromatograms were visualized under UV light at 254 nm. Different solvent systems were utilized based on the polarity of each compound. In this research, methanol in dichloromethane and ethyl acetate in dichloromethane were predominantly used.

Column chromatography was performed with silica gel (SiO_2, particle size 0.040–0.055 mm, 230–400 mesh) for the purification of all compounds in this series. The column was packed with silica gel and eluted with various solvent systems, primarily 50% EtOAc/ 50% Hexane and 95% DCM/ 1% MeOH.

3.1.3 Chemical reagents

The reagents, building blocks and solvents obtained from commercial suppliers were used without further purification.

3.2 Computational Method

3.2.1 Study 1 Comparison of Feline and Human Immunodeficiency Virus Reverse Transcriptase Enzymes Through Chemical Screening and Computational Analysis.

Quantum Chemical Calculations

Multiple conformation of the **1-10**, and references drugs (**Table 2**), were generated by rotating amine/alcohol groups attached to the 2- and 4-positions of pyrimidine/quinazoline as shown in **Figure 4**. These were used for quantum mechanical geometry optimization at the HF/6-31G(d) level in Gaussian G16 [71] using default settings. These optimized conformations were used for subsequent virtual screening exercises.

Table 1 shows the 10 compounds, and 3 anti-HIV-1 RT drugs assessed

ID	Structure	Mass	ID	Structure	Mass
1	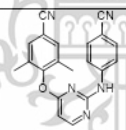	341.4	8	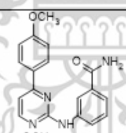	320.4
2	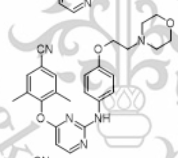	445.5	9	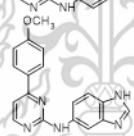	317.4
3	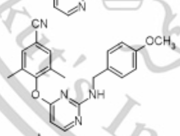	360.4	10	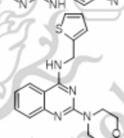	326.4
4	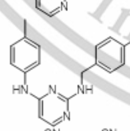	369.3	RPV	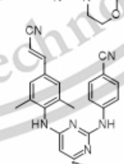	366.4
5	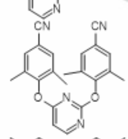	370.4	NEV	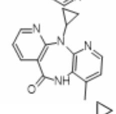	266.3
6	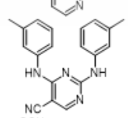	315.4	EFV	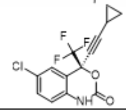	315.7
7	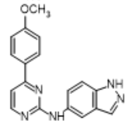	317.4			

[a] *mean, [max](S.D.)*

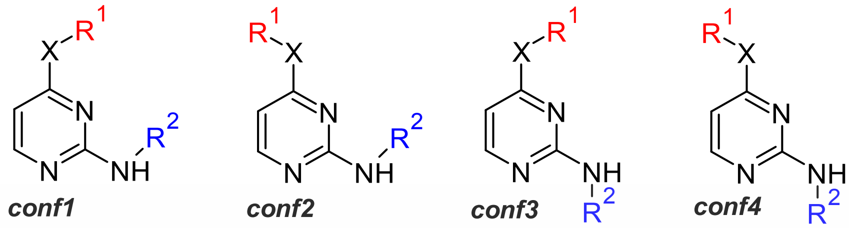

Figure 4 The 4 conformations of pyrimidine-2,4-diamine inhibitors were optimized.

Ligand-based Similarity Methods

Shape-based and pharmacophore-based similarity between the QM optimized conformations of compounds **1-10** and the active conformation of reference NNRTI inhibitors that H-bond to Gln101/Lys101 were undertaken. The active conformations of Rilpivirine (PDB ID: 3MEE) [72], Efavirenz (PDB ID: 7KJW) [73], Delavirdine (PDB ID: 1KLM) [74], and development compounds; TNK651 (PDB ID: 1JLA) [75] and CHEMBL1923492 (PDB ID: 4H4O) [76] were extracted from their PDB structure. Note, the 1st generation drug Nevirapine was not included as a reference as it does not form H-bonds as found in later generations.

Shape-based similarity analysis of the QM optimized conformation of **1-10** compared to the known HIV-inhibitors were performed using the combined volume-based and charge-based overlap option in ShaEP [77]. A 3D pharmacophore-based similarity analysis was also performed using PharmaGist [78, 79]. The default setting was used and the overlap score of each p air was evaluated.

Molecular Docking

Molecular docking of **1-10** to HIV (3MEE, resolution 2.80 Å) [72], and an FIV homology model based on the same structure was performed using GOLD5.3 [80]. All co-factors, ligands and water molecules were removed from the protein. Docking solutions had an enforced H-bond between ligands and Gln101/Lys101, otherwise default settings were used.

3.2.2 Study 2 Design, Synthesis and Biological Evaluation of Feline and Human immunodeficiency virus Inhibitors

Molecular Docking

The docking protocol used in this study has been described in detail elsewhere [81]. Briefly, **35-37** was docked to the HIV-1 RT (3MEC and 2ZD1, resolution 2.30 Å and 1.80 Å) [72, 82]. Proteins were prepared without water molecules or other co-factors, fixed 2 hydrogens.

Quantum Mechanics

The conformations of compound **35-37** were generated in Discovery studio. The difference of 3 compounds are position of methoxy on benzylamines which 2-position, 3-position and 4-position and Quantum mechanical geometry optimization (PM3) [83] was performed in Gaussian G16 [71] using default settings to assess how their bind to HIV1-RT left wing pocket.

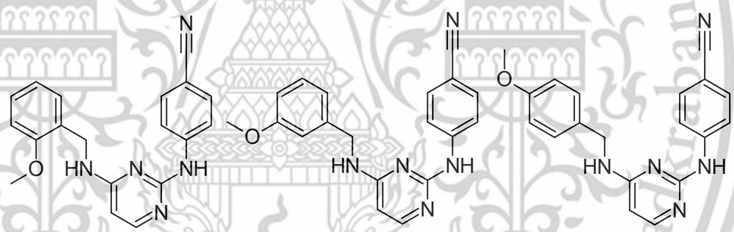

Figure 5 The 3 conformations of inhibitors were optimized.

3.3 Synthesis

3.3.1 Study 1 Comparison of Feline and Human Immunodeficiency Virus Reverse Transcriptase Enzymes Through Chemical Screening and Computational Analysis.

A total of 10 final compounds were synthesized as outlined in **Scheme 1**, including 6 novel compounds (compounds **1-6**) and 4 previously published compounds (compounds **7-9** [84] and **10** [85]) The overall reaction yields varied, ranging from low (14%) to excellent (63%).

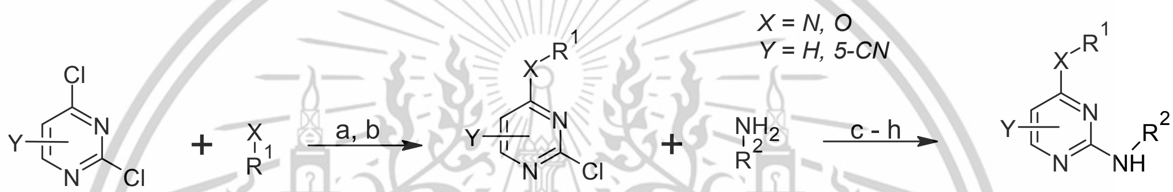

Scheme 1 General route synthesis of compound **1-6**: Y = H or 5-CN; (a) 4-hydroxy-3,5-dimethyl benzonitrile, K_2CO_3, DMF, rt., 8 h, (b) *p*-toluidine, DIPEA, 1-butanol, 110°C, 6 h, (c) 4-aminobenzonitrile, $Pd_2(dba)_3$, xantphos,Na_2CO_3, anhydrous toluene, 160°C, 6h, (d) 4-[2-(morpholin-4-yl)ethoxy]aniline, TFA, *i*-PrOH, 90°C, overnight, (e) 1-(4-methoxyphenyl)methanamine, TEA, NMP, 80°C, 18 h, (f) 1-(4 bromophenyl)methanamine, TEA, NMP, 80°C, 18 h, (g) 4-hydroxy-3,5-dimethyl benzonitrile, K_2CO_3, DMF, 150°C, overnight, (h) 3-methylaniline, DIPEA, DMF, rt., 4 h.

General procedure A for the preparation of intermediate compound **I1**

A mixture of 2,4-dichloropyrimidine (2.0 eq), 4-Hydroxy-3,5-dimethylbenzonitrile (1.0 eq) and K_2CO_3 (1.2 eq) were dissolved in DMF was stirred at rt for 8 h The precipitate was filtered, washed with ethanol or the resultant was evaporated under vacuum and extracted with DI water and ethyl acetate 3 times. The organic layer was collected and combined, dried over anhydrous Na_2SO_4, filtered, and crude mixture required additional purification via silica gel column chromatography to give the desired product as the white solid.

General procedure B for the preparation of intermediate compound **I2**

A mixture of 2,4-dichloropyrimidine (1.0 eq), p-toluidine (1.0 eq) and DIPEA (5.0 eq) were dissolved in 1-butanol and was stirred at 110°C for 6 h. The reaction mixture was cooled down to room temperature. The precipitate was filtered and washed with ethanol to give the desired product as the light yellow solid.

General procedure C for the preparation of final compound **1**

To a solution of **I1** (1.0 eq), 4-aminobenzonitrile (2.0 eq) in anhydrous toluene (4 mL), Na_2CO_3 (2.0 eq), Xantphos (0.1 eq) and $Pd_2(dba)_3$ (0.3 eq) were added. The reaction mixture was stirred at 160°C for 6 h. The reaction mixture was filtered and concentrated under reduced pressure. The residue was extracted with water/EtOAc 3 times, the organic layers were combined, dried over anhydrous Na_2SO_4 and evaporated. Finally, column chromatography was used to purify with DCM/MeOH = 99/1 to afford the desired compound as the light yellow solid.

General procedure D for the preparation of final compound **2**

To a solution of **I1** (1.0 eq), 4-[2-(morpholin-4-yl) ethoxy] aniline (1.2 eq) in i-PrOH (5 mL) and TFA (0.5 ml) were added. The reaction mixture was stirred at 90°C overnight. The reaction mixture was filtered and concentrated under reduced pressure. The residue was extracted with water/EtOAc 3 times, the organic layers were combined, dried over anhydrous Na_2SO_4 and evaporated. Finally, column chromatography was used to purify with EtOAC/Hexane 50/50 to afford the desired compound as the beige solid.

General procedure E for the preparation of final compound **3**

To a solution of **I1** (1.0 eq), 1-(4-methoxyphenyl) methanamine (1.2 eq) in NMP (5 mL) and TEA (2.0 eq)) were added. The reaction mixture was stirred at 80°C for 18 h. The reaction mixture was filtered and concentrated under reduced pressure. The residue was extracted with water/EtOAc 3 times, the organic layers were combined, dried over anhydrous Na_2SO_4 and evaporated. Finally, column chromatography was used to purify with EtOAC/Hexane 50/50 to afford the desired compound as the light yellow solid.

General procedure F for the preparation of final compound **4**

To a solution of **I2** (1.0 eq), 1-(4 bromophenyl)methanamine (1.2 eq) in NMP (5 mL) and TEA (2.0 eq)) were added. The reaction mixture was stirred at 80°C for 18 h. The reaction mixture was filtered and concentrated under reduced pressure. The residue was extracted with water/EtOAc 3 times, the organic layers were combined, dried over anhydrous Na_2SO_4 and evaporated. Finally, column chromatography was used to purify with EtOAC/Hexane 50/50 to afford the desired compound as the orange solid.

General procedure G for the preparation of final compound **5**

To a solution of 2,4-dichloropyrimidine (1.0 eq), 4-hydroxy-3,5-dimethyl benzonitrile (1.2 eq) in DMF (4 mL) and K_2CO_3 (1.2 eq)) were added. The reaction mixture was stirred at 150°C overnight. The reaction mixture was filtered and concentrated under reduced pressure. The residue was extracted with water/EtOAc 3 times, the organic layers were combined, dried over anhydrous Na_2SO_4 and evaporated. Finally, column chromatography was used to purify with EtOAC/Hexane 50/50 to afford the desired compound as the white solid.

General procedure H for the preparation of final compound **6**

To a solution of 2,4-dichloropyrimidine-5-carbonitrile (1.0 eq), 3-methylaniline (1.0 eq) in DMF (5 mL) and DIPEA (5.0 eq) were added. The reaction mixture was stirred at rt for 4.5 h. The reaction mixture was filtered and concentrated under reduced pressure. The residue was extracted with water/EtOAc 3 times, the organic layers were combined, dried over anhydrous Na_2SO_4 and evaporated. Finally, column chromatography was used to purify with EtOAC/Hexane 50/50 to afford the desired compound as the light gray solid.

3.3.2 Study 2 Design, Synthesis and Biological Evaluation of Feline and Human immunodeficiency virus Inhibitors

22 final novel compounds were synthesized in total according to **Scheme 2** with overall reaction yields ranging from very low (6 %) to excellent (72 %).

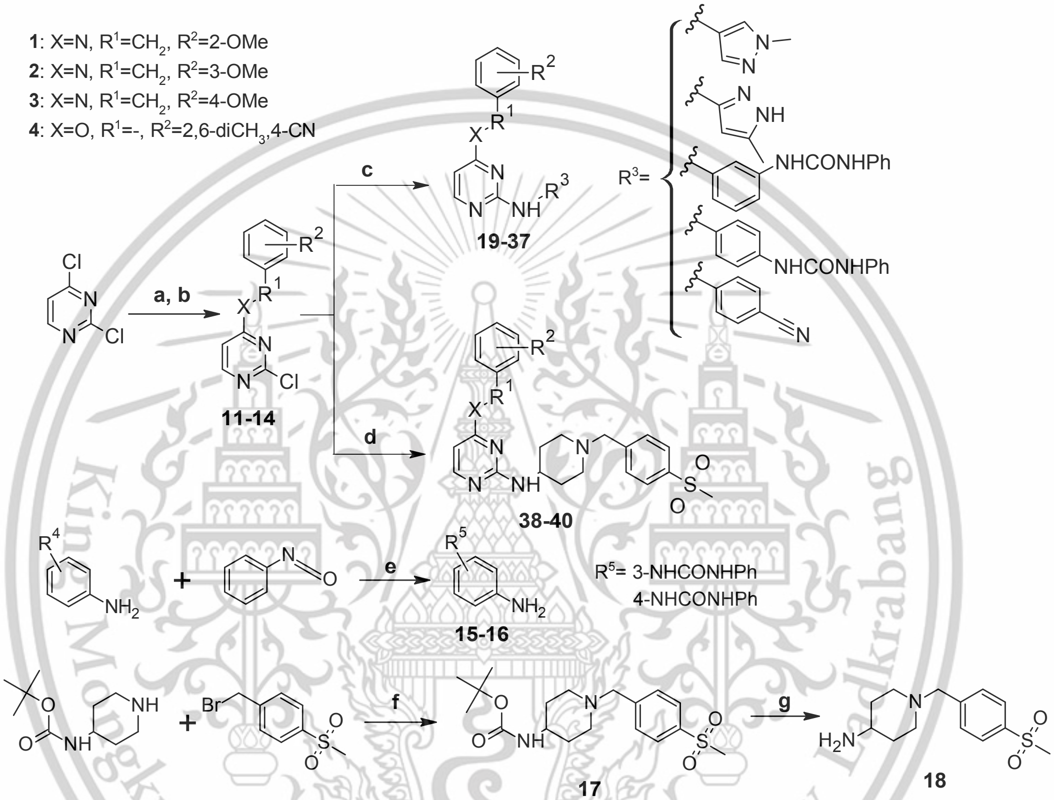

Scheme 2. General synthesis of FIV/HIV inhibitors; **11-13:** (a) $NaHCO_3$, 1,4-dioxane, 100°C, 30min-2h, (50-75%), **14:** (b) K_2CO_3, DMF, rt, overnight, (75%), (c) TFA, i-PrOH, 60-100°C, overnight, (6-72%), (d) DIPEA, 1-butanol, 120°C, overnight, (15-18%), (e) DCM, rt, overnight, (95%), (f) TEA, DCM, rt, 5h, (95%), (g) TFA, DCM, rt, overnight, (95%).

General procedure A for the preparation of intermediate compound **11-13**

A mixture of 2,4-dichloropyrimidine (1.0 eq), benzylamine derivatives (1.2 eq) and $NaHCO_3$ (3.0 eq) were dissolved in 1,4-dioxane was stirred at 100°C for 30 min – 2 h. The reaction mixture was extracted with DI water and ethyl acetate 3 times. The organic layer was collected and combined, dried over anhydrous Na_2SO_4, filtered, and crude mixture required additional purification via silica gel column chromatography to give the desired product as the light yellow solid.

General procedure B for the preparation of intermediate compound **14**

A mixture of 2,4-dichloropyrimidine (1.0 eq), 4-hydroxy-3,5-dimethylbenzonitrile (1.2 eq) and K_2CO_3 (1.2 eq) were dissolved in DMF was stirred at rt overnight. The reaction mixture was extracted with DI water and ethyl acetate 3 times. The organic layer was collected and combined, dried over anhydrous Na_2SO_4, filtered, and crude mixture required additional purification via silica gel column chromatography to give the desired product as the white solid.

General procedure C for the preparation of intermediate compound **15-16**

A mixture of phenyl isocyanate (1.0 eq), phenylenediamine (1.0 eq) were dissolved in DCM was stirred at rt overnight. The precipitate was filtered and washed with DCM to give the desired product as light gray and purple solid, respectively.

General procedure D for the preparation of intermediate compound **17**

A mixture of 4-Boc-aminopiperidine (1.0 eq), 1-(Bromomethyl)-4-methanesulfonylbenzene (1.0 eq) and TEA (1.2 eq) were dissolved in DCM was stirred at rt for 5h. The reaction mixture was extracted with DI water and ethyl acetate 3 times. The organic layer was collected and combined, dried over anhydrous Na_2SO_4, filtered to give the desired product as the yellow viscous liquid.

General procedure E for the preparation of intermediate compound **18**

To a solution of **17** (1.0 eq) in DCM (1 mL) and TFA (30.0 eq) were added. The reaction mixture was stirred at rt overnight. A base was then added to adjust the pH from strongly acidic to strongly basic, followed by extraction with deionized water and ethyl acetate three times. The organic layers were collected, combined, and dried over anhydrous Na_2SO_4, then filtered to yield the desired product as the light-yellow viscous liquid.

General procedure F for the preparation of final compound **19-37**

A solution of product in general synthetic compound **11-14** (1.0 eq) and aromatic derivatives (1.5 eq) was stirred in isopropanol (3 ml), TFA (0.50 ml) was slowly added, the resulting mixture was stirred at 90°C overnight. The reaction mixture was filtered and concentrated under reduced pressure. The residue was extracted with water/EtOAc 3 times, the organic layers were combined, dried over anhydrous Na_2SO_4 and evaporated. Finally, column chromatography was used to purify with DCM/MeOH = 99/1 or EtOAc/Hexane 50/50 to afford the desired compound as the white or/and yellow solid.

General procedure G for the preparation of final compound **38-40**

A solution of product in general synthetic compound **11-13** (1.0 eq) and product in general synthetic compound **18** (1.2 eq) was stirred in 1-butanol (3 ml), DIPEA (3 eq) was slowly added, the resulting mixture was stirred at 120°C overnight. The reaction mixture was filtered and concentrated under reduced pressure. The residue was extracted with water/EtOAc 3 times, the organic layers were combined, dried over anhydrous Na_2SO_4 and evaporated. Finally, column chromatography was used to purify with DCM/MeOH = 1/99 to afford the desired compound as the white or/and yellow solid.

3.4 Biological testing

The EnzChek^{TM} reverse transcriptase assay kit (E-22064) and dimethyl sulfoxide (DMSO) were purchased from Molecular Probes (USA) and Sigma-Aldrich (Germany), respectively. Compounds **1-10** and **19-40** were prepared and characterized as described in the following section. Screening standards Efavirenz (EFV), Rilpivirine (RPV) and Nevirapine (NEV) were purchased commercially.

3.4.1 HIV/ FIV reverse transcription relative inhibition assay

The FIV RT relative inhibition assay was performed using the EnzChek^{TM} reverse transcriptase assay kit (E-22064) as previously reported [86-88]. to screen their ability to inhibit. EnkChek^{TM} Reverse Transcriptase assay kit was purchased from (E-22064) and dimethyl sulfoxide (DMSO) were purchased from Molecular Probes (USA) and Sigma-Aldrich (Germany), respectively. This protocol used a final volume of 25 µL in 96-well black plate. Firstly, 2 µL of 625 µM of each compound or 12.5 µM of drug standards was added to a 96-well plate. Next, 3 µL of RT reaction buffer (50 mM TE $pH_{7.6}$, 2 mM DTT, and 20% glycerol) and 15 µL of 1:400 template/primer substrate were added into each well. After that, the reaction was started by adding 5 µL of 12.5 nM of FIV RT enzyme. For a negative control, 2 µL of 0.2 M EDTA (stop solution) was added before starting the reaction. The reaction was incubated at 25°C for 30 min and adding 2 µL of 0.2 M EDTA for stopped the reaction except for the negative control. Finally, 173 µL of 1:1500 Picogreen fluorescence dye was added into each well and the reaction was measured by using a microplate reader (Infinite M200 microplate reader, Tecan, Männedorf, Switzerland) at an excitation wavelength of 485 nm and emission of 528 nm. The percent relative inhibition (%) of all studied compounds was calculated using Equation (1):

$$\%\ \textbf{Relative Inhibition} = \frac{[(\textbf{positive}-\textbf{negative})-(\textbf{sample}-\textbf{negative})]}{(\textbf{positive}-\textbf{negative})}\ \textbf{x100} \quad (1)$$

Compounds were also screened for their ability to inhibit the HIV-1 RT enzyme using the same EnzChek^{TM} reverse transcriptase assay kit (E-22064).

3.4.2 Determination of IC_{50}

For IC_{50} calculations, the different concentrations of focused compounds and drug standards around ten concentrations were performed to calculate the IC_{50} values as previously described.

The reaction was started by adding 2 µL of focused compounds in each concentration into 96-well black plate. After that, 3 µL of RT reaction buffer and 15 µL of 1:400 template/primer substrate were added into each well, respectively. The reaction was incubated, stopped, and the fluorescence intensity was measured as previously described. The IC_{50} was calculated from the non-linear regression dose–response curve generated using the GraphPad Prism program (GraphPad Software Inc., San Diego, CA, USA).

3.5 Aqueous Solubility

The equilibrium solubility was determined in phosphate buffer (PBS) at pH 7.4 [89]. Approximately 1 mg of each sample was dissolved in 2 mL of 0.02 M PBS at pH7.4 in a 10 mL glass screw top vial, sonicated and shaken for 1 h and 6 h, respectively, to make the saturated solution, and then filtered using a syringe filter (13mm, 0.20 mm, filter, Xiboshi). A standard solution for each sample was prepared by dissolving a known amount of sample in 1 mL of DMSO, pre-diluted 10 times using DMSO. The amount of sample present in the PBS and DMSO solutions was determined by HPLC-UV (HITACHI/Chromaster HPLC with a Poroshell 120 EC-C8 2.7 µM column). A 100 µL injection of the aqueous sample and 10 µL of DMSO solution were used. The solubility was calculated based on the ratio of the area under the curve obtained from the 2 samples, corrected for the dilution factors and injection volume.

3.6 Partition coefficient ($logD_{7.4}$)

The 1-octanol, pre-saturated with 0.02M PBS at $pH_{7.4}$ was determined using the shake flask technique [90]. Roughly 1 mg of the sample was added into a 10 mL glass screw-top vial to which 2 mL of octanol was added. The solution was sonicated for 1 hr. Compounds that were incompletely dissolved were diluted in further octanol and sonicated until a completely clear solution resulted. A final volume of 2 mL of octanol solution and 8 mL of 0.02 M of PBS at $pH_{7.4}$ were shaken for 6 hrs. The resulting solutions were centrifuged (4000 rpm for 15 min), and the octanol and aqueous layers were extracted separately. The amount of sample present in the octanol and PBS solutions was determined by HPLC-UV (HITACHI/Chromaster HPLC with a Poroshell 120 EC-C8 2.7 μM column).

Chapter 4

Result and Discussion

4.1 Study 1 Comparison of Feline and Human Immunodeficiency Virus Reverse Transcriptase Enzymes Through Chemical Screening and Computational Analysis.

In this research, we place particular emphasis on probe compounds structurally similar to the 4th generation inhibitor Rilpirivirine and its related derivatives [91-93]. The central criteria for compound selection were the ability of the molecule to form the key binding motif found in the majority of NNRTIs (**Figure 2**). To this end, we first employed substructure searching, followed by shaped-based and pharmacophore-based similarity searching and molecular docking. This procedure allowed us to identify a set of structurally diverse molecules that had the potential to bind to the NNRTI pocket of FIV and HIV. We wished to select Ten molecules to screen experimentally against the two enzymes. Three knowns HIV-1 RT inhibitors, Rilpivirine (RPV), Efavirenz (EFV) and Nevirapine (NEV) were also considered for the purpose of comparison.

4.1.1. Computational Screening

Compounds **1-10** were identified as potential HIV inhibitors from substructure searching. The compounds were then assessed in terms of their shape-based, pharmacophore-based similarity analysis and ability to dock to FIV-RT and HIV-1 RT.

Shape-based and pharmacophore-based similarity assessment was performed using the programs ShaEP and Pharmagist. First, multiple low energy conformations of **1-10** were prepared and optimized at the HF/6-31G* level of theory. These conformations were used in the virtual screening comparisons against experimentally known conformations of 5 inhibitors/drugs extracted from X-ray crystal structures of HIV-1 RT (Figure 1). Molecular docking to both HIV-1 RT and an FIV-RT homology model were also performed (Table 1). Two drug molecules, RPV and EFV, were also analyzed using the same protocol to act as a benchmark.

The protocol led to mean shape similarity values for RPV and EFV against the 2 reference HIV inhibitors of 0.57 and 0.59 (Table 1). It was found that the max ShAEP value obtained for Rilpivirine was 0.72, and Efavirenz, 0.69, both against themselves. A value of 1 was not obtained since it was gasphase optimized QM-based geometries being compared to those taken directly from the 3D X-ray structures. We therefore concluded that a mean shape similarity score of ~0.5, and a mean PharmaGist score of ~8.0 represented molecules with acceptable shape and pharmacophoric similarity to the 5 HIV references. Compound **1-10** met this threshold.

Table 2 Computational results from ShAEP and and docking scores to FIV, HIV using GOLD docking.

ID	Structure	Ligand Similarity[a]		Molecular Docking	
		ShAEP Score	PharmaGist Score	FIV	HIV
1	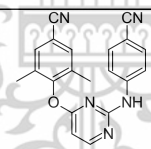	0.50, [0.61] (±0.06)	8.75, [14.44] (±2.6)	78.83	81.21
2	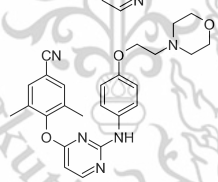	0.40, [0.56] (±0.08)	7.26, [11.29] (±2.3)	65.17	69.30
3	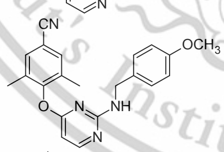	0.50, [0.61] (±0.07)	8.22, [12.93] (±2.3)	72.38	69.16
4	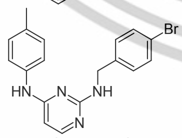	0.50, [0.61] (±0.07)	7.72, [12.67] (±2.4)	67.65	72.17
5	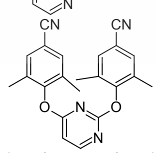	0.52, [0.62] (±0.06)	8.59, [12.39] (±2.3)	66.97	52.53
6	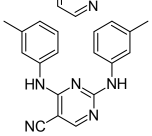	0.51, [0.65] (±0.07)	7.92, [13.25] (±2.4)	70.35	66.39

7	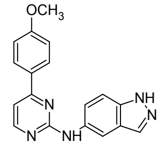	0.53, [0.61] (±0.07)	8.53, [10.65] (±1.6)	61.06	62.66
8	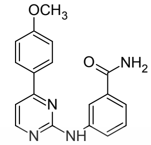	0.53, [0.62] (±0.05)	7.38, [9.03] (±1.4)	58.91	62.32
9	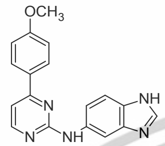	0.53, [0.61] (±0.06)	8.49, [10.68] (±1.6)	62.32	60.42
10	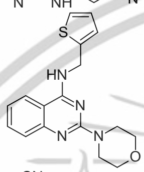	0.53, [0.67] (±0.07)	8.12, [9.02] (±0.8)	60.82	61.12
RPV	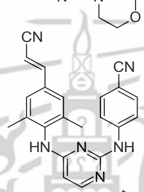	0.57, [0.72] (±0.09)	9.02, [16.93] (±3.7)	89.45	88.12
EFV	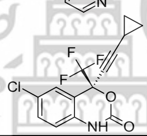	0.59, [0.69] (±0.08)	7.00, [8.77] (±1.6)	57.93	57.49

[a] *mean, [max](S.D.)*

Molecular docking of compounds to FIV and HIV demonstrated that molecules **1-4** and **6-9** could bind to the NNRTI site and make at least 2 H-bond interactions with GLN/LYS101. The docking scores of reference drugs **RPV** and **EFV** were 89.5 and 57.9 to FIV, and 88.1 and 57.5, respectively. The docking scores of **1-10** to FIV ranged from 61.1 to 89.5, and 57.5-81.1 suggesting they could be potential binders. **5** and **10** could make only 1 H-bond interaction with GLN/LYS101 meaning their docking scores were on average lower at both targets.

The results obtained from virtual screening suggested that the selected molecules have the potential to bind to both FIV and HIV. Furthermore, the structural diversity of the features possessed by the molecules (connectivity, functional groups etc.) mean that they can be used to probe differences between the two related RT enzymes.

4.1.2 In vitro Screening against FIV-RT and HIV-1 RT

Compounds were initially screened against FIV-RT and HIV-1 RT at 1 μM concentration (**Table 2**). Compounds tested against FIV showed %inhibition (%I) values ranging from 14.9-87.8% while the corresponding %I values at HIV-1 RT ranged from 15.5-93.6%. IC_{50} values against FIV were subsequently obtained for all compounds as this was the primary target of interest here. IC_{50} values were determined against HIV-1 RT only where %I > 40%. RPV, NEV and EFV were evaluated at both enzymes for the purpose of comparison.

The IC_{50} values at FIV-RT ranged 0.03 to >800 μM. The corresponding values for HIV-1RT were 0.01 to >252 μM. RPV, NEV and EFV displayed IC_{50}s against FIV-RT of 0.04, 160 and 0.22 μM while the corresponding values at HIV-1RT were 0.05, 3.1 and 0.01 μM, respectively. The rather dramatic loss in activity for NEV in felines is in line with previous reports [86, 88, 94]. The most potent compound against FIV was found to be compound **1** (0.03 μM). This compound is structurally similar to the HIV-1 RT inhibitor RPV**,** which was is marginally less potent (0.04 μM). Close analogs **2** and **3** were considerably less potent at both FIV and HIV (μM range). All but **9** and **10** showed better FIV-RT activity than NEV.

Next, we assessed the correlation between the FIV and HIV-1RT IC_{50}s (**Figure 6**). FIV and HIV-1 RT show reasonably strong correlation for the 9 compounds having both values (r^2 = 0.87). This is perhaps unsurprising as the amino-acid sequence similarities between the two enzymes are 68%, or approximately 88% at the active site level.

The inhibition values obtained for HIV-1 RT were on average 4-fold lower than those obtained for FIV. The non-pyrimidine compound NEV was a distinct outlier, being considerably less potent against FIV than HIV. The observation that **1** was marginally more potent at FIV than HIV-1 RT confirms that small active site differences within the two protein can have significant effects on the activity [10].

4.1.3 Structure Activity Relationships (SAR)

Molecular docking of compounds to HIV-1RT, and a FIV-RT homology model, was used to facilitate SAR rationalization. A crystal structure of RPV bound to wild-type HIV-1 RT was used for HIV-1 RT docking (3MEE, resolution 2.80 Å) [72] and to generate a FIV-RT homology model. Compounds were then docked to the allosteric site (**Figure 1**). The docked conformation and score were then employed to help rationalize the experimental inhibition values.

Of the new compounds evaluated here, those with greater similarity to the marketed drug RPV had the best activity (**1** & **2** in particular). **1** differs from RPV by replacing the 4-position aniline with phenol, as well as the deletion of the ethene linker connecting to the nitrile group. Addition of a larger, polar morpholino group to give **2** results in reduced activity, albeit better at HIV-1RT than FIV.

Compounds **3** & **4** differ more substantially from RPV, incorporating a benzyl ring at the 2-position of pyrimidine as opposed to aniline. This change results in a more sizeable drop-in activity suggesting it is detrimental to the H-bond with GLN/LYS101. **5** incorporates a phenol as opposed to aniline at the pyrimidine 2-position, again reducing the H-bonding with GLN/LYS101 as it lacks the required H-bond acceptor to form a bidentate interaction. Compound **6** possesses a less polar, less sterically hindered 3-methyl aniline, with the nitrile group now at the 5-position of pyrimidine. This led to an even greater drop-in activity. Molecular docking points to clashes with residues including ALA/GLU138.

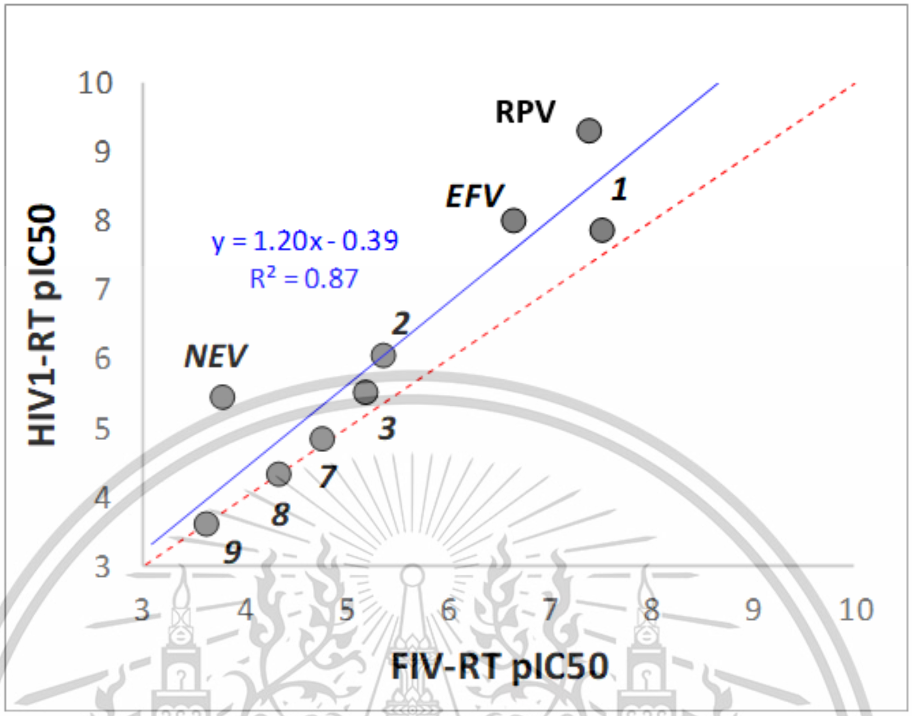

Figure 6 Relationship between HIV-1 RT pIC_{50} vs FIV-RT

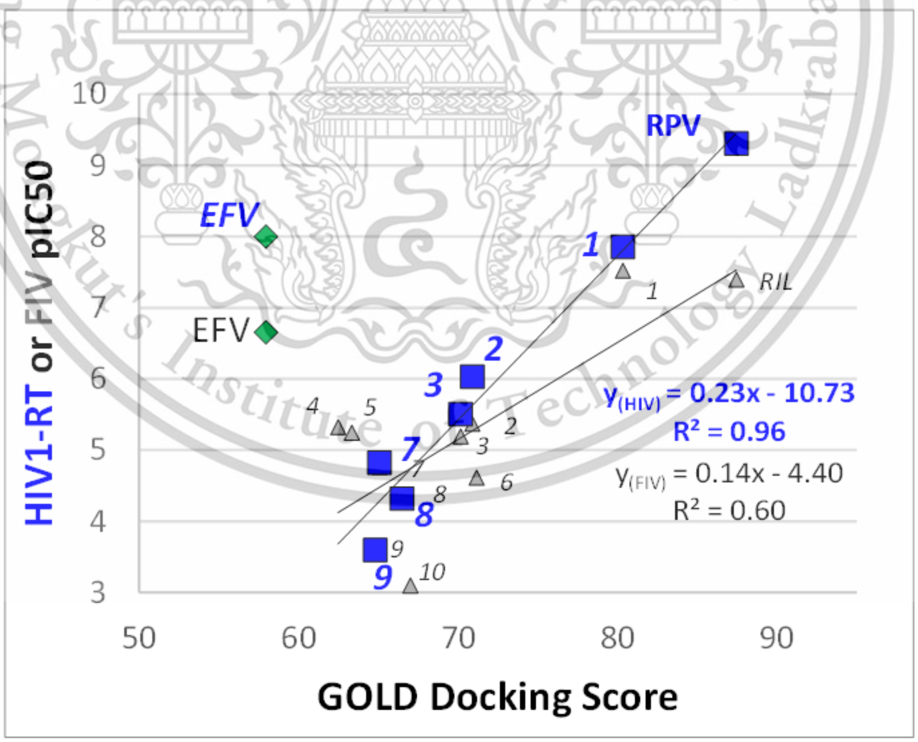

Figure 7 The correlation between the HIV-1 RT and FIV pIC_{50} docking score for pyrimidine analogs.

Compounds **7-10** were structurally less similar to RPV than compounds **1-6** so it was not unexpected that they displayed the weakest inhibitory effect at both RT enzymes. The 4-phenyl pyrimidine compounds have a distinctly different shape profile meaning that forming H-bond interactions with GLN/LYS101 will result in the 4-position phenyl rings entering the adjacent pocket at a sub-optimal angle as confirmed from docking. The direct attachment of a morpholine ring to the quinazoline of **10** resulted in weaker interaction with GLN/LYS101 due to steric clash, explaining the very poor inhibition of the compound.

Lastly, we plotted the docking scores of compounds with the experimental pIC_{50}s (**Figure 7**). A good correlation between the docking score and HIV-1 RT activity was observed for RPV-like compounds. The r^2 was 0.96, excluding the structurally less similar EFV molecule. The trend was less pronounced for FIV (r^2=0.60), due to the presence of additional benzyl analogs **4** and **5**, and potentially since docking was to a HIV-1 RT derived homology model of the enzyme. This observation suggests that for close structural analogs to RPV at least, the docking program can differentiate between those that can and cannot (a) H-bond to GLN/LYS101 and (b) maintain a favorable vector for the 4-subsituted moiety into the adjacent pocket. This finding could potentially be useful for future virtual screening efforts.

4.1.4 Synthesis Results

Compounds **1**, **2**, **3**, **4**, **5** and **6** were prepared according to **Scheme 1**. The preparation of compounds **7-9** [84] and **10** [85] have been reported elsewhere. All final compounds (**Table 3**) were confirmed through ^1H NMR spectroscopy and high-resolution mass spectrometry (HRMS), providing detailed structural information for each compound. Additionally, the purity of each compound was assessed by HPLC, confirming a purity level of over 95%.

Table 3 Screening data for the 10 compounds and 3 anti-HIV-1 RT drugs assessed in this study. Reported are calculated physicochemical properties, HIV-1 RT % I values (at 50 μM) HIV-1 RT IC_{50}s for compounds with %I > 40% and IC_{50}s for FIV-RT

ID	Structure	Mass	clogP	FIV RT: WT		HIV-1 RT: WT	
				%I[a]	IC_{50}[b] /μM	%I[b]	IC_{50}[b] / μM
1	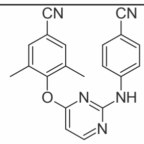	341.4	5.0	83.7 ±2.86	0.03 ±0.01	88.8 ±1.98	0.01 ±0.00
2	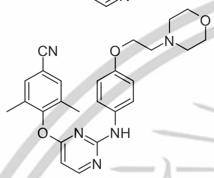	445.5	4.8	58.5 ±1.04	4.27 ±0.30	93.6 ±0.88	0.93 ±0.01
3	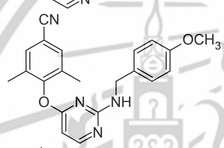	360.4	4.7	58.5 ±6.48	6.42 ±1.06	43.6 ±8.89	3.09 ±0.24
4	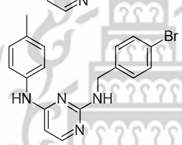	369.3	5.2	48.1 ±0.36	4.73 ±2.35	37.5 ±1.11	nd
5	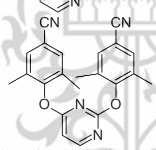	370.4	6.1	54.6 ±4.51	5.67 ±1.96	22.6 ±8.81	nd
6	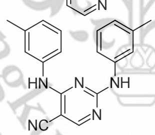	315.4	5.1	66.0 ±4.84	24.1 ±8.60	23.1 ±2.38	nd
7	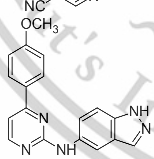	317.4	2.9	87.8 ±3.65	17.2 ±2.00	76.8 ±0.97	15.1 ±2.90
8	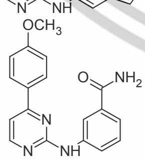	320.4	2.9	48.2 ±2.99	45.8 ±5.40	45.7 ±8.05	47.7 ±3.69
9	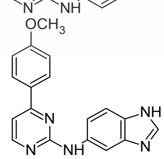	317.4	3.6	23.6 ±3.56	232 ±5.40	71.9 ±6.08	252 ±6.68
10	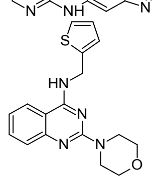	326.4	3.7	14.9 ±5.84	>800	15.5 ±6.23	nd

RPV	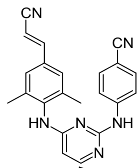	366.4	5.5	79.9 ±1.04	0.04 ±0.01	-	0.049 ±0.001
NEV	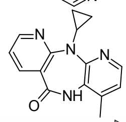	266.3	2.5	14.8 ±2.18	>160	48.7 ±7.50	3.06 ±0.01
EFV	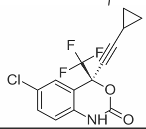	315.7	4.5	48.5 ±1.17	0.22 ±0.17	-	0.01 ±0.01

[a] %I at 1 μM, [b] %I at 50 μM, nd not determined.

4.2 Study 2 Design, Synthesis and Biological Evaluation of Feline and Human immunodeficiency virus Inhibitors

4.2.1 Structure-based Design Method

Docking studies were conducted to evaluate how the optimized conformations of compounds **35**, **36**, and **37**, featuring 2-methoxy, 3-methoxy, and 4-methoxy groups, respectively, bind to the left wing of HIV-1 reverse transcriptase (RT). The analysis was performed using two different protein structures: 3MEC, which has Etravirine in its active site, and 2ZD1, which contains Rilpivirine in its active site.

Protein preparation for docking involved the removal of bound inhibitors, water molecules, and other cofactors. Additionally, a docking constraint was applied, requiring each ligand pose to form a hydrogen bond interaction with LYN101.

Docking results with 3MEC (**Table 4**) revealed that the **36** exhibited the lowest binding energy, followed by the **37** and **38**. The binding pose for the **36** was found predominantly in the "left wing", a region pointing away from the active site, where the final position of the aromatic ring was associated with the lowest energy. In contrast, docking results with 2ZD1 (**Table 5**) indicated that **37** had the lowest binding energy, followed by **36** and **35**. Similarly, most binding poses for **37** were found in the "left wing", pointing away from the active site, with the aromatic ring occupying the final low-energy position.

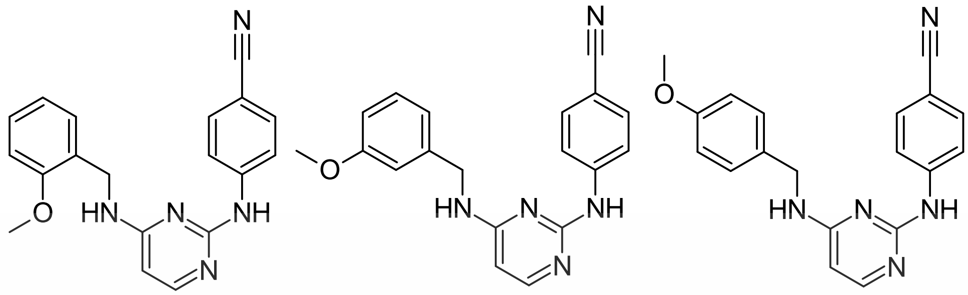

35 36 37

Figure 8 shown the structure of compounds **35-37**

Table 4 The docking results for 3 different positions (compound **35-37**) with HIV-1 RT (PDB: 3MEC) [72] are shown.

ID	Step	Pose	Docking score	ΔE in each group (kcal/mol)
35	Dock 1	in	72.82	4.6
	Dock 8	out	71.81	1.6
	Dock 12	out	66.97	7.0
	Dock 15	out	76.54	**0.0**
36	Dock 4	out	80.83	2.0
	Dock 6	out	76.84	**0.0**
	Dock 10	out	67.19	4.0
	Dock 14	out	69.84	6.4
37	Dock 7	out	77.62	**0.0**
RPV	Dock 1	-	91.14	-
	Dock 3	-	88.42	-
ETR	Dock 3	-	89.46	-

Table 5 The docking results for 3 different positions (compound **35-37**) with HIV-1 RT (PDB: 2ZD1) [82] are shown.

ID	Step	Pose	Docking score	**Δ**E in each group (kcal/mol)
35	Dock 1	out	70.50	25.9
	Dock 3	out	76.29	**0.0**
36	Dock 1	out	75.52	26.8
	Dock 2	out	78.20	23.4
	Dock 3	in	72.98	**0.0**
37	Dock 2	in	73.29	9.2
	Dock 3	out	74.62	26.4
	Dock 4	out	73.20	**0.0**
RPV	Dock 1	-	89.95	-
ETR	Dock 2	-	84.01	-

Figure 37 compares the docking scores of various methoxy-substituted compounds (2-methoxy, 3-methoxy, and 4-methoxy groups) with 2 reference compounds, Rilpivirine (RPV) and Etravirine (ETR), across two protein structures, 3MEC and 2ZD1, demonstrating a strong correlation between the 2 datasets. **35** exhibits the highest docking score in both 3MEC and 2ZD1, followed by **37** and **36**. The reference compounds, RPV and ETR, show significantly higher docking scores than the methoxy derivatives in both protein structures, with RPV having the highest docking score overall. This suggests that the methoxy derivatives have weaker binding affinities compared to the reference NNRTIs, RPV and ETR. Furthermore, the strong correlation between the docking scores for 3MEC and 2ZD1 indicates that the binding behavior of these compounds is consistent across both protein structures.

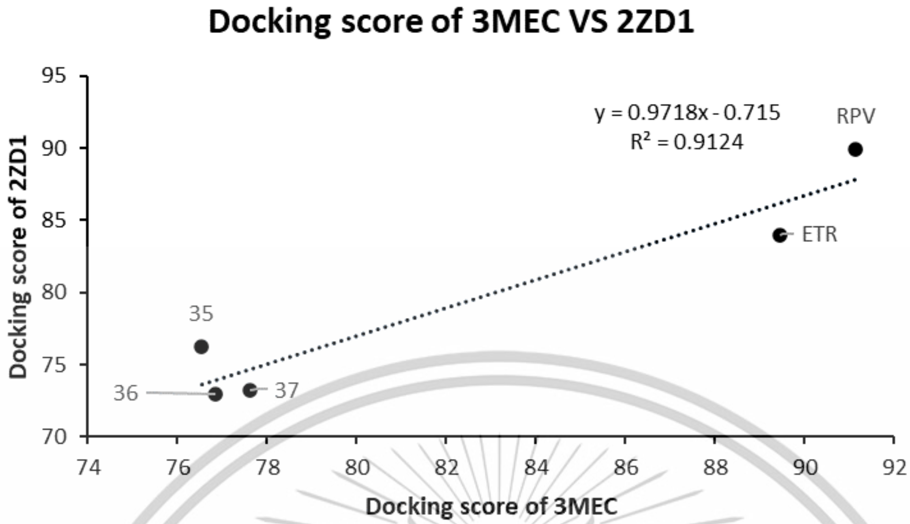

Figure 9 shows the docking score of 3MEC vs 2ZD1

After performing docking, I conducted quantum mechanics (QM) calculations on the lowest energy structures for compound **35-37**, as well as on the protein without the ligand and the protein-ligand complexes to obtain binding energies. The results showed that in 3MEC (**Table 6**), the **35** had the lowest energy, followed by **36** and **37**. In 2ZD1 (**Table 7**), **35** again had the lowest energy, followed by **37** and **36**.

Table 6 The QM results for 3 different positions (compound **35-37**) to determine binding energy with HIV-1 RT (PDB: 3MEC) [72] are presented.

ID	Position	All energy	Energy of ligand	Energy of protein	Binding energy
35	Dock 15	-1.19	0.13	-1.28	-25.5
36	Dock 1	-1.19	0.12	-1.28	-22.1
37	Dock 7	-1.19	0.12	-1.28	-18.4
RPV	Dock 1	-1.06	0.25	-1.28	-18.3
ETR	Dock 3	-1.04	0.27	-1.28	-17.2

Table 7 The QM results for 3 different positions (compound **35-37**) to determine binding energy with HIV-1 RT (PDB: 2ZD1) [82] are presented.

ID	Position	All energy	Energy of ligand	Energy of protein	Binding energy
35	Dock 3	-0.98	0.13	-1.10	-3.0
36	Dock 3	-0.98	0.12	-1.10	-1.8
37	Dock 4	-0.98	0.12	-1.10	-2.1
RPV	Dock 1	-0.86	0.25	-1.10	-7.9
ETR	Dock 2	-0.83	0.27	-1.10	-3.8

The graph (**Figure 38**) illustrates the relationship between the docking scores and the binding energies for various methoxy-substituted compounds **35-37** (2-methoxy, 3-methoxy, and 4-methoxy groups) as well as two reference compounds, Rilpivirine (RPV) and Etravirine (ETR), against the 2ZD1 protein structure, suggesting a strong linear relationship between these two variables. In the graph, **35** shows the lowest binding energy among the methoxy derivatives, followed by **37** and **36**. The reference compounds, RPV and ETR, exhibit lower binding energies compared to the methoxy derivatives, with RPV showing the lowest binding energy and highest docking score, indicating strong binding to the 2ZD1 protein. This analysis highlights the inverse relationship between binding energy and docking score, where lower binding energies are associated with higher docking scores, indicating better binding affinity. Rilpivirine (RPV) stands out with the most favorable binding energy and docking score, suggesting it is a more potent inhibitor in comparison to the methoxy-substituted compounds.

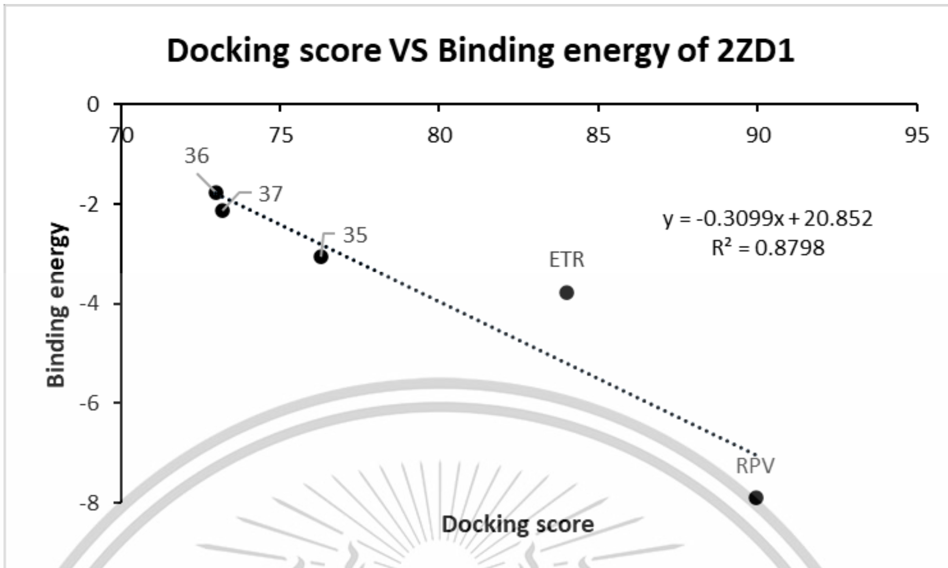

Figure 10 shown graph of docking score vs binding energy of 2ZD1

The structure-guided design of new compounds was based on computational predictions, including docking and quantum mechanics (QM), as described in the structure-based methods section. The design was also influenced by reference drugs from the NNRTI class, particularly Rilpivirine (RPV) and Etravirine (ETR), as well as by compounds 4ab and 21a, which have shown promising inhibition and notable results in previous research [91] [95].

4.2.2 Synthesis Results

Synthetic modifications were developed by focusing on three key areas: the left wing, the right wing, and the core structure. For the left wing, I was inspired by the design of compound 4ab [91] and Etravirine [95], incorporating methoxy groups to enhance conformational flexibility, expecting π-π stacking interactions with aromatic amino acid residues such as Tyr181, Tyr188, and Trp229. For the right wing, the goal was to extend towards the solvent and protein surface. Two types of 5-membered rings were added to investigate differences in the hydrophobic region. Rilpivirine [72] and Etravirine were used to guide the incorporation of cyano groups. Additionally, the aliphatic ring groups were inspired by compound 21a [95]. In the core structure, the nitrogen atom in the pyrimidine and the NH group of the compounds form critical hydrogen bonds with Lys101.

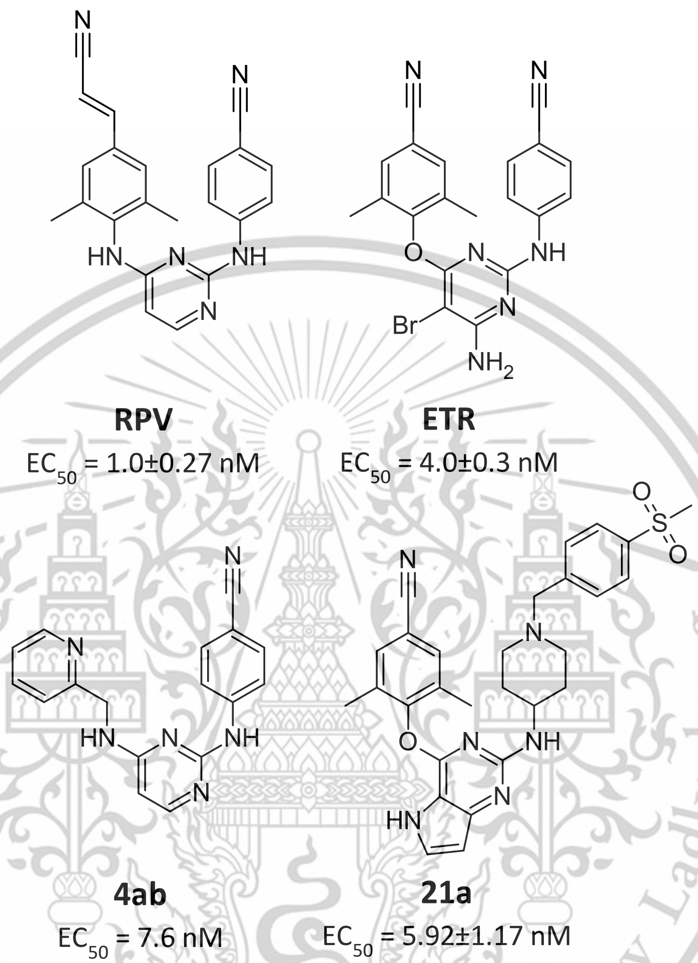

Figure 11 Structures of HIV drugs and development compounds: Rilpivirine (RPV) [72], Etravirine (ETR) [95], 4ab [91] and 21a [95]

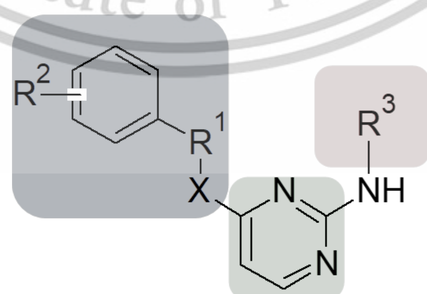

Figure 12 Scope of design HIV-1 RT inhibitors

All compounds were prepared according to the synthetic route described in **Scheme 2**. Briefly, intermediate **11-13** was prepared from the reaction of 2,4-dichloropyrimine and benzylamine derivatives with $NaHCO_3$ in 1,4-dioxane, at 100^{o}C, for 30 min - 2 h, with a yield of 50-75%. Intermediate **14** was prepared from the reaction of 2,4-dichloropyrimine and 4-hydroxy-3,5-dimethylbenzonitrile with K_2CO_3 in DMF at rt overnight with a yield of 75%. Intermediate **15-16** was prepared from the reaction of phenyl isocyanate and phenylenediamine in DCM at rt overnight with a yield of 95%. Intermediate **17** was prepared from the reaction of 4-Boc-aminopiperidine and 1-(Bromomethyl)-4-methanesulfonylbenzene with TEA in DCM at rt for 5h with a yield of 95%. Intermediate **18** was prepared from the reaction of compound **17** with TFA in DCM at rt overnight with a yield of 95%. **11-14** was then reacted with aromatic derivatives under acidic conditions (TFA) in i-PrOH at 60-100^{o}C overnight to give final **19-37** with yields ranging from 6-72%. And **11-13** was then reacted with compound **18** under DIPEA in 1-butanol at 12^{o}C overnight to give final **38-40** with yields ranging from 15-18%.

All final compounds (**Table 8**) were confirmed through ^{1}H NMR spectroscopy and high-resolution mass spectrometry (HRMS), providing detailed structural information for each compound. Additionally, the purity of each compound was assessed by HPLC, confirming a purity level of over 95%.

Table 8. 19-40 and standard assessed in this study. Reported are R-groups, yields, and HIV and FIV activities (%I at 50 μM).

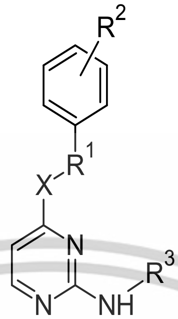

ID	X	R^1	R^2	R^3	clogD[a]	MWT[a]	Yield (%)	FIV-RT: WT		HIV1-RT: WT	
								%I	IC_{50}/μM	%I	IC_{50}/μM
19	NH	CH_2	2-methoxy	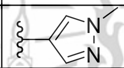	2.90	310.35	27	76.9	-	77.2	-
20	NH	CH_2	3- methoxy	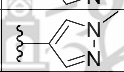	2.90	310.35	65	50.0	-	51.9	-
21	NH	CH_2	4- methoxy	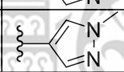	2.90	310.35	14`	54.3	-	54.2	-
22	O	-	2,6-diCH_4	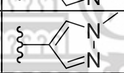	3.24	320.35	30	43.7	-	75.3	-
23	NH	CH_2	2-methoxy	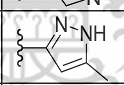	2.82	310.35	6	50.5	-	56.5	-
24	NH	CH_2	3- methoxy	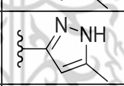	2.82	310.35	14	52.4	-	78.1	-
25	NH	CH_2	4- methoxy	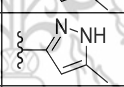	2.82	310.35	9	42.4	-	55.1	-
26	O	-	2,6-diCH_4	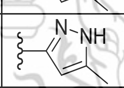	3.24	320.35	9	40.0	-	71.2	-
27	NH	CH_2	2-methoxy	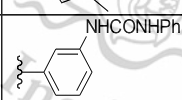	4.95	440.50	30	97.4	-	92.56	-
28	NH	CH_2	3- methoxy	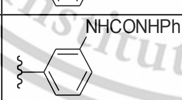	4.95	440.50	72	99.4	-	92.7	-
29	NH	CH_2	4- methoxy	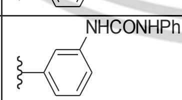	4.95	440.50	46	100	-	83.1	-
30	O	-	2,6-diCH_4	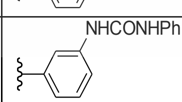	4.86	450.49	15	54.	-	67.	-
31	NH	CH_2	2-methoxy	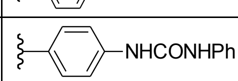	4.95	440.50	26	100	-	90.5	-
32	NH	CH_2	3- methoxy	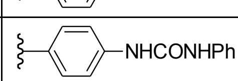	4.95	440.50	70	100	-	100	-
33	NH	CH_2	4- methoxy	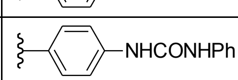	4.95	440.50	18	82.4	-	64.5	-

34	O	-	2,6-diCH_4	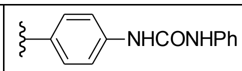	4.86	450.49	16	85.5	-	90.5	-
35	NH	CH_2	2-methoxy	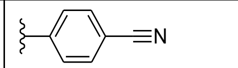	3.66	331.37	35	69.1	-	72.0	-
36	NH	CH_2	3- methoxy	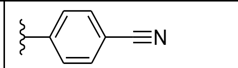	3.66	331.37	40	84.1	-	86.6	-
37	NH	CH_2	4- methoxy	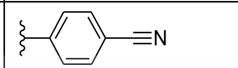	3.66	331.37	27	51.1	-	84.9	-
38	NH	CH_2	2-methoxy	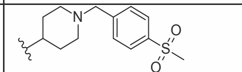	2.43	481.61	15	52.6	-	69.0	-
39	NH	CH_2	3- methoxy	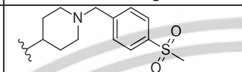	2.43	481.61	16	66.4	-	75.6	-
40	NH	CH_2	4- methoxy	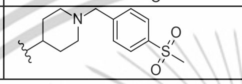	2.43	481.61	18	626	-	47.7	-
Rilpivirine (RPV)					5.50	366.41	-	70.4	-	90.5	-
Efavirenz (EFV)					4.50	315.70	-	80.5	-	85.	-
Nevirapine (NVP)					2.50	266.30	-	65.27	-	79.72	-

[a]calculated using MarvinSketch[96].

4.2.3 FIV and HIV Inhibition

All compounds were tested for their activity against HIV WT and FIV WT at a concentration of 50 μM. The % inhibition (%I) values for HIV and FIV ranged from 47.7% to 100% and 40.0% to 100%, respectively (**Table 9**). 12 compounds exhibited higher %I than the reference HIV drug.

The graph in **Figure 61** indicates that 5 compounds exhibit significant inhibition of HIV: compounds **27**, **28**, **31**, **32**, and **34**. In addition, 5 compounds show notable inhibition of FIV: compounds **27**, **28**, **29**, **31**, and **32**. These 12 compounds, including 6 that demonstrate strong inhibition of both HIV and FIV, were further evaluated for logD7.4 and solubility to assess their correlation.

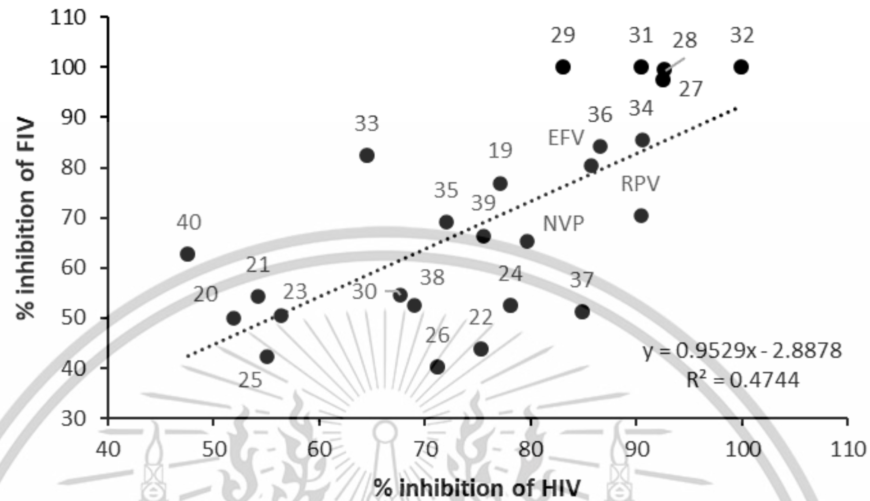

Figure 13 shown graph comparing the % inhibition (%I) of HIV and FIV

Table 9 Partition coefficient ($logD_{7.4}$), aqueous solubility and HIV and FIV activity of compounds **19**, **27-36** and **39**

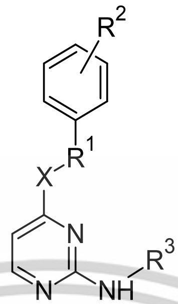

ID	X	R1	R2	R3	%inhibition HIV	%inhibition FIV	Solubility (µg/mL)	clogD[a]	logD7.4
19	NH	CH_2	2-methoxy	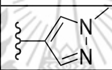	77.2	79.9	313	2.82	2.86
27	NH	CH_2	2-methoxy	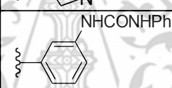	92.6	97.4	9.52	4.95	3.82
28	NH	CH_2	3- methoxy	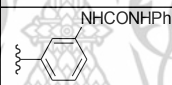	92.7	99.4	2.96	4.95	3.58
29	NH	CH_2	4- methoxy	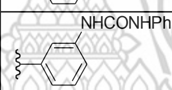	83.1	100	<1	4.95	>4
30	O	-	2,6-diCH_4	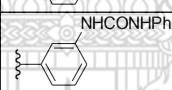	67.6	54.5	4.09	4.86	2.50
31	NH	CH_2	2-methoxy	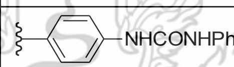	90.5	100	1.79	4.95	3.43
32	NH	CH_2	3- methoxy	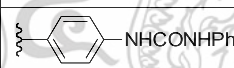	100	100	1.36	4.95	>4
33	NH	CH_2	4- methoxy	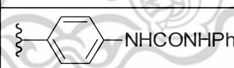	64.5	82.4	17.4	4.95	3.67
34	O	-	2,6-diCH_4	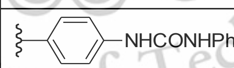	90.5	85.4	1.82	4.86	3.25
35	NH	CH_2	2-methoxy	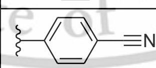	72.0	69.1	3.99	3.66	2.56
36	NH	CH_2	3- methoxy		86.6	84.1	8.83	3.66	3.34
39	NH	CH_2	3- methoxy	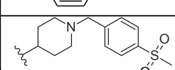	75.6	66.4	639	2.43	2.06
Rilpivirine (RPV)					90.4	70.4	1.19	5.50	3.71
Efavirenz (EFV)					85.7	80.4	69.6	4.50	>4
Nevirapine (NVP)					79.7	65.2	610	2.50	1.44

[a]calculated using MarvinSketch[96].

We observed a good correlation between the calculated and measured logD value for compounds reported here (**Figure 62**) giving confidence in our results. Furthermore, the experimentally reported logD values for RPV, EFV and NEV are 4.5 [97], 5.40 [97] and 2.5 [97] in good agreement with the values reported here of 3.71, >4 and 1.44.

The experimentally reported phosphate buffer solubility values for RPV, EFV and NEV are 18.5 μg/mL [98], 9 μg/ml [99, 100] and 100 μg/ml [101] using a different protocol. The values are broadly similar to those reported here of 1.19 μg/ml, 69.6 μg/ml and 610 μg/ml (i.e. NEV is markedly more soluble than RIL and EFV.)

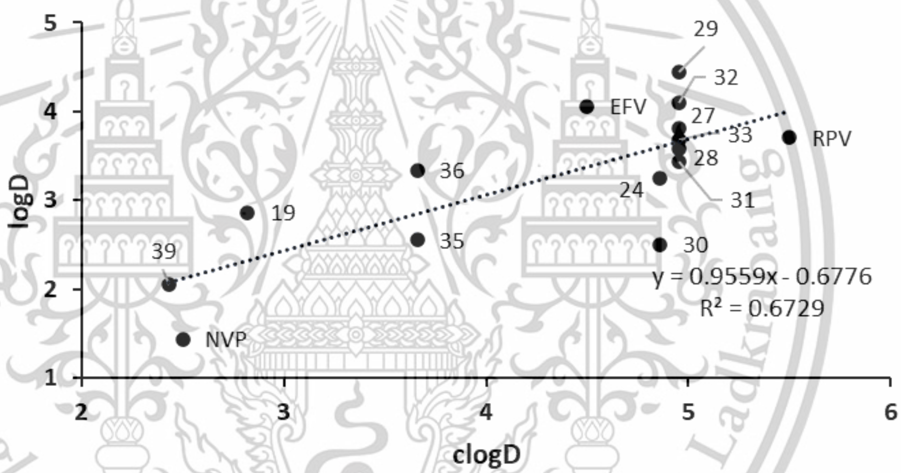

Figure 14 A graph of calculated logD and experiment logD

Analysis of the correlation between the %inhibition data collected for compounds **19-37** shows a reasonable strong relationship between the 2 enzymes. A correlation coefficient r scale of 0.47 is in line with the fact that while these are both transcriptase enzymes, they share only 67% similarity. These finding are in line with our previous reports elsewhere [102].

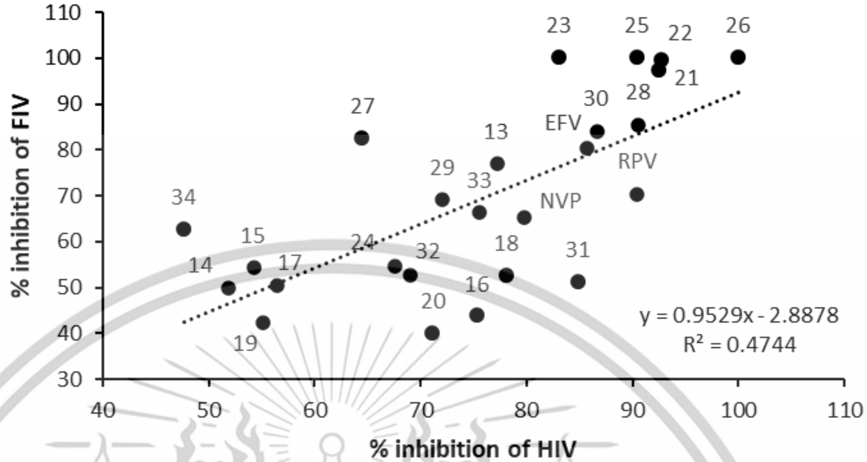

Figure 15 Correlation between the FIV and HIV1-RT inhibition values obtained here.

Finally, we evaluated the correlation between the calculated docking scores, binding energies, and the experimental % inhibition values presented in **Table 10**. A strong correlation was observed between binding energy and % inhibition for HIV, with an r^2 value of 0.97 (**Figure 64**). However, no correlation was found between the computed parameters and % inhibition (**Table 10**). When analyzing the position of the methoxy group attached to the benzyl group, as detailed in **Table 8** and **Figure 61**, a reasonable correlation with the GOLD docking results was observed.

Table 10 show the docking scores and binding energies for both 3MEC and 2ZD1, along with the experimental % inhibition values for HIV and FIV.

ID	Docking score		Binding energy		%Inhibition	
	3MEC	2ZD1	3MEC	2ZD1	HIV	FIV
35	76.54	76.29	-25.54	-3.05	72.04	69.08
36	76.84	72.98	-22.09	-1.78	86.62	84.12
37	77.62	73.20	-18.36	-2.12	84.91	51.08
RIL	91.14	89.95	-18.34	-7.89	90.47	70.41

Chapter 5

Conclusion

Study 1 Comparison of Feline and Human Immunodeficiency Virus Reverse Transcriptase Enzymes Through Chemical Screening and Computational Analysis.

The treatment of felines suffering FIV has traditionally relied on drugs developed for human with the similar underlying mechanisms. This has prompted the repurposing of anti-HIV-1 RT drugs for felines, despite significant differences in their ultimate targets. Indeed, Galilee *et al*[10] noted that human drugs may not be ideal for felines due to differences in key active site residues as well as protein flexibility.

The goal of this work was to explore the SAR differences between FIV-RT and HIV-1 RT, and in particular to understand how the inhibitory activity at both enzymes differs when exposed to molecules that can bind in subtly different conformations within their respective active sites. To this end we selected 10 Rilpirivirine-like molecules that also demonstrated good shape and pharmacophore similarity to the latest NNRTI drugs and development compounds. These were then screened experimentally against FIV-RT and HIV-1 RT.

We demonstrated that there was a reasonably strong correlation between FIV-RT and HIV-1 RT (r^2=0.87), despite the relatively low enzyme similarity (~67%). Nevertheless, it was clear subtle SAR differences were present, including **NEV** being considerably less potent at FIV-RT and HIV-1 RT. While **EFV** (0.01 μM) was the most potent compound at HIV-1 RT, **1** was the most potent at FIV-RT (0.03 μM). These results confirm that the optimal compound to inhibit the human target may not necessarily be the best for the related feline target and vice versa.

Study 2 Design, Synthesis and Biological Evaluation of Feline and Human immunodeficiency virus Inhibitors

We have designed and synthesized **22** novel inhibitors of HIV-1RT and FIV by incorporating a benzyl linker at 4-posotion of pyrimidine. The designed molecules were assessed in terms of their fit within the HIV-1RT and FIV active site pockets using molecular docking using GOLD5.3 and using a QM-based method.

All molecules were predicted to bind well with the pocket and were therefore prepared experimentally. Compounds were tested against HIV1-RT and FIV at 50 μM concentration with exemplars including **27**, **28**, **29**, **31, 32**, **34** and **36** showing greater activity that the known reverse transcriptase inhibitors Rilirivirine, Etravirine and Nevirapine. IC_{50} values will be obtained later.

Compounds were also tested in terms of the physicochemical properties and we identified **19** and **33** and **39** as a moderately potent inhibitors of HIV and FIV but with excellent solubility (313, 17.4 and 639 ug/ml, respectively) and logD (2.86, 3.67 and 2.06 respectively). These molecules could potentially overcome one of the key deficiencies of the drug Rilpirivirine, which has consisted suffered in the clinic due to its poor solubility (3.71 ug/ml).

Finally, compounds **19** and **27** demonstrate balanced potency as inhibitors, showing potential to inhibit HIV with rates of 77.2% and 92.6%, respectively, and FIV with rates of 79.9% and 97.4%. Additionally, they exhibit good solubility, with values of 313 μg/ml and 9.52 μg/ml."

Reference

1. Long, M., et al., *Identification of a Potential Inhibitor of the FIV p24 Capsid Protein and Characterization of Its Binding Site.* Biochemistry, 2021. **60**(24): p. 1896-1908.
2. Medeiros Sde, O., et al., *Follow-up on long-term antiretroviral therapy for cats infected with feline immunodeficiency virus.* J Feline Med Surg, 2016. **18**(4): p. 264-72.
3. Saparpakorn, P., et al., *Insight investigation of rilpivirine and compounds from mushrooms as feline immunodeficiency virus reverse transcriptase inhibitors using molecular dynamics simulations and quantum chemical calculations.* Molecular Simulation, 2022. **48**(6): p. 463-476.
4. Brown, M.A., et al., *Feline immunodeficiency virus (FIV) in wild Pallas' cats.* Veterinary Immunology and Immunopathology, 2010. **134**(1): p. 90-95.
5. Bendinelli, M., et al., *Feline immunodeficiency virus: an interesting model for AIDS studies and an important cat pathogen.* Clin Microbiol Rev, 1995. **8**(1): p. 87-112.
6. Pedersen, N.C., et al., *Isolation of a T-lymphotropic virus from domestic cats with an immunodeficiency-like syndrome.* Science, 1987. **235**(4790): p. 790-3.
7. Sparger, E.E., *FIV as a Model for HIV: An Overview.* In vivo Models of HIV Disease and Control, 2006: p. 149-237.
8. De Clercq, E., *Antiviral therapy for human immunodeficiency virus infections.* Clin Microbiol Rev, 1995. **8**(2): p. 200-39.
9. Das, K. and E. Arnold, *HIV-1 reverse transcriptase and antiviral drug resistance. Part 1.* Curr Opin Virol, 2013. **3**(2): p. 111-8.
10. Galilee, M. and A. Alian, *The structure of FIV reverse transcriptase and its implications for non-nucleoside inhibitor resistance.* PLOS Pathogens, 2018. **14**(1): p. e1006849.
11. Amacker, M., M. Hottiger, and U. Hübscher, *Feline immunodeficiency virus reverse transcriptase: expression, functional characterization, and reconstitution of the 66- and 51-kilodalton subunits.* J Virol, 1995. **69**(10): p. 6273-9.
12. Kenyon, J.C. and A.M. Lever, *The molecular biology of feline immunodeficiency virus (FIV).* Viruses, 2011. **3**(11): p. 2192-213.
13. Schwartz, A.M., et al., *Antiviral efficacy of nine nucleoside reverse transcriptase inhibitors against feline immunodeficiency virus in feline peripheral blood mononuclear cells.* Am J Vet Res, 2014. **75**(3): p. 273-81.
14. Savarino, A., et al., *Human immunodeficiency virus integrase inhibitors efficiently suppress feline immunodeficiency virus replication in vitroand provide a rationale to redesign antiretroviral treatment for feline AIDS.* Retrovirology, 2007. **4**(1): p. 79.
15. Bisset, L.R., et al., *Combined effect of zidovudine (ZDV), lamivudine (3TC) and abacavir (ABC) antiretroviral therapy in suppressing in vitro FIV replication.* Antiviral Res, 2002. **53**(1): p. 35-45.
16. Nolan, D. and S. Mallal, *Complications associated with NRTI therapy: update on clinical features and possible pathogenic mechanisms.* Antivir Ther, 2004. **9**(6): p. 849-63.
17. Usach, I., V. Melis, and J.E. Peris, *Non-nucleoside reverse transcriptase inhibitors: a review on pharmacokinetics, pharmacodynamics, safety and tolerability.* J Int AIDS Soc, 2013. **16**(1): p. 1-14.
18. Auwerx, J., et al., *Susceptibility of feline immunodeficiency virus/human immunodeficiency virus type 1 reverse transcriptase chimeras to non-nucleoside RT inhibitors.* Mol Pharmacol, 2004. **65**(1): p. 244-51.

19. Sluis-Cremer, N. and G. Tachedjian, *Mechanisms of inhibition of HIV replication by non-nucleoside reverse transcriptase inhibitors.* Virus Res, 2008. **134**(1-2): p. 147-56.
20. Xu, S., et al., *Opportunities and challenges in new HIV therapeutic discovery: what is the next step?* Expert Opinion on Drug Discovery, 2023. **18**(11): p. 1195-1199.
21. Zuo, X., et al., *Current insights into anti-HIV drug discovery and development: a review of recent patent literature (2014–2017).* Expert Opinion on Therapeutic Patents, 2018. **28**(4): p. 299-316.
22. Kang, D., et al., *Structure-Based Bioisosterism Yields HIV-1 NNRTIs with Improved Drug-Resistance Profiles and Favorable Pharmacokinetic Properties.* Journal of Medicinal Chemistry, 2020. **63**(9): p. 4837-4848.
23. Hsiou, Y., et al., *The Lys103Asn mutation of HIV-1 RT: a novel mechanism of drug resistance.* J Mol Biol, 2001. **309**(2): p. 437-45.
24. Boyer, P.L., et al., *Analysis of nonnucleoside drug-resistant variants of human immunodeficiency virus type 1 reverse transcriptase.* J Virol, 1993. **67**(4): p. 2412-20.
25. Hartmann, K., A. Wooding, and M. Bergmann, *Efficacy of Antiviral Drugs against Feline Immunodeficiency Virus.* Veterinary sciences, 2015. **2**(4): p. 456-476.
26. Hartmann, K., *Efficacy of antiviral chemotherapy for retrovirus-infected cats: What does the current literature tell us?* J Feline Med Surg, 2015. **17**(11): p. 925-39.
27. Power, C., *Neurologic disease in feline immunodeficiency virus infection: disease mechanisms and therapeutic interventions for NeuroAIDS.* J Neurovirol, 2018. **24**(2): p. 220-228.
28. Beebe, A.M., et al., *Evaluation of in vivo and in vitro interactions of feline immunodeficiency virus and feline leukemia virus.* Aids, 1994. **8**(7): p. 873-8.
29. Medinas, R.J., D.M. Lambert, and W.A. Tompkins, *C-Terminal gp40 peptide analogs inhibit feline immunodeficiency virus: cell fusion and virus spread.* J Virol, 2002. **76**(18): p. 9079-86.
30. Reubel, G.H., et al., *Effects of incidental infections and immune activation on disease progression in experimentally feline immunodeficiency virus-infected cats.* J Acquir Immune Defic Syndr (1988), 1994. **7**(10): p. 1003-15.
31. Pedersen, N.C., et al., *Feline immunodeficiency virus infection.* Vet Immunol Immunopathol, 1989. **21**(1): p. 111-29.
32. Hartmann, K., *Clinical aspects of feline immunodeficiency and feline leukemia virus infection.* Vet Immunol Immunopathol, 2011. **143**(3-4): p. 190-201.
33. Gottlieb, M.S., et al., *Pneumocystis carinii pneumonia and mucosal candidiasis in previously healthy homosexual men: evidence of a new acquired cellular immunodeficiency.* N Engl J Med, 1981. **305**(24): p. 1425-31.
34. Palella, F.J., Jr., et al., *Declining morbidity and mortality among patients with advanced human immunodeficiency virus infection. HIV Outpatient Study Investigators.* N Engl J Med, 1998. **338**(13): p. 853-60.
35. De Clercq, E., *Anti-HIV drugs: 25 compounds approved within 25 years after the discovery of HIV.* Int J Antimicrob Agents, 2009. **33**(4): p. 307-20.
36. Paton, N.I., et al., *Nucleoside reverse-transcriptase inhibitor cross-resistance and outcomes from second-line antiretroviral therapy in the public health approach: an observational analysis within the randomised, open-label, EARNEST trial.* The Lancet HIV, 2017. **4**(8): p. e341-e348.
37. Kline, E.R., et al., *Long-term exposure to AZT, but not d4T, increases endothelial cell oxidative stress and mitochondrial dysfunction.* Cardiovasc Toxicol, 2009. **9**(1): p. 1-12.

38. Flexner, C., *HIV drug development: the next 25 years.* Nat Rev Drug Discov, 2007. **6**(12): p. 959-66.
39. Spence, R.A., et al., *Mechanism of inhibition of HIV-1 reverse transcriptase by nonnucleoside inhibitors.* Science, 1995. **267**(5200): p. 988-93.
40. Ena, J., et al., *Pharmacological and clinical evidence of nevirapine immediate- and extended-release formulations.* HIV AIDS (Auckl), 2012. **4**: p. 169-79.
41. Costa, B. and N. Vale *Efavirenz: History, Development and Future*. Biomolecules, 2023. **13**, DOI: 10.3390/biom13010088.
42. Minuto, J.J. and R. Haubrich, *Etravirine: a second-generation NNRTI for treatment-experienced adults with resistant HIV-1 infection.* Futur HIV Ther, 2008. **2**(6): p. 525-537.
43. Schafer, J.J. and W.R. Short, *Rilpivirine, a novel non-nucleoside reverse transcriptase inhibitor for the management of HIV-1 infection: a systematic review.* Antivir Ther, 2012. **17**(8): p. 1495-502.
44. Flexner, C., *HIV-protease inhibitors.* N Engl J Med, 1998. **338**(18): p. 1281-92.
45. Cahn, P., et al., *Dolutegravir versus raltegravir in antiretroviral-experienced, integrase-inhibitor-naive adults with HIV: week 48 results from the randomised, double-blind, non-inferiority SAILING study.* Lancet, 2013. **382**(9893): p. 700-8.
46. Dorr, P., et al., *Maraviroc (UK-427,857), a potent, orally bioavailable, and selective small-molecule inhibitor of chemokine receptor CCR5 with broad-spectrum anti-human immunodeficiency virus type 1 activity.* Antimicrob Agents Chemother, 2005. **49**(11): p. 4721-32.
47. Bangsberg, D.R., D.L. Kroetz, and S.G. Deeks, *Adherence-resistance relationships to combination HIV antiretroviral therapy.* Curr HIV/AIDS Rep, 2007. **4**(2): p. 65-72.
48. Hartmann, K., A. Wooding, and M. Bergmann, *Efficacy of Antiviral Drugs against Feline Immunodeficiency Virus.* Vet Sci, 2015. **2**(4): p. 456-476.
49. Scarsi, K.K., et al., *HIV-1 Integrase Inhibitors: A Comparative Review of Efficacy and Safety.* Drugs, 2020. **80**(16): p. 1649-1676.
50. Szymański, P., M. Markowicz, and E. Mikiciuk-Olasik, *Adaptation of high-throughput screening in drug discovery-toxicological screening tests.* Int J Mol Sci, 2012. **13**(1): p. 427-52.
51. Murray, C.W. and D.C. Rees, *The rise of fragment-based drug discovery.* Nat Chem, 2009. **1**(3): p. 187-92.
52. Meng, X.Y., et al., *Molecular docking: a powerful approach for structure-based drug discovery.* Curr Comput Aided Drug Des, 2011. **7**(2): p. 146-57.
53. Kozakov, D., et al., *PIPER: an FFT-based protein docking program with pairwise potentials.* Proteins, 2006. **65**(2): p. 392-406.
54. Ghosh, A.K., et al., *Design of HIV Protease Inhibitors Targeting Protein Backbone: An Effective Strategy for Combating Drug Resistance.* Accounts of Chemical Research, 2008. **41**(1): p. 78-86.
55. Trott, O. and A.J. Olson, *AutoDock Vina: improving the speed and accuracy of docking with a new scoring function, efficient optimization, and multithreading.* J Comput Chem, 2010. **31**(2): p. 455-61.
56. Verdonk, M.L., et al., *Improved protein-ligand docking using GOLD.* Proteins, 2003. **52**(4): p. 609-23.
57. Neese, F., et al., *Chemistry and Quantum Mechanics in 2019: Give Us Insight and Numbers.* Journal of the American Chemical Society, 2019. **141**(7): p. 2814-2824.

58. Ryde, U. and P. Söderhjelm, *Ligand-Binding Affinity Estimates Supported by Quantum-Mechanical Methods.* Chemical Reviews, 2016. **116**(9): p. 5520-5566.
59. Sinnokrot, M.O., E.F. Valeev, and C.D. Sherrill, *Estimates of the ab initio limit for pi-pi interactions: the benzene dimer.* J Am Chem Soc, 2002. **124**(36): p. 10887-93.
60. Sangster, J.M., *Octanol-Water Partition Coefficients: Fundamentals and Physical Chemistry.* European Journal of Medicinal Chemistry, 1997. **11**: p. 842.
61. Landry, M.L. and J.J. Crawford, *LogD Contributions of Substituents Commonly Used in Medicinal Chemistry.* ACS Med Chem Lett, 2020. **11**(1): p. 72-76.
62. Lipinski, C.A., et al., *Experimental and computational approaches to estimate solubility and permeability in drug discovery and development settings.* Adv Drug Deliv Rev, 2001. **46**(1-3): p. 3-26.
63. Amidon, G.L., *Drug Bioavailability: Estimation of Solubility, Permeability, Absorption and Bioavailability Edited by H. van de Waterbeemd, H. Lennemas, and P. Artursson. Wiley-VCH, Weinheim, Germany. 2003. xvii + 579 pp. 18 × 24.5 cm. ISBN 3-527-30438-X. $195.00.* Journal of Medicinal Chemistry, 2004. **47**(7): p. 1868-1868.
64. Liliasari, L., L. Amsad, and A. Wahyudi, *Innovative chemistry education: An alternative course models in the disruption era.* Journal of Physics: Conference Series, 2021. **1731**: p. 012023.
65. Di, L., E.H. Kerns, and G.T. Carter, *Drug-like property concepts in pharmaceutical design.* Curr Pharm Des, 2009. **15**(19): p. 2184-94.
66. Baka, E., J.E.A. Comer, and K. Takács-Novák, *Study of equilibrium solubility measurement by saturation shake-flask method using hydrochlorothiazide as model compound.* Journal of Pharmaceutical and Biomedical Analysis, 2008. **46**(2): p. 335-341.
67. Lipinski, C.A., et al., *Experimental and computational approaches to estimate solubility and permeability in drug discovery and development settings.* Advanced Drug Delivery Reviews, 1997. **23**(1): p. 3-25.
68. Jorgensen, W.L. and E.M. Duffy, *Prediction of drug solubility from structure.* Advanced Drug Delivery Reviews, 2002. **54**(3): p. 355-366.
69. Hancock, B.C. and M. Parks, *What is the true solubility advantage for amorphous pharmaceuticals?* Pharm Res, 2000. **17**(4): p. 397-404.
70. Savjani, K.T., A.K. Gajjar, and J.K. Savjani, *Drug solubility: importance and enhancement techniques.* ISRN Pharm, 2012. **2012**: p. 195727.
71. Frisch, M.J., et al., *Gaussian 16 Rev. C.01*. 2016: Wallingford, CT.
72. Lansdon, E.B., et al., *Crystal Structures of HIV-1 Reverse Transcriptase with Etravirine (TMC125) and Rilpivirine (TMC278): Implications for Drug Design.* Journal of Medicinal Chemistry, 2010. **53**(10): p. 4295-4299.
73. Ha, B., et al., *High-resolution view of HIV-1 reverse transcriptase initiation complexes and inhibition by NNRTI drugs.* Nature Communications, 2021. **12**(1): p. 2500.
74. Esnouf Robert, M., et al., *Unique features in the structure of the complex between HIV-1 reverse transcriptase and the bis(heteroaryl)piperazine (BHAP) U-90152 explain resistance mutations for this nonnucleoside inhibitor.* Proceedings of the National Academy of Sciences, 1997. **94**(8): p. 3984-3989.
75. Ren, J., et al., *Structural mechanisms of drug resistance for mutations at codons 181 and 188 in HIV-1 reverse transcriptase and the improved resilience of second generation non-nucleoside inhibitors11Edited by J. Karn.* Journal of Molecular Biology, 2001. **312**(4): p. 795-805.

76. Frey, K.M., et al., *Crystal Structures of HIV-1 Reverse Transcriptase with Picomolar Inhibitors Reveal Key Interactions for Drug Design.* Journal of the American Chemical Society, 2012. **134**(48): p. 19501-19503.
77. Vainio, M.J., J.S. Puranen, and M.S. Johnson, *ShaEP: Molecular Overlay Based on Shape and Electrostatic Potential.* Journal of Chemical Information and Modeling, 2009. **49**(2): p. 492-502.
78. Schneidman-Duhovny, D., et al., *PharmaGist: a webserver for ligand-based pharmacophore detection.* Nucleic Acids Research, 2008. **36**(suppl_2): p. W223-W228.
79. Schneidman-Duhovny, D., et al., *Deterministic pharmacophore detection via multiple flexible alignment of drug-like molecules.* J Comput Biol, 2008. **15**(7): p. 737-54.
80. *GOLD5.3: https://www.ccdc.cam.ac.uk/solutions/csd-discovery/components/gold/.*
81. Gleeson, M.P. and D. Gleeson, *QM/MM As a Tool in Fragment Based Drug Discovery. A Cross-Docking, Rescoring Study of Kinase Inhibitors.* Journal of Chemical Information and Modeling, 2009. **49**(6): p. 1437-1448.
82. Das, K., et al., *High-resolution structures of HIV-1 reverse transcriptase/TMC278 complexes: Strategic flexibility explains potency against resistance mutations.* Proceedings of the National Academy of Sciences, 2008. **105**(5): p. 1466-1471.
83. Liu, X., et al., *A quantum-mechanical study on the geometry of a hexacyclopeptide dichotomin A.* Journal of Molecular Structure: THEOCHEM, 2007. **818**(1): p. 77-83.
84. Toviwek, B., et al., *Synthesis and evaluation of the NSCLC anti-cancer activity and physical properties of 4-aryl-N-phenylpyrimidin-2-amines.* Bioorganic & Medicinal Chemistry Letters, 2017. **27**(20): p. 4749-4754.
85. Nattakarn, P., et al., *Synthesis, Plasmodium falciparum Inhibitory Activity, Cytotoxicity and Solubility of N2 ,N4 -Disubstituted Quinazoline-2,4-diamines.* Medicinal Chemistry, 2019. **15**(6): p. 693-704.
86. Silprasit, K., et al., *Simple and rapid determination of the enzyme kinetics of HIV-1 reverse transcriptase and anti-HIV-1 agents by a fluorescence based method.* Journal of Virological Methods, 2011. **171**(2): p. 381-387.
87. Seetaha, S., et al., *Novel peptides with HIV-1 reverse transcriptase inhibitory activity derived from the fruits of Quercus infectoria.* Chem Biol Drug Des, 2021. **97**(1): p. 157-166.
88. Seetaha, S., et al., *Anti-feline immunodeficiency virus reverse transcriptase properties of some medicinal and edible mushrooms.* Vet World, 2020. **13**(9): p. 1798-1806.
89. Wenlock, M.C., et al., *A Highly Automated Assay for Determining the Aqueous Equilibrium Solubility of Drug Discovery Compounds.* J. Assoc. Lab. Auto., 2011. **16**(4): p. 276-284.
90. Wenlock, M.C., et al., *A Method for Measuring the Lipophilicity of Compounds in Mixtures of 10.* J. Biomol. Screen., 2011. **16**(3): p. 348-355.
91. Lu, H.-H., et al., *Structural modifications of diarylpyrimidines (DAPYs) as HIV-1 NNRTIs: Synthesis, anti-HIV activities and SAR.* Bioorganic & Medicinal Chemistry, 2017. **25**(8): p. 2491-2497.
92. Gu, S.-X., et al., *A novel family of diarylpyrimidines (DAPYs) featuring a diatomic linker: Design, synthesis and anti-HIV activities.* Bioorganic & Medicinal Chemistry, 2015. **23**(20): p. 6587-6593.
93. Zeng, Z.-S., et al., *Hybrid diarylbenzopyrimidine non-nucleoside reverse transcriptase inhibitors as promising new leads for improved anti-HIV-1 chemotherapy.* Bioorganic & Medicinal Chemistry, 2010. **18**(14): p. 5039-5047.
94. Choengpanya, K., et al., *Anti-HIV-1 reverse transcriptase property of some edible mushrooms in Asia.* Saudi J Biol Sci, 2021. **28**(5): p. 2807-2815.

95. Kang, D., et al., *Further Exploring Solvent-Exposed Tolerant Regions of Allosteric Binding Pocket for Novel HIV-1 NNRTIs Discovery.* ACS Medicinal Chemistry Letters, 2018. **9**(4): p. 370-375.
96. Rudolph, T., et al., *MARVIN: a medical research application framework based on open source software.* Computer Methods and Programs in Biomedicine, 2008. **91**(2): p. 165-174.
97. Wang, Y., et al., *LogD7.4 prediction enhanced by transferring knowledge from chromatographic retention time, microscopic pKa and logP.* Journal of Cheminformatics, 2023. **15**(1): p. 76.
98. kommavarapu, P., et al., *Preparation and characterization of rilpivirine solid dispersions with the application of enhanced solubility and dissolution rate.* Beni-Suef University Journal of Basic and Applied Sciences, 2015. **4**(1): p. 71-79.
99. Srivalli, K.M. and B. Mishra, *Improved Aqueous Solubility and Antihypercholesterolemic Activity of Ezetimibe on Formulating with Hydroxypropyl-β-Cyclodextrin and Hydrophilic Auxiliary Substances.* AAPS PharmSciTech, 2016. **17**(2): p. 272-83.
100. Vyas, M., et al., *SOLUBILITY ENHANCEMENT OF EFAVIRENZ (BCS CLASS II DRUG) BY CYCLODEXTRIN INCLUSION COMPLEX TECHNIQUE.* Journal of Drug Delivery and Therapeutics, 2017. **7**: p. 41-43.
101. Wang, R., et al., *Solubility determination and thermodynamic model analysis of nevirapine in different organic solvents from 278.15 K to 328.15 K.* Journal of Molecular Liquids, 2022. **365**: p. 120173.
102. Thammajong, P., et al., *Comparison of feline and human immunodeficiency virus reverse transcriptase enzymes through chemical screening and computational analysis.* Chem Biol Drug Des, 2024. **103**(5): p. e14530.

1. Long, M., et al., *Identification of a Potential Inhibitor of the FIV p24 Capsid Protein and Characterization of Its Binding Site.* Biochemistry, 2021. **60**(24): p. 1896-1908.
2. Medeiros Sde, O., et al., *Follow-up on long-term antiretroviral therapy for cats infected with feline immunodeficiency virus.* J Feline Med Surg, 2016. **18**(4): p. 264-72.
3. Saparpakorn, P., et al., *Insight investigation of rilpivirine and compounds from mushrooms as feline immunodeficiency virus reverse transcriptase inhibitors using molecular dynamics simulations and quantum chemical calculations.* Molecular Simulation, 2022. **48**(6): p. 463-476.
4. Brown, M.A., et al., *Feline immunodeficiency virus (FIV) in wild Pallas' cats.* Veterinary Immunology and Immunopathology, 2010. **134**(1): p. 90-95.
5. Bendinelli, M., et al., *Feline immunodeficiency virus: an interesting model for AIDS studies and an important cat pathogen.* Clin Microbiol Rev, 1995. **8**(1): p. 87-112.
6. Pedersen, N.C., et al., *Isolation of a T-lymphotropic virus from domestic cats with an immunodeficiency-like syndrome.* Science, 1987. **235**(4790): p. 790-3.
7. Sparger, E.E., *FIV as a Model for HIV: An Overview.* In vivo Models of HIV Disease and Control, 2006: p. 149-237.
8. De Clercq, E., *Antiviral therapy for human immunodeficiency virus infections.* Clin Microbiol Rev, 1995. **8**(2): p. 200-39.
9. Das, K. and E. Arnold, *HIV-1 reverse transcriptase and antiviral drug resistance. Part 1.* Curr Opin Virol, 2013. **3**(2): p. 111-8.
10. Galilee, M. and A. Alian, *The structure of FIV reverse transcriptase and its implications for non-nucleoside inhibitor resistance.* PLOS Pathogens, 2018. **14**(1): p. e1006849.
11. Amacker, M., M. Hottiger, and U. Hübscher, *Feline immunodeficiency virus reverse transcriptase: expression, functional characterization, and reconstitution of the 66- and 51-kilodalton subunits.* J Virol, 1995. **69**(10): p. 6273-9.
12. Kenyon, J.C. and A.M. Lever, *The molecular biology of feline immunodeficiency virus (FIV).* Viruses, 2011. **3**(11): p. 2192-213.
13. Schwartz, A.M., et al., *Antiviral efficacy of nine nucleoside reverse transcriptase inhibitors against feline immunodeficiency virus in feline peripheral blood mononuclear cells.* Am J Vet Res, 2014. **75**(3): p. 273-81.
14. Savarino, A., et al., *Human immunodeficiency virus integrase inhibitors efficiently suppress feline immunodeficiency virus replication in vitroand provide a rationale to redesign antiretroviral treatment for feline AIDS.* Retrovirology, 2007. **4**(1): p. 79.
15. Bisset, L.R., et al., *Combined effect of zidovudine (ZDV), lamivudine (3TC) and abacavir (ABC) antiretroviral therapy in suppressing in vitro FIV replication.* Antiviral Res, 2002. **53**(1): p. 35-45.
16. Nolan, D. and S. Mallal, *Complications associated with NRTI therapy: update on clinical features and possible pathogenic mechanisms.* Antivir Ther, 2004. **9**(6): p. 849-63.
17. Usach, I., V. Melis, and J.E. Peris, *Non-nucleoside reverse transcriptase inhibitors: a review on pharmacokinetics, pharmacodynamics, safety and tolerability.* J Int AIDS Soc, 2013. **16**(1): p. 1-14.
18. Auwerx, J., et al., *Susceptibility of feline immunodeficiency virus/human immunodeficiency virus type 1 reverse transcriptase chimeras to non-nucleoside RT inhibitors.* Mol Pharmacol, 2004. **65**(1): p. 244-51.
19. Sluis-Cremer, N. and G. Tachedjian, *Mechanisms of inhibition of HIV replication by non-nucleoside reverse transcriptase inhibitors.* Virus Res, 2008. **134**(1-2): p. 147-56.

20. Xu, S., et al., *Opportunities and challenges in new HIV therapeutic discovery: what is the next step?* Expert Opinion on Drug Discovery, 2023. **18**(11): p. 1195-1199.
21. Zuo, X., et al., *Current insights into anti-HIV drug discovery and development: a review of recent patent literature (2014–2017).* Expert Opinion on Therapeutic Patents, 2018. **28**(4): p. 299-316.
22. Kang, D., et al., *Structure-Based Bioisosterism Yields HIV-1 NNRTIs with Improved Drug-Resistance Profiles and Favorable Pharmacokinetic Properties.* Journal of Medicinal Chemistry, 2020. **63**(9): p. 4837-4848.
23. Hsiou, Y., et al., *The Lys103Asn mutation of HIV-1 RT: a novel mechanism of drug resistance.* J Mol Biol, 2001. **309**(2): p. 437-45.
24. Boyer, P.L., et al., *Analysis of nonnucleoside drug-resistant variants of human immunodeficiency virus type 1 reverse transcriptase.* J Virol, 1993. **67**(4): p. 2412-20.
25. Hartmann, K., A. Wooding, and M. Bergmann, *Efficacy of Antiviral Drugs against Feline Immunodeficiency Virus.* Veterinary sciences, 2015. **2**(4): p. 456-476.
26. Hartmann, K., *Efficacy of antiviral chemotherapy for retrovirus-infected cats: What does the current literature tell us?* J Feline Med Surg, 2015. **17**(11): p. 925-39.
27. Power, C., *Neurologic disease in feline immunodeficiency virus infection: disease mechanisms and therapeutic interventions for NeuroAIDS.* J Neurovirol, 2018. **24**(2): p. 220-228.
28. Beebe, A.M., et al., *Evaluation of in vivo and in vitro interactions of feline immunodeficiency virus and feline leukemia virus.* Aids, 1994. **8**(7): p. 873-8.
29. Medinas, R.J., D.M. Lambert, and W.A. Tompkins, *C-Terminal gp40 peptide analogs inhibit feline immunodeficiency virus: cell fusion and virus spread.* J Virol, 2002. **76**(18): p. 9079-86.
30. Reubel, G.H., et al., *Effects of incidental infections and immune activation on disease progression in experimentally feline immunodeficiency virus-infected cats.* J Acquir Immune Defic Syndr (1988), 1994. **7**(10): p. 1003-15.
31. Pedersen, N.C., et al., *Feline immunodeficiency virus infection.* Vet Immunol Immunopathol, 1989. **21**(1): p. 111-29.
32. Hartmann, K., *Clinical aspects of feline immunodeficiency and feline leukemia virus infection.* Vet Immunol Immunopathol, 2011. **143**(3-4): p. 190-201.
33. Gottlieb, M.S., et al., *Pneumocystis carinii pneumonia and mucosal candidiasis in previously healthy homosexual men: evidence of a new acquired cellular immunodeficiency.* N Engl J Med, 1981. **305**(24): p. 1425-31.
34. Palella, F.J., Jr., et al., *Declining morbidity and mortality among patients with advanced human immunodeficiency virus infection. HIV Outpatient Study Investigators.* N Engl J Med, 1998. **338**(13): p. 853-60.
35. De Clercq, E., *Anti-HIV drugs: 25 compounds approved within 25 years after the discovery of HIV.* Int J Antimicrob Agents, 2009. **33**(4): p. 307-20.
36. Paton, N.I., et al., *Nucleoside reverse-transcriptase inhibitor cross-resistance and outcomes from second-line antiretroviral therapy in the public health approach: an observational analysis within the randomised, open-label, EARNEST trial.* The Lancet HIV, 2017. **4**(8): p. e341-e348.
37. Kline, E.R., et al., *Long-term exposure to AZT, but not d4T, increases endothelial cell oxidative stress and mitochondrial dysfunction.* Cardiovasc Toxicol, 2009. **9**(1): p. 1-12.
38. Flexner, C., *HIV drug development: the next 25 years.* Nat Rev Drug Discov, 2007. **6**(12): p. 959-66.

39. Spence, R.A., et al., *Mechanism of inhibition of HIV-1 reverse transcriptase by nonnucleoside inhibitors.* Science, 1995. **267**(5200): p. 988-93.
40. Ena, J., et al., *Pharmacological and clinical evidence of nevirapine immediate- and extended-release formulations.* HIV AIDS (Auckl), 2012. **4**: p. 169-79.
41. Costa, B. and N. Vale *Efavirenz: History, Development and Future*. Biomolecules, 2023. **13**, DOI: 10.3390/biom13010088.
42. Minuto, J.J. and R. Haubrich, *Etravirine: a second-generation NNRTI for treatment-experienced adults with resistant HIV-1 infection.* Futur HIV Ther, 2008. **2**(6): p. 525-537.
43. Schafer, J.J. and W.R. Short, *Rilpivirine, a novel non-nucleoside reverse transcriptase inhibitor for the management of HIV-1 infection: a systematic review.* Antivir Ther, 2012. **17**(8): p. 1495-502.
44. Flexner, C., *HIV-protease inhibitors.* N Engl J Med, 1998. **338**(18): p. 1281-92.
45. Cahn, P., et al., *Dolutegravir versus raltegravir in antiretroviral-experienced, integrase-inhibitor-naive adults with HIV: week 48 results from the randomised, double-blind, non-inferiority SAILING study.* Lancet, 2013. **382**(9893): p. 700-8.
46. Dorr, P., et al., *Maraviroc (UK-427,857), a potent, orally bioavailable, and selective small-molecule inhibitor of chemokine receptor CCR5 with broad-spectrum anti-human immunodeficiency virus type 1 activity.* Antimicrob Agents Chemother, 2005. **49**(11): p. 4721-32.
47. Bangsberg, D.R., D.L. Kroetz, and S.G. Deeks, *Adherence-resistance relationships to combination HIV antiretroviral therapy.* Curr HIV/AIDS Rep, 2007. **4**(2): p. 65-72.
48. Hartmann, K., A. Wooding, and M. Bergmann, *Efficacy of Antiviral Drugs against Feline Immunodeficiency Virus.* Vet Sci, 2015. **2**(4): p. 456-476.
49. Scarsi, K.K., et al., *HIV-1 Integrase Inhibitors: A Comparative Review of Efficacy and Safety.* Drugs, 2020. **80**(16): p. 1649-1676.
50. Szymański, P., M. Markowicz, and E. Mikiciuk-Olasik, *Adaptation of high-throughput screening in drug discovery-toxicological screening tests.* Int J Mol Sci, 2012. **13**(1): p. 427-52.
51. Murray, C.W. and D.C. Rees, *The rise of fragment-based drug discovery.* Nat Chem, 2009. **1**(3): p. 187-92.
52. Meng, X.Y., et al., *Molecular docking: a powerful approach for structure-based drug discovery.* Curr Comput Aided Drug Des, 2011. **7**(2): p. 146-57.
53. Kozakov, D., et al., *PIPER: an FFT-based protein docking program with pairwise potentials.* Proteins, 2006. **65**(2): p. 392-406.
54. Ghosh, A.K., et al., *Design of HIV Protease Inhibitors Targeting Protein Backbone: An Effective Strategy for Combating Drug Resistance.* Accounts of Chemical Research, 2008. **41**(1): p. 78-86.
55. Trott, O. and A.J. Olson, *AutoDock Vina: improving the speed and accuracy of docking with a new scoring function, efficient optimization, and multithreading.* J Comput Chem, 2010. **31**(2): p. 455-61.
56. Verdonk, M.L., et al., *Improved protein-ligand docking using GOLD.* Proteins, 2003. **52**(4): p. 609-23.
57. Neese, F., et al., *Chemistry and Quantum Mechanics in 2019: Give Us Insight and Numbers.* Journal of the American Chemical Society, 2019. **141**(7): p. 2814-2824.
58. Ryde, U. and P. Söderhjelm, *Ligand-Binding Affinity Estimates Supported by Quantum-Mechanical Methods.* Chemical Reviews, 2016. **116**(9): p. 5520-5566.

59. Sinnokrot, M.O., E.F. Valeev, and C.D. Sherrill, *Estimates of the ab initio limit for pi-pi interactions: the benzene dimer.* J Am Chem Soc, 2002. **124**(36): p. 10887-93.
60. Sangster, J.M., *Octanol-Water Partition Coefficients: Fundamentals and Physical Chemistry.* European Journal of Medicinal Chemistry, 1997. **11**: p. 842.
61. Landry, M.L. and J.J. Crawford, *LogD Contributions of Substituents Commonly Used in Medicinal Chemistry.* ACS Med Chem Lett, 2020. **11**(1): p. 72-76.
62. Lipinski, C.A., et al., *Experimental and computational approaches to estimate solubility and permeability in drug discovery and development settings.* Adv Drug Deliv Rev, 2001. **46**(1-3): p. 3-26.
63. Amidon, G.L., *Drug Bioavailability: Estimation of Solubility, Permeability, Absorption and Bioavailability Edited by H. van de Waterbeemd, H. Lennemas, and P. Artursson. Wiley-VCH, Weinheim, Germany. 2003. xvii + 579 pp. 18 × 24.5 cm. ISBN 3-527-30438-X. $195.00.* Journal of Medicinal Chemistry, 2004. **47**(7): p. 1868-1868.
64. Di, L., E.H. Kerns, and G.T. Carter, *Drug-like property concepts in pharmaceutical design.* Curr Pharm Des, 2009. **15**(19): p. 2184-94.
65. Baka, E., J.E.A. Comer, and K. Takács-Novák, *Study of equilibrium solubility measurement by saturation shake-flask method using hydrochlorothiazide as model compound.* Journal of Pharmaceutical and Biomedical Analysis, 2008. **46**(2): p. 335-341.
66. Lipinski, C.A., et al., *Experimental and computational approaches to estimate solubility and permeability in drug discovery and development settings.* Advanced Drug Delivery Reviews, 1997. **23**(1): p. 3-25.
67. Jorgensen, W.L. and E.M. Duffy, *Prediction of drug solubility from structure.* Advanced Drug Delivery Reviews, 2002. **54**(3): p. 355-366.
68. Hancock, B.C. and M. Parks, *What is the true solubility advantage for amorphous pharmaceuticals?* Pharm Res, 2000. **17**(4): p. 397-404.
69. Savjani, K.T., A.K. Gajjar, and J.K. Savjani, *Drug solubility: importance and enhancement techniques.* ISRN Pharm, 2012. **2012**: p. 195727.
70. Frisch, M.J., et al., *Gaussian 16 Rev. C.01*. 2016: Wallingford, CT.
71. Lansdon, E.B., et al., *Crystal Structures of HIV-1 Reverse Transcriptase with Etravirine (TMC125) and Rilpivirine (TMC278): Implications for Drug Design.* Journal of Medicinal Chemistry, 2010. **53**(10): p. 4295-4299.
72. Ha, B., et al., *High-resolution view of HIV-1 reverse transcriptase initiation complexes and inhibition by NNRTI drugs.* Nature Communications, 2021. **12**(1): p. 2500.
73. Esnouf Robert, M., et al., *Unique features in the structure of the complex between HIV-1 reverse transcriptase and the bis(heteroaryl)piperazine (BHAP) U-90152 explain resistance mutations for this nonnucleoside inhibitor.* Proceedings of the National Academy of Sciences, 1997. **94**(8): p. 3984-3989.
74. Ren, J., et al., *Structural mechanisms of drug resistance for mutations at codons 181 and 188 in HIV-1 reverse transcriptase and the improved resilience of second generation non-nucleoside inhibitors11Edited by J. Karn.* Journal of Molecular Biology, 2001. **312**(4): p. 795-805.
75. Frey, K.M., et al., *Crystal Structures of HIV-1 Reverse Transcriptase with Picomolar Inhibitors Reveal Key Interactions for Drug Design.* Journal of the American Chemical Society, 2012. **134**(48): p. 19501-19503.
76. Vainio, M.J., J.S. Puranen, and M.S. Johnson, *ShaEP: Molecular Overlay Based on Shape and Electrostatic Potential.* Journal of Chemical Information and Modeling, 2009. **49**(2): p. 492-502.

77. Schneidman-Duhovny, D., et al., *PharmaGist: a webserver for ligand-based pharmacophore detection.* Nucleic Acids Research, 2008. **36**(suppl_2): p. W223-W228.
78. Schneidman-Duhovny, D., et al., *Deterministic pharmacophore detection via multiple flexible alignment of drug-like molecules.* J Comput Biol, 2008. **15**(7): p. 737-54.
79. *GOLD5.3: https://www.ccdc.cam.ac.uk/solutions/csd-discovery/components/gold/.*
80. Gleeson, M.P. and D. Gleeson, *QM/MM As a Tool in Fragment Based Drug Discovery. A Cross-Docking, Rescoring Study of Kinase Inhibitors.* Journal of Chemical Information and Modeling, 2009. **49**(6): p. 1437-1448.
81. Das, K., et al., *High-resolution structures of HIV-1 reverse transcriptase/TMC278 complexes: Strategic flexibility explains potency against resistance mutations.* Proceedings of the National Academy of Sciences, 2008. **105**(5): p. 1466-1471.
82. Liu, X., et al., *A quantum-mechanical study on the geometry of a hexacyclopeptide dichotomin A.* Journal of Molecular Structure: THEOCHEM, 2007. **818**(1): p. 77-83.
83. Toviwek, B., et al., *Synthesis and evaluation of the NSCLC anti-cancer activity and physical properties of 4-aryl-N-phenylpyrimidin-2-amines.* Bioorganic & Medicinal Chemistry Letters, 2017. **27**(20): p. 4749-4754.
84. Nattakarn, P., et al., *Synthesis, Plasmodium falciparum Inhibitory Activity, Cytotoxicity and Solubility of N2 ,N4 -Disubstituted Quinazoline-2,4-diamines.* Medicinal Chemistry, 2019. **15**(6): p. 693-704.
85. Silprasit, K., et al., *Simple and rapid determination of the enzyme kinetics of HIV-1 reverse transcriptase and anti-HIV-1 agents by a fluorescence based method.* Journal of Virological Methods, 2011. **171**(2): p. 381-387.
86. Seetaha, S., et al., *Novel peptides with HIV-1 reverse transcriptase inhibitory activity derived from the fruits of Quercus infectoria.* Chem Biol Drug Des, 2021. **97**(1): p. 157-166.
87. Seetaha, S., et al., *Anti-feline immunodeficiency virus reverse transcriptase properties of some medicinal and edible mushrooms.* Vet World, 2020. **13**(9): p. 1798-1806.
88. Wenlock, M.C., et al., *A Highly Automated Assay for Determining the Aqueous Equilibrium Solubility of Drug Discovery Compounds.* J. Assoc. Lab. Auto., 2011. **16**(4): p. 276-284.
89. Wenlock, M.C., et al., *A Method for Measuring the Lipophilicity of Compounds in Mixtures of 10.* J. Biomol. Screen., 2011. **16**(3): p. 348-355.
90. Lu, H.-H., et al., *Structural modifications of diarylpyrimidines (DAPYs) as HIV-1 NNRTIs: Synthesis, anti-HIV activities and SAR.* Bioorganic & Medicinal Chemistry, 2017. **25**(8): p. 2491-2497.
91. Gu, S.-X., et al., *A novel family of diarylpyrimidines (DAPYs) featuring a diatomic linker: Design, synthesis and anti-HIV activities.* Bioorganic & Medicinal Chemistry, 2015. **23**(20): p. 6587-6593.
92. Zeng, Z.-S., et al., *Hybrid diarylbenzopyrimidine non-nucleoside reverse transcriptase inhibitors as promising new leads for improved anti-HIV-1 chemotherapy.* Bioorganic & Medicinal Chemistry, 2010. **18**(14): p. 5039-5047.
93. Choengpanya, K., et al., *Anti-HIV-1 reverse transcriptase property of some edible mushrooms in Asia.* Saudi J Biol Sci, 2021. **28**(5): p. 2807-2815.
94. Kang, D., et al., *Further Exploring Solvent-Exposed Tolerant Regions of Allosteric Binding Pocket for Novel HIV-1 NNRTIs Discovery.* ACS Medicinal Chemistry Letters, 2018. **9**(4): p. 370-375.
95. Rudolph, T., et al., *MARVIN: a medical research application framework based on open source software.* Computer Methods and Programs in Biomedicine, 2008. **91**(2): p. 165-174.

96. Wang, Y., et al., *LogD7.4 prediction enhanced by transferring knowledge from chromatographic retention time, microscopic pKa and logP.* Journal of Cheminformatics, 2023. **15**(1): p. 76.

97. kommavarapu, P., et al., *Preparation and characterization of rilpivirine solid dispersions with the application of enhanced solubility and dissolution rate.* Beni-Suef University Journal of Basic and Applied Sciences, 2015. **4**(1): p. 71-79.

98. Srivalli, K.M. and B. Mishra, *Improved Aqueous Solubility and Antihypercholesterolemic Activity of Ezetimibe on Formulating with Hydroxypropyl-β-Cyclodextrin and Hydrophilic Auxiliary Substances.* AAPS PharmSciTech, 2016. **17**(2): p. 272-83.

99. Vyas, M., et al., *SOLUBILITY ENHANCEMENT OF EFAVIRENZ (BCS CLASS II DRUG) BY CYCLODEXTRIN INCLUSION COMPLEX TECHNIQUE.* Journal of Drug Delivery and Therapeutics, 2017. **7**: p. 41-43.

100. Wang, R., et al., *Solubility determination and thermodynamic model analysis of nevirapine in different organic solvents from 278.15 K to 328.15 K.* Journal of Molecular Liquids, 2022. **365**: p. 120173.

101. Thammajong, P., et al., *Comparison of feline and human immunodeficiency virus reverse transcriptase enzymes through chemical screening and computational analysis.* Chem Biol Drug Des, 2024. **103**(5): p. e14530.

Appendix A

Study 1: Chemical Characterization Data & Spectra for compound 1-6

Chemical Characterization Data

4-[(2-chloropyrimidin-4-yl)oxy]-3,5-dimethylbenzonitrile (I1)

A mixture of 2,4-dichloropyrimidine (6.71 mmol) and 4-hydroxy-3,5-dimethyl benzonitrile (3.40 mmol) were dissolved in DMF (5 mL) and K_2CO_3 (4.07 mmol) were added. The reaction mixture was refluxed at room temperature for 8 h. The precipitate was filtered, washed with ethanol or the resultant was evaporated under vacuum and extracted with ethyl acetate. The organic layers were combined, washed with a brine, dried over anhydrous Na_2SO_4, and concentrated in vacuo. The crude mixture required additional purification via column chromatography. The resultant solid was collected to give 4-[(2-chloropyrimidin-4-yl) oxy]-3,5-dimethylbenzonitrile as white solid, 751 mg, 85% yield. ^{1}H NMR (400 MHz, DMSO-d_6) δ 8.65 (d, J = 4.6 Hz), 7.70 (s), 7.27 (d, J = 4.6 Hz), 2.05 (s).MS-ESI: m/z $C_{13}H_{10}ClN_3O$ $[M+H]^+$calculated 260.1 found 260.0.

2-chloro-N-(4-methylphenyl)pyrimidin-4-amine (I2)

A mixture of p-toluidine (0.93 mmol) and, 2,4-dichloropyrimidine (0.93 mmol) were dissolved in 1-butanol (3 mL) and DIPEA (4.65 mmol) were added. The reaction mixture was stirred at 110°C for 6 hr. The reaction mixture was cooled down to room temperature. The precipitate was filtered and washed with ethanol. The resultant solid was collected to give 2-chloro-*N*-(4-methylphenyl)pyrimidin-4-amine as a white solid 93 mg, 45% yield. ^{1}H NMR (400 MHz, DMSO-d_6) δ 9.92 (s, 1H), 8.12 (d, J = 5.9 Hz, 1H), 7.51 (dd, J = 52.6, 8.2 Hz, 2H), 7.15 (dd, J = 26.5, 8.1 Hz, 2H), 6.70 (d, J = 5.9 Hz, 1H), 2.36 – 2.22 (m, 3H). MS-ESI: m/z $C_{11}H_{10}ClN_3$ $[M+H]^+$calculated 220.1 found 220.6.

4-([2-(4-cyanoanilino)pyrimidin-4-yl]oxy)-3,5-dimethylbenzonitrile (1)

To a solution of 4-[(2-chloropyrimidin-4-yl)oxy]-3,5-dimethylbenzonitrile (**I1**) (0.39

mmol) in anhydrous toluene (4 mL), 4-aminobenzonitrile (0.78 mmol), Na_2CO_3 (0.77 mmol), xantphos (0.04 mmol) and $Pd_2(dba)_3$ (0.12 mmol) were added. The reaction mixture was stirred at 160°C for 6 h. The reaction mixture was concentrated in vacuo and redissolved in ethyl acetate, washed with brine. The organic layer was collected and dried over Na_2SO_4, filtered, and crude mixture required additional purification via column chromatography to give the desired product, 35 mg, 26% yield as a light yellow solid, mp = 260°C. ^{1}H NMR (400 MHz, DMSO-d$_6$) δ 10.16 (s, 1H), 8.50 (d, J = 5.6 Hz, 1H), 7.78 (s, 2H), 7.53 (dd, J = 22.0, 8.8 Hz, 4H), 6.72 (d, J = 5.6 Hz, 1H), 2.12 (s, 6H). ^{13}C NMR (300 MHz, DMSO-d_6) δ 168.41, 161.22, 159.57, 153.85, 144.96, 133.26, 133.15, 119.12, 118.72, 109.12, 103.16, 99.53, 31.82, 31.24, 29.55, 16.32. HPLC-UV retention time = 3.742 min. HRMS-ESI: m/z $C_{20}H_{15}N_5NaO$ [M+Na]$^+$ calculated 364.1169 found 364.1176.

4-([2-(morpholin-4-yl) ethoxyanilino]pyrimidin-4-yl)oxy-3,5-dimethylbenzonitrile (2)

To a solution of 4-[(2-chloropyrimidin-4-yl)oxy]-3,5-dimethylbenzonitrile (**I1**) (0.39 mmol) in *i*-PrOH (5 mL), 4-[2-(morpholin-4-yl)ethoxy]aniline (0.46 mmol) and TFA (500 µL) were added. The reaction mixture was stirred at 90°C overnight. The reaction mixture was extracted with ethyl acetate. The organic layer was collected, washed with brine, dried over anhydrous Na_2SO_4, filtered, and crude mixture required additional purification via column chromatography to give the desired product, 109 mg, 63% yield as a beigesolid, mp = 196 °C. ^{1}H NMR (400 MHz, DMSO-d_6) δ 9.44 (s, 1H), 8.36 (d, J = 5.5 Hz, 1H), 7.75 (s, 2H), 7.21 (s, 2H), 6.64 (d, J = 7.9 Hz, 2H), 6.50 (d, J = 5.5 Hz, 1H), 3.99 (t, J = 5.7 Hz, 2H), 3.61 – 3.54 (m, 4H), 2.65 (t, J = 5.7 Hz, 2H), 2.11 (s, 6H), 2.09 (s, 4H). ^{13}C NMR (300 MHz, DMSO-d_6) δ 168.36, 161.02, 160.15, 158.80, 158.56, 154.08, 152.82, 134.54, 133.30, 133.10, 120.50, 119.21, 118.89, 116.51, 114.87, 108.84, 97.41, 63.87, 62.73, 55.70, 52.24, 19.09, 16.35.HPLC-UV retention time = 2.368 min. HRMS-ESI: m/z $C_{25}H_{27}N_5NaO_3$ [M+Na]$^+$ calculated 468.2006 found 468.2022.

4-[(2-([(4-methoxyphenyl)methyl]amino}pyrimidin-4-yl)oxy]-3,5-dimethylbenzonitrile (3)

To a solution of 4-[(2-chloropyrimidin-4-yl)oxy]-3,5-dimethylbenzonitrile (**I1**) (0.39 mmol) in NMP (5 ml), 1-(4-methoxyphenyl)methanamine (0.46 mmol) and TEA (0.77 mmol) were added. The reaction mixture was stirred at 80°C for 18 h. The reaction mixture was extracted with ethyl acetate. The organic layer was collected, washed with brine, dried over Na_2SO_4, filtered, and crude mixture required additional purification via column chromatography to give the desired product, 86 mg, 61% yield as a light yellow solid, mp = 134 °C. ^{1}H NMR (400 MHz, DMSO-d_6) δ 8.18 (d, J = 4.7 Hz, 1H), 7.70 (s, 2H), 6.26 (d, J = 5.5 Hz, 1H), 3.87 (s, 1H), 3.72 (s, 3H), 2.09 (s, 12H). ^{13}C NMR (300 MHz, DMSO-d_6) δ 168.33, 162.65, 161.01, 158.52, 153.95, 133.31, 132.86, 129.18, 119.24, 113.79, 108.61, 95.21, 55.54, 43.94, 16.27. HPLC-UV retention time = 2.902 min. HRMS-ESI: m/z $C_{21}H_{20}N_4NaO_2$ $[M+Na]^+$ calculated 383.1478 found 383.1491.

N^2-[(4-bromophenyl)methyl]-N^4-(4-methylphenyl) pyrimidine-2,4-diamine (4)

To a solution of 2-chloro-*N*-(4-methylphenyl)pyrimidin-4-amine (**I2**) (0.39 mmol) in NMP (5 mL), 1-(4 bromophenyl)methanamine (0.46 mmol) and TEA (0.77 mmol) were added. The reaction mixture was stirred at 80°C for 18 h. The reaction mixture was extracted with ethyl acetate. The organic layer was collected, washed with brine, dried over Na_2SO_4, filtered, and crude mixture required additional purification via column chromatography to give the desired product, 20 mg, 14% yield as an orange solid, mp = 72 °C. ^{1}H NMR (400 MHz, DMSO-d_6) δ 10.00 (s, 1H), 8.50 (s, 3H), 7.85 (d, J = 1.6 Hz, 2H), 7.74 (d, J = 8.6 Hz, 6H), 7.67 (d, J = 8.5 Hz, 6H), 7.54 (d, J = 8.4 Hz, 6H), 7.31 (d, J = 8.4 Hz, 6H), 4.75 (s, 6H), 1.24 (s, 9H). ^{13}C NMR (300 MHz, DMSO-d_6) δ 161.79, 139.45, 135.63, 132.86, 132.30, 132.23, 131.78, 130.61, 130.40, 124.87, 120.43, 63.44. HPLC-UV retention time = 3.265 min. MS-ESI: m/z 369.2 $[M+H]^+$. HRMS-ESI: m/z $C_{18}H_{18}BrN_4$ $[M+H]^+$ calculated 369.0709 found 369.0713.

4,4'-[pyrimidine-2,4-diylbis(oxy)]bis(3,5-dimethyl benzonitrile) (5)

To a solution of 2,4-dichloropyrimidine (0.39 mmol) in DMF (4 mL), 4-hydroxy-3,5-dimethyl benzonitrile (0.46 mmol) and K_2CO_3 (0.46 mmol) were added. The reaction mixture was stirred at 150°C overnight. The reaction mixture was extracted with ethyl acetate. The organic layer was collected, washed with brine, dried over Na_2SO_4, filtered, and crude mixture required additional purification via column chromatography to give the desired product, 30 mg, 21% yield as a white solid, mp = 220 °C. ^{1}H NMR (400 MHz, DMSO-d_6) δ 8.53 (d, *J* = 5.7 Hz, 1H), 7.64 (s, 2H), 7.57 (s, 2H), 7.03 (d, *J* = 5.7 Hz, 1H), 2.04 (s, 6H), 1.98 (s, 6H). ^{13}C NMR (300 MHz, DMSO-d_6) δ 170.06, 163.58, 162.56, 153.57, 153.05, 133.00, 132.83, 132.70, 118.95, 118.84, 109.31, 108.77, 103.27, 16.10, 16.01. HPLC-UV retention time = 3.980 min. HRMS-ESI: m/z $C_{22}H_{18}N_4NaO_2$ $[M+Na]^+$ calculated 393.1322 found 393.1347.

2,4-bis(3-methylanilino)pyrimidine-5-carbonitrile (6)

To a solution of 2,4-dichloropyrimidine-5-carbonitrile (0.39 mmol) in DMF (5 mL), 3-methylaniline (0.39 mmol) and DIPEA (1.95 mmol) were added. The reaction mixture was stirred at room temperature for 4.5 h. The reaction mixture was extracted with ethyl acetate. The organic layer was collected, washed with brine, dried over Na_2SO_4, filtered, and dried under reduced pressure to give the desired product, 61 mg, 50% yield as a light gray solid, mp = 194 °C. ^{1}H NMR (500 MHz, DMSO-d_6) δ 9.80 (s, 1H), 9.40 (s, 1H), 8.48 (s, 1H), 7.40 (s, 1H), 7.36 (q, *J* = 18.1, 10.4 Hz, 4H), 7.30 (t, *J* = 8.1 Hz, 1H), 7.24 (t, *J* = 8.0 Hz, 1H), 7.09 (d, *J* = 7.6 Hz, 1H), 7.03 (d, *J* = 4.9 Hz, 3H), 6.99 (d, *J* = 7.7 Hz, 1H), 6.78 (d, *J* = 7.4 Hz, 1H), 2.28 (s, 3H), 2.14 (s, 3H). ^{13}C NMR (300 MHz, DMSO-d_6) δ 163.16, 160.10, 139.64, 138.51, 138.20, 138.11, 128.85, 128.71, 125.81, 123.84, 120.90, 117.22, 21.65, 21.59. HPLC-UV retention time = 7.540 min. MS-ESI: m/z 316.3 $[M+H]^+$. HRMS-ESI: m/z $C_{19}H_{17}N_5Na$ $[M+Na]^+$ calculated 338.1376 found 338.1379.

Spectra for compound 1-6

Characterization data confirming the structure (H-NMR, C-NMR and HR-MS) and purity (HPLC-UV) of the following compounds are reported; **1**, **2**, **3**, **4**, **5** and **6**.

4-([2-(4-cyanoanilino)pyrimidin-4-yl]oxy)-3,5-dimethylbenzonitrile (1)

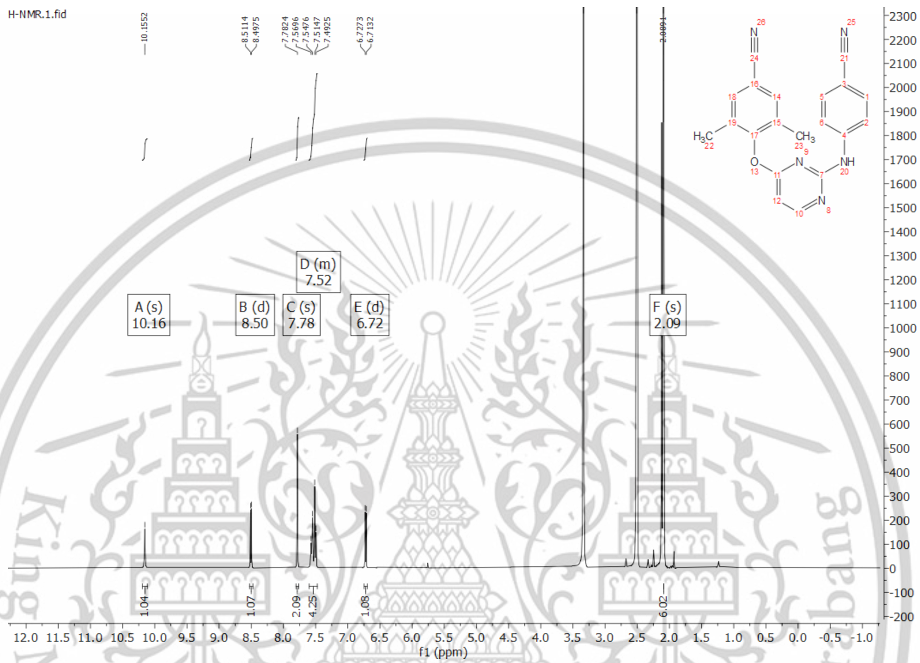

^{1}H-NMR spectra of **1**

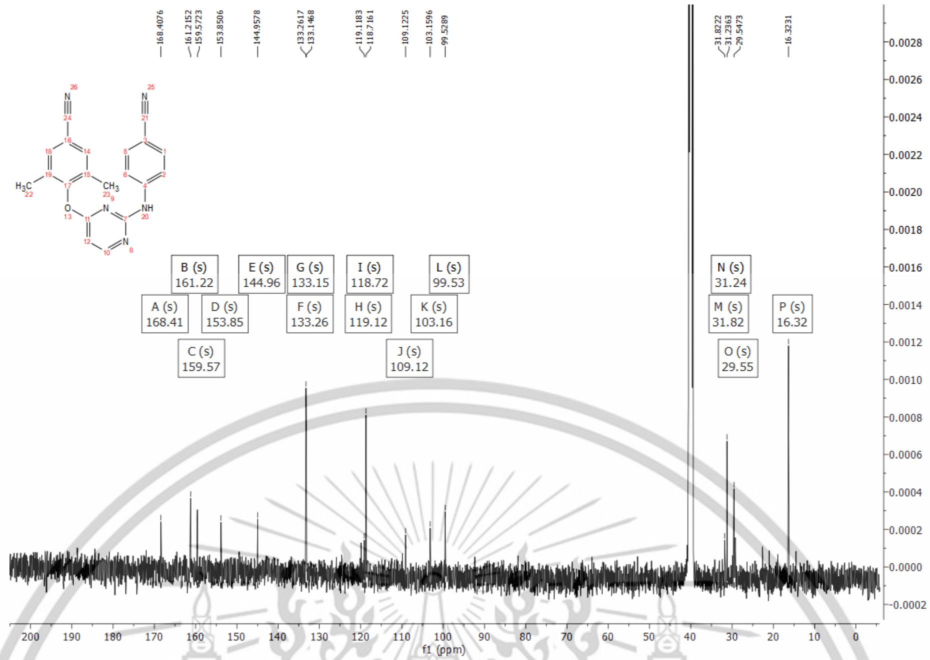

^{13}C-NMR spectra of **1**

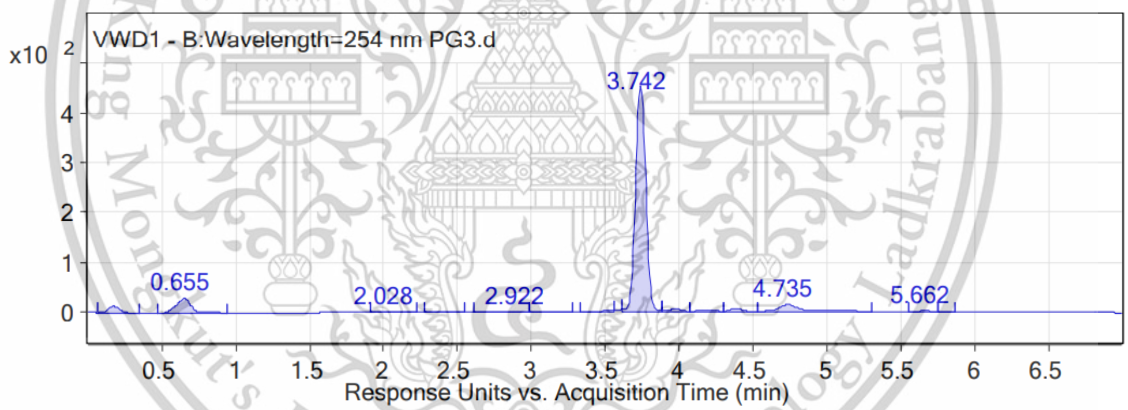

HPLC spectra of **1**

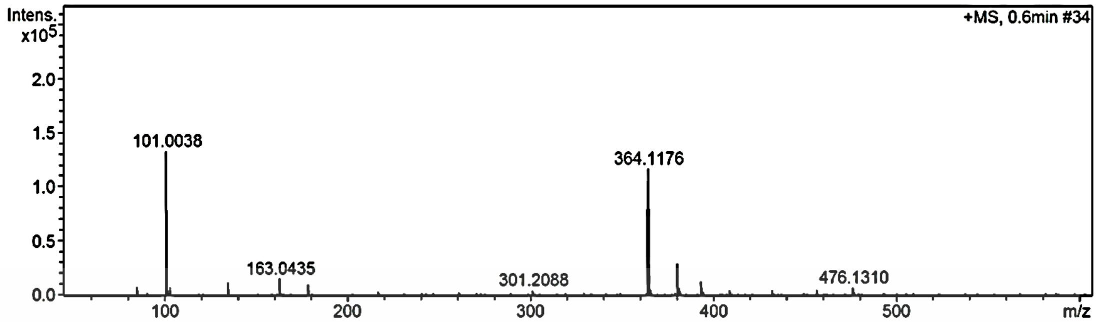

Meas. m/z	#	Ion Formula	m/z	err [mDa]	mSigma	# Sigma	Score	rdb	e⁻ Conf	N-Rule
364.1176	1	C20H15N5NaO	364.1169	**0.7**	0.6	1	100.00	15.5	even	ok

HRMS spectra of **1**

4-([2-(morpholin-4-yl) ethoxyanilino]pyrimidin-4-yl)oxy-3,5-dimethylbenzonitrile (2)

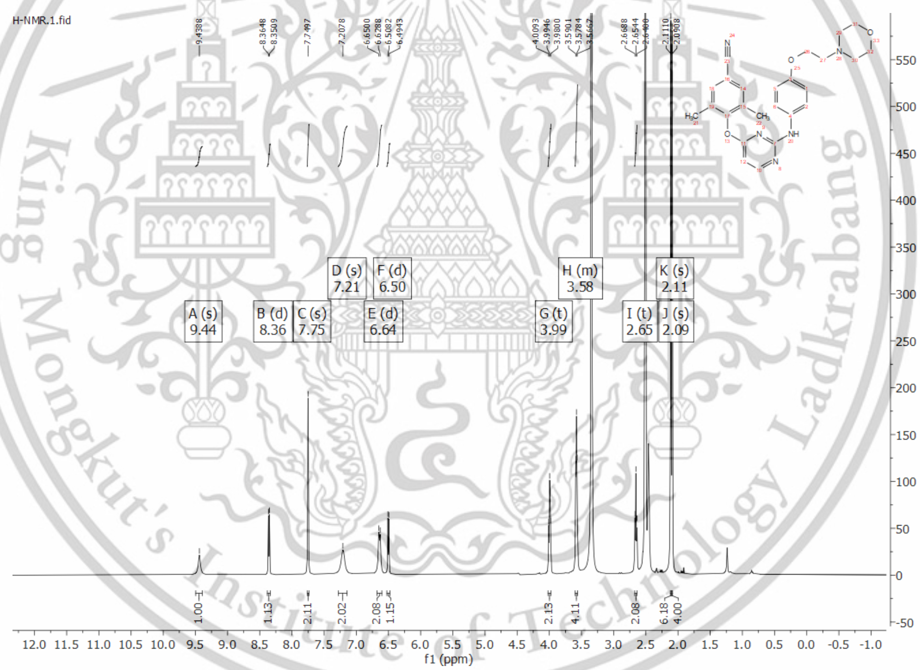

^{1}H-NMR spectra of **2**

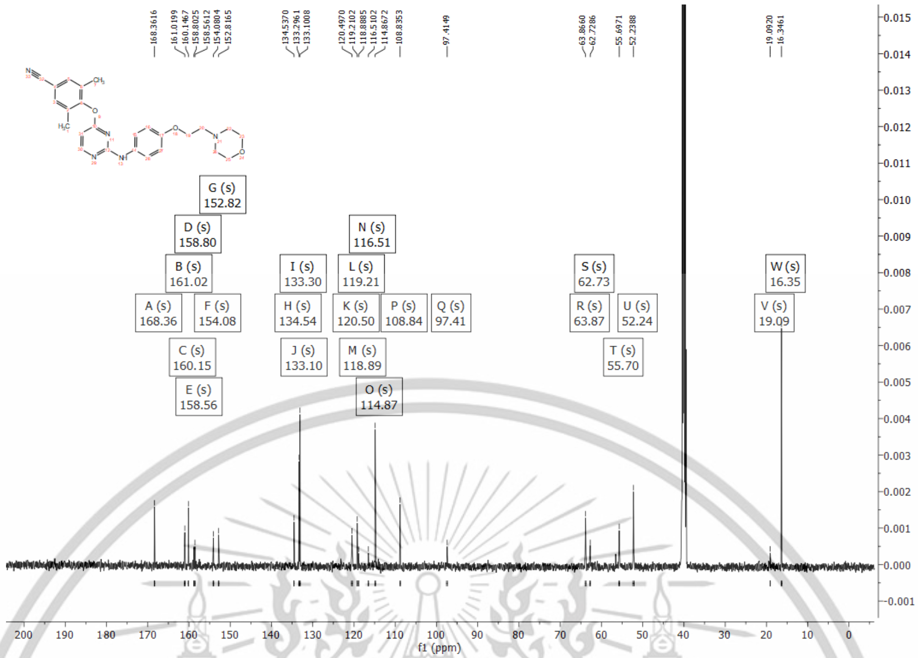

^{13}C-NMR spectra of **2**

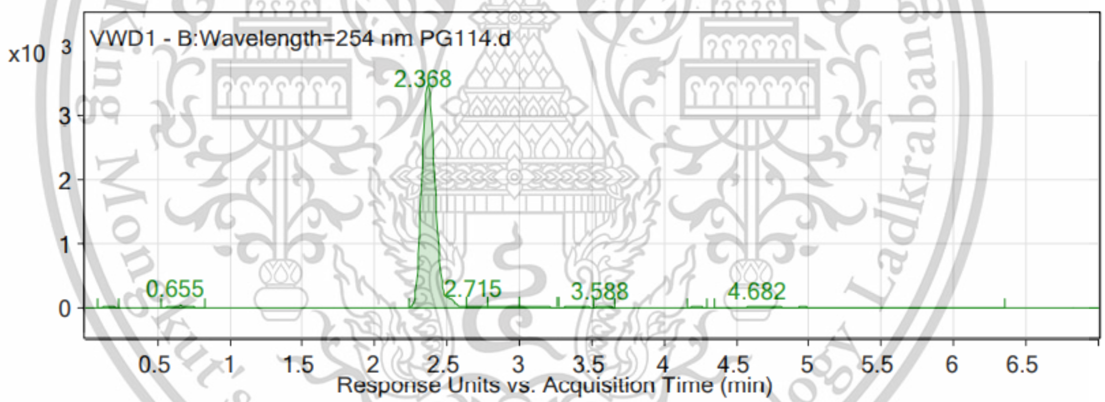

HPLC spectra of **2**

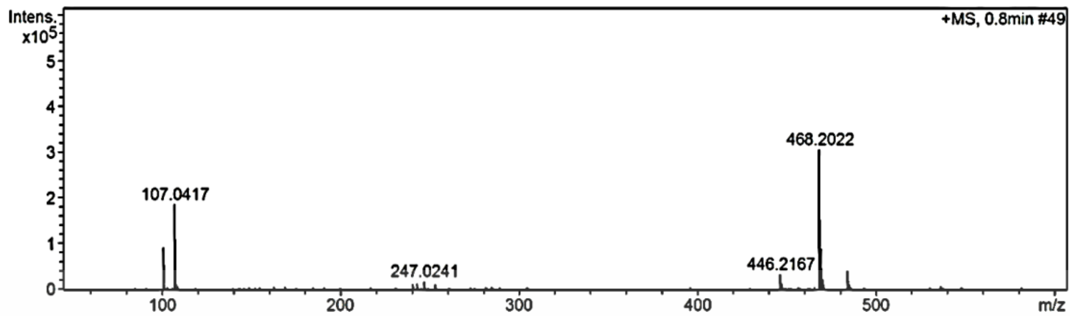

Meas. m/z	#	Ion Formula	m/z	err [mDa]	mSigma	# Sigma	Score	rdb	e⁻ Conf	N-Rule
445.2136	1	C25H27N5O3	445.2108	2.8	620.6	1	100.00	15.0	odd	ok
	1	C25H27N5O3	445.2108	2.8	620.6	1	100.00	15.0	odd	ok
446.2167	1	C25H28N5O3	446.2187	-2.0	3.7	1	100.00	14.5	even	ok
	1	C25H28N5O3	446.2187	-2.0	3.7	1	100.00	14.5	even	ok
468.2022	1	C25H27N5NaO3	468.2006	-1.6	12.1	1	100.00	14.5	even	ok

HRMS spectra of **2**

4-[(2-([(4-methoxyphenyl)methyl]amino)pyrimidin-4-yl)oxy]-3,5-dimethylbenzonitrile (3)

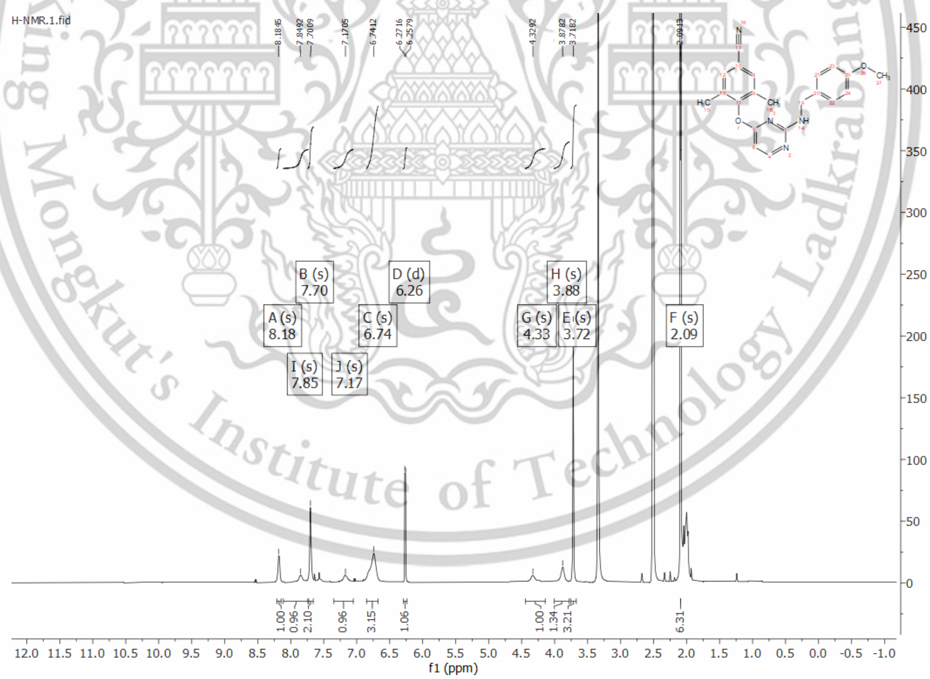

^{1}H-NMR spectra of **3**

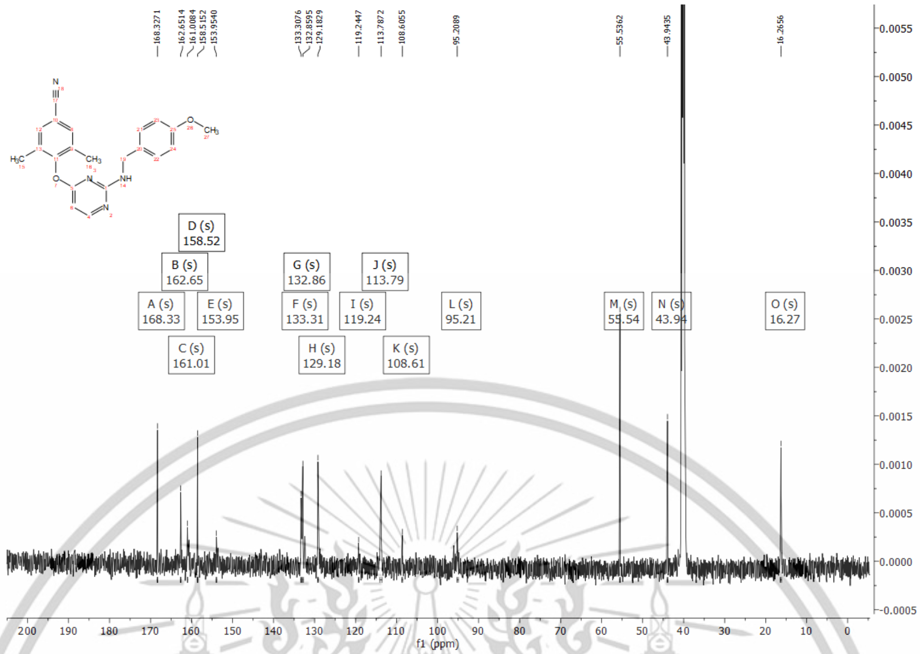

^{13}C-NMR spectra of **3**

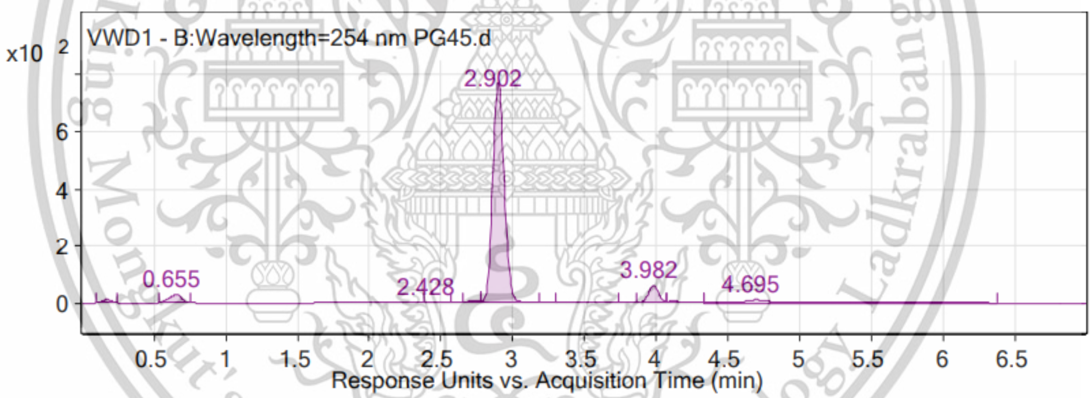

HPLC spectra of **3**

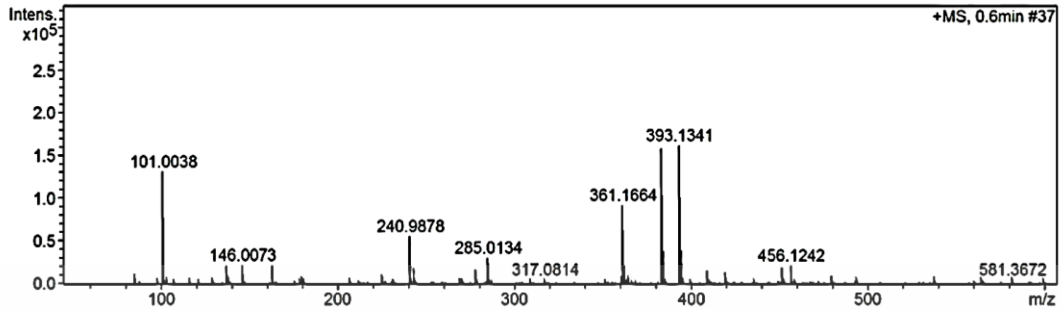

Meas. m/z	#	Ion Formula	m/z	err [mDa]	mSigma	# Sigma	Score	rdb	e⁻ Conf	N-Rule
360.1589	1	C21H20N4O2	360.1581	0.8	725.7	1	100.00	14.0	odd	ok
	1	C21H20N4O2	360.1581	0.8	725.7	1	100.00	14.0	odd	ok
361.1664	1	C21H21N4O2	361.1659	-0.5	1.9	1	100.00	13.5	even	ok
383.1491	1	C21H20N4NaO2	383.1478	1.2	2.3	1	100.00	13.5	even	ok
	1	C21H20N4NaO2	383.1478	1.2	2.3	1	100.00	13.5	even	ok

HRMS spectra of **3**

N^{2}-[(4-bromophenyl)methyl]-*N*^{4}-(4-methylphenyl)pyrimidine-2,4-diamine (**4**)

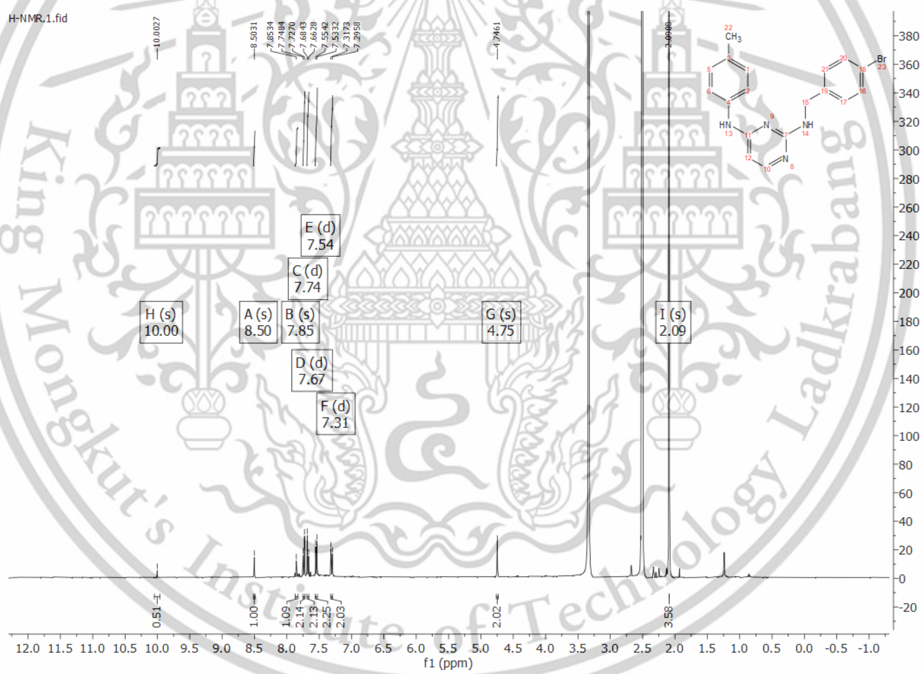

^{1}H-NMR spectra of **4**

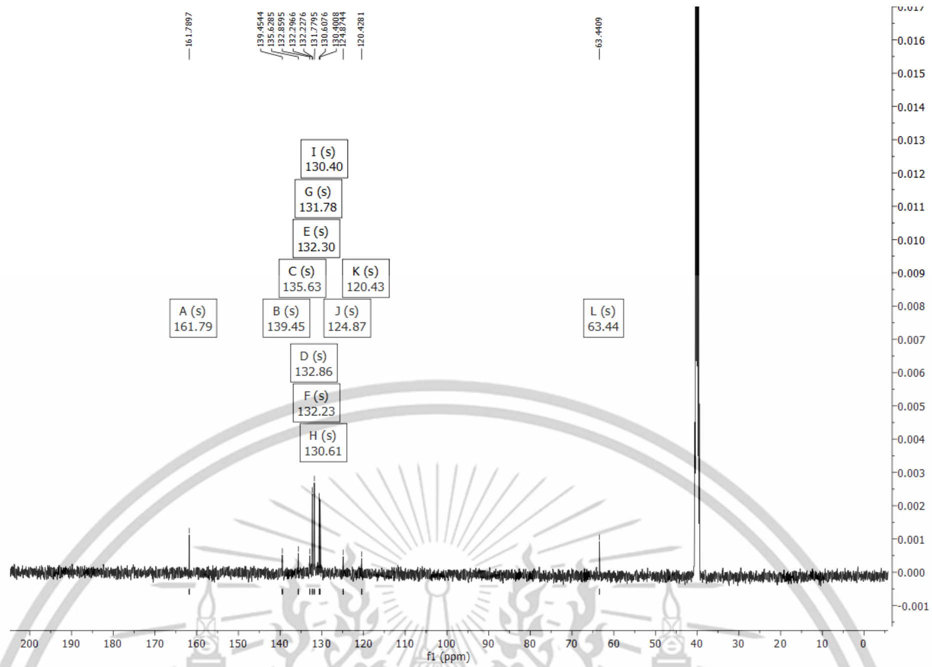

^{13}C-NMR spectra of **4**

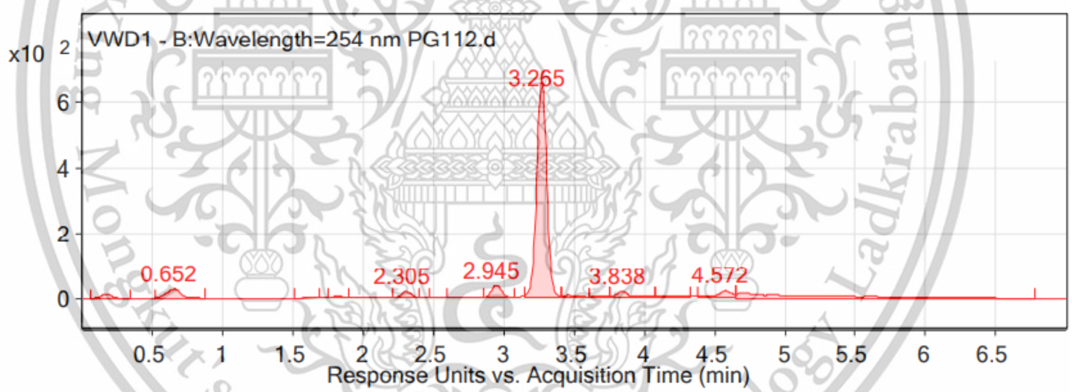

HPLC spectra of **4**

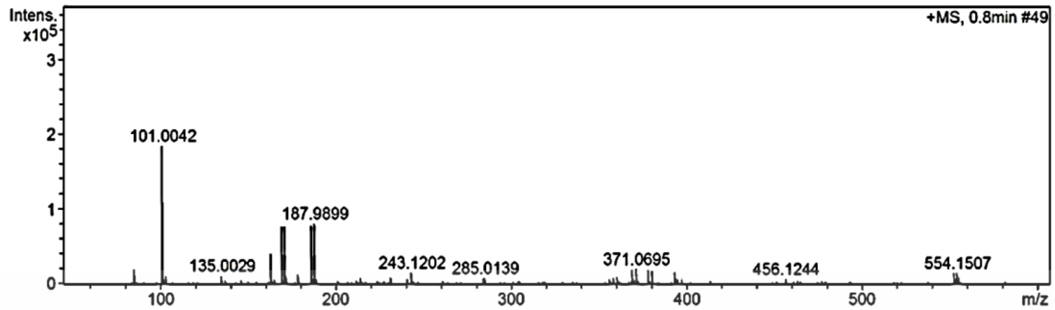

Meas. m/z	#	Ion Formula	m/z	err [mDa]	mSigma	# Sigma	Score	rdb	e⁻ Conf	N-Rule
369.0713	1	C18H18BrN4	369.0709	0.4	14.9	1	100.00	11.5	even	ok
391.0546	1	C18H17BrN4Na	391.0529	-1.7	506.3	1	100.00	11.5	even	ok
	1	C18H17BrN4Na	391.0529	-1.7	506.3	1	100.00	11.5	even	ok

HRMS spectra of **4**

4,4'-[pyrimidine-2,4-diylbis(oxy)]bis(3,5-dimethylbenzonitrile) (5)

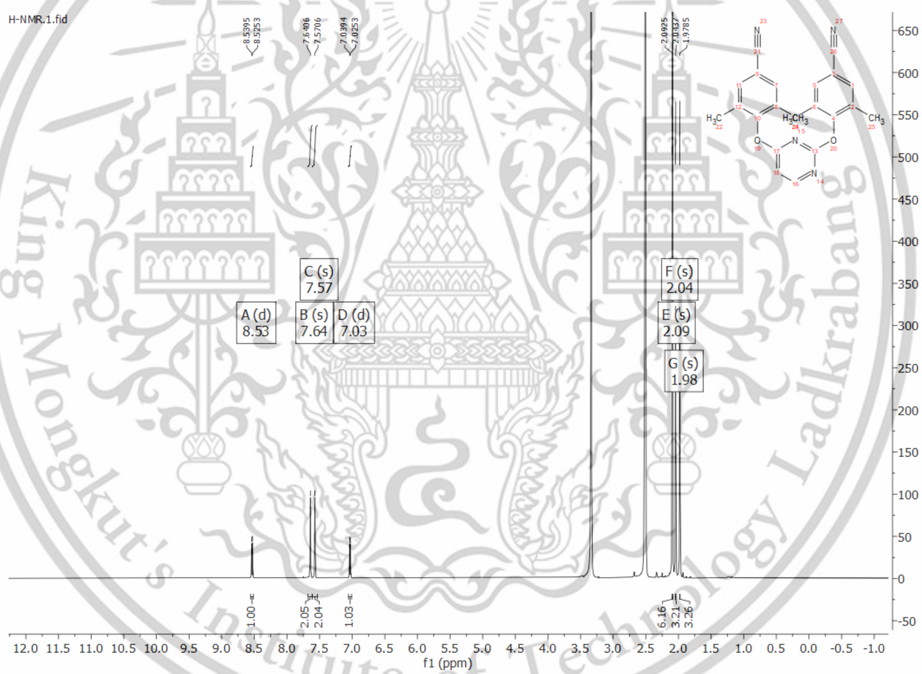

[1]H-NMR spectra of **5**

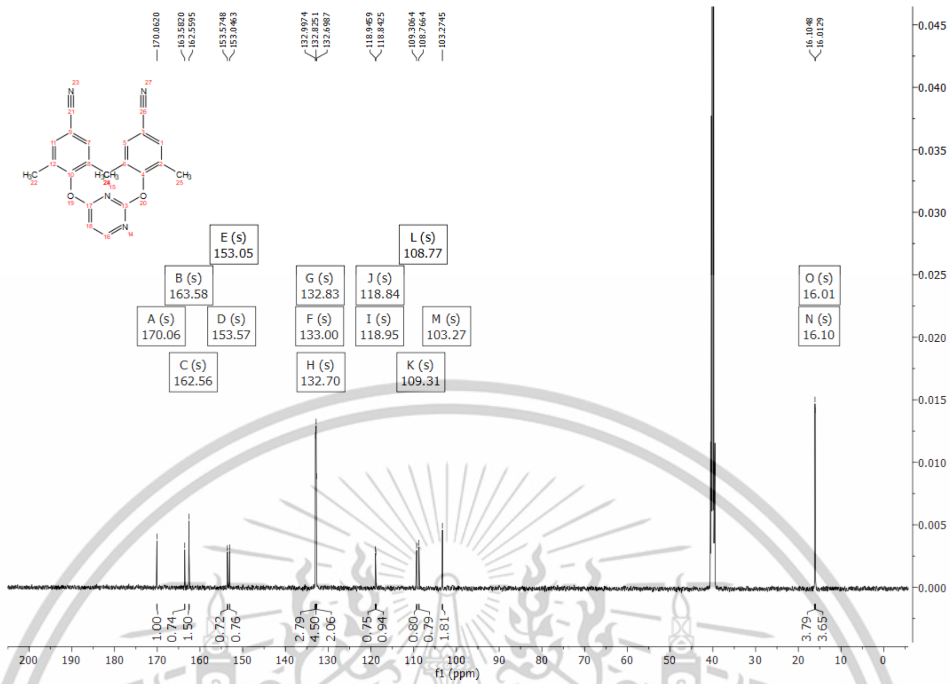

^{13}C-NMR spectra of **5**

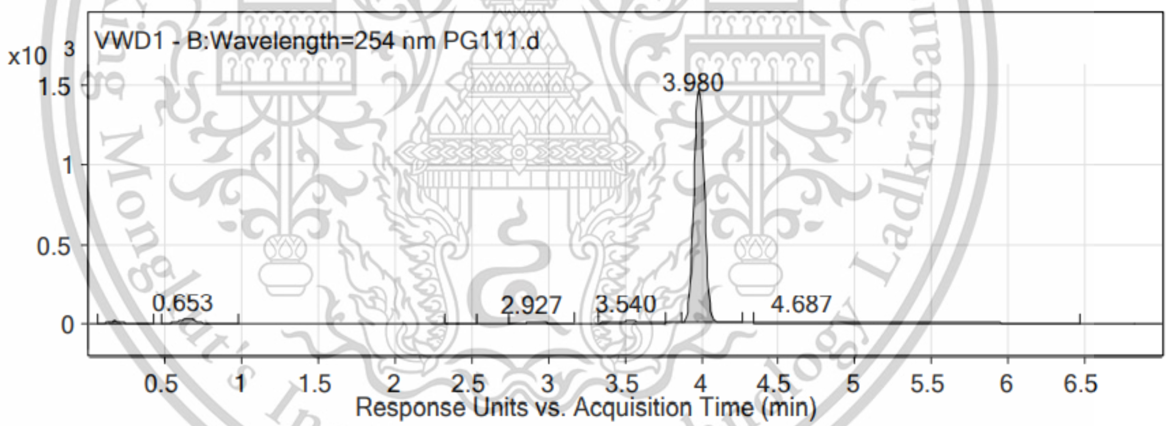

HPLC spectra of **5**

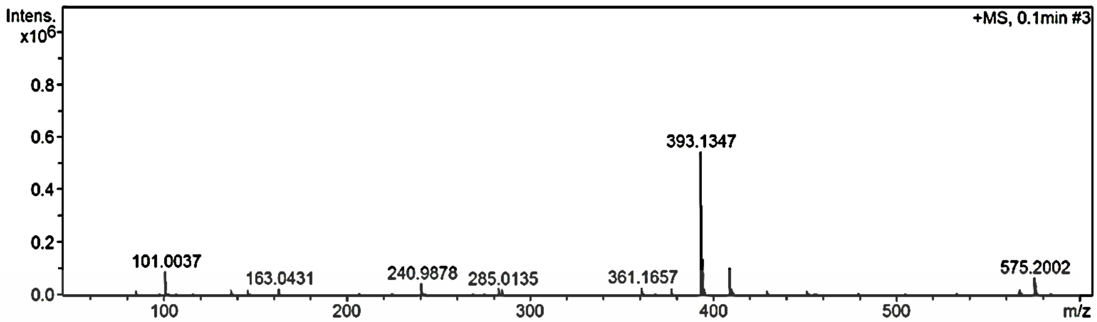

Meas. m/z	#	Ion Formula	m/z	err [mDa]	mSigma	# Sigma	Score	rdb	e⁻ Conf	N-Rule
371.1544	1	C22H19N4O2	371.1503	-4.1	787.0	1	-1.#J	15.5	even	ok
	1	C22H19N4O2	371.1503	-4.1	787.0	1	-1.#J	15.5	even	ok
393.1347	1	C22H18N4NaO2	393.1322	2.5	0.7	1	100.00	15.5	even	ok

HRMS spectra of **5**

2,4-bis(3-methylanilino)pyrimidine-5-carbonitrile (6)

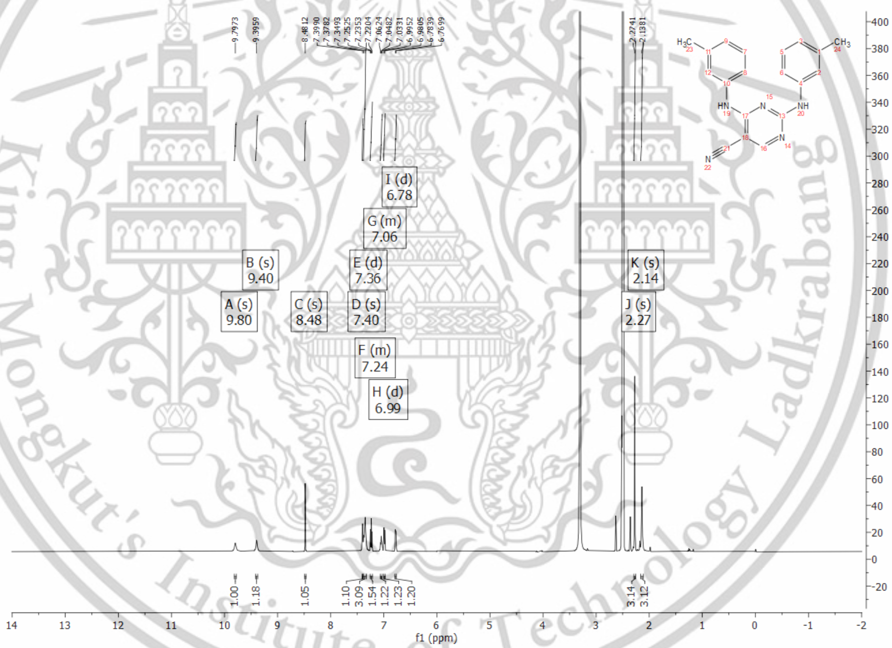

^{1}H-NMR spectra of **6**

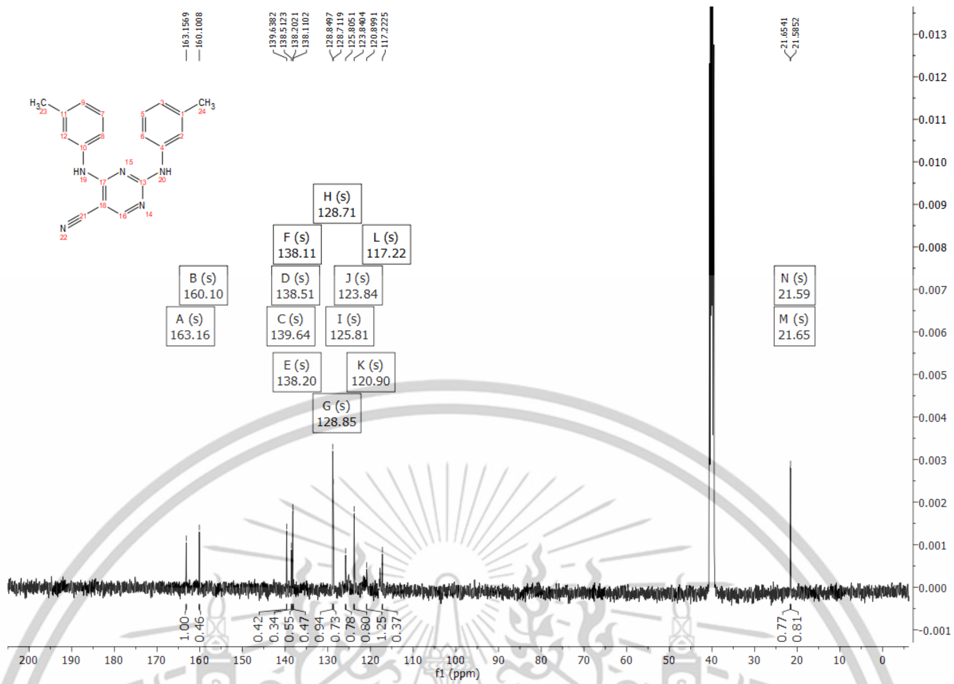

^{13}C-NMR spectra of **6**

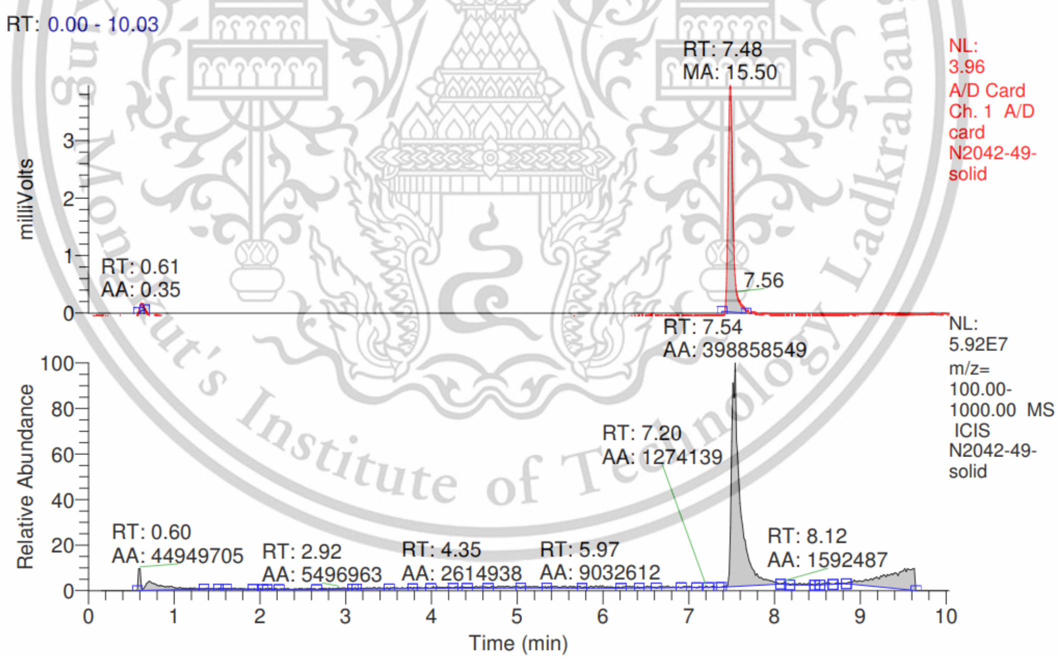

HPLC spectra of **6**

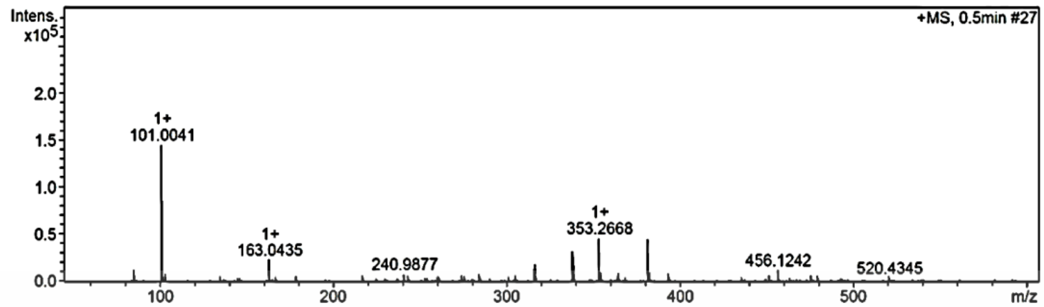

Meas. m/z	#	Ion Formula	m/z	err [mDa]	mSigma	# Sigma	Score	rdb	e⁻ Conf	N-Rule
316.1557	1	C19H18N5	316.1557	0.0	31.9	1	100.00	13.5	even	ok
338.1379	1	C19H17N5Na	338.1376	-0.2	1.6	1	100.00	13.5	even	ok
	1	C19H17N5Na	338.1376	-0.2	1.6	1	100.00	13.5	even	ok

HRMS spectra of **6**

FIV and HIV Inhibition

Biological testing data confirming the inhibitory activity of compounds at 50μM against HIV and FIV are reported. Full IC_{50} curves are reported for HIV and FIV.

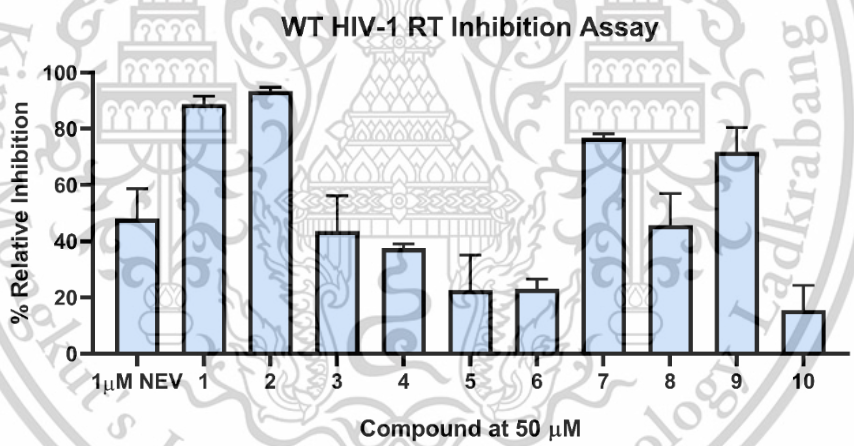

Screening data of compounds **1-10** and drug standard against WT HIV-1 RT.

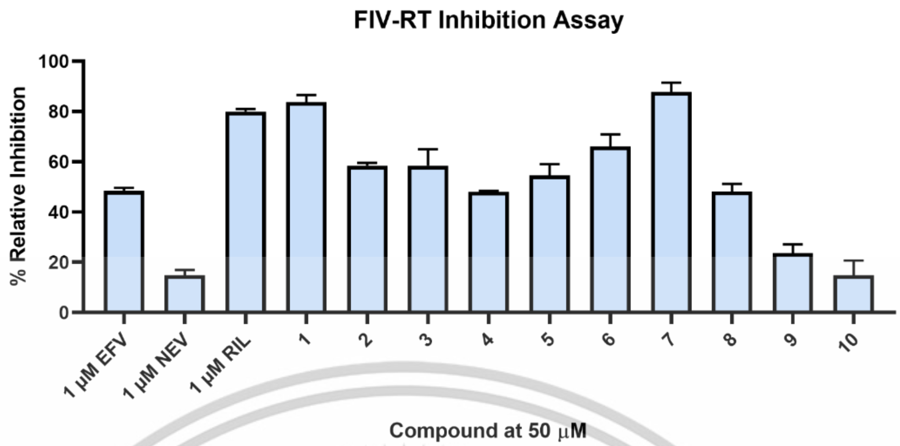

Screening data of compounds **1-10** and drug standards against FIV RT.

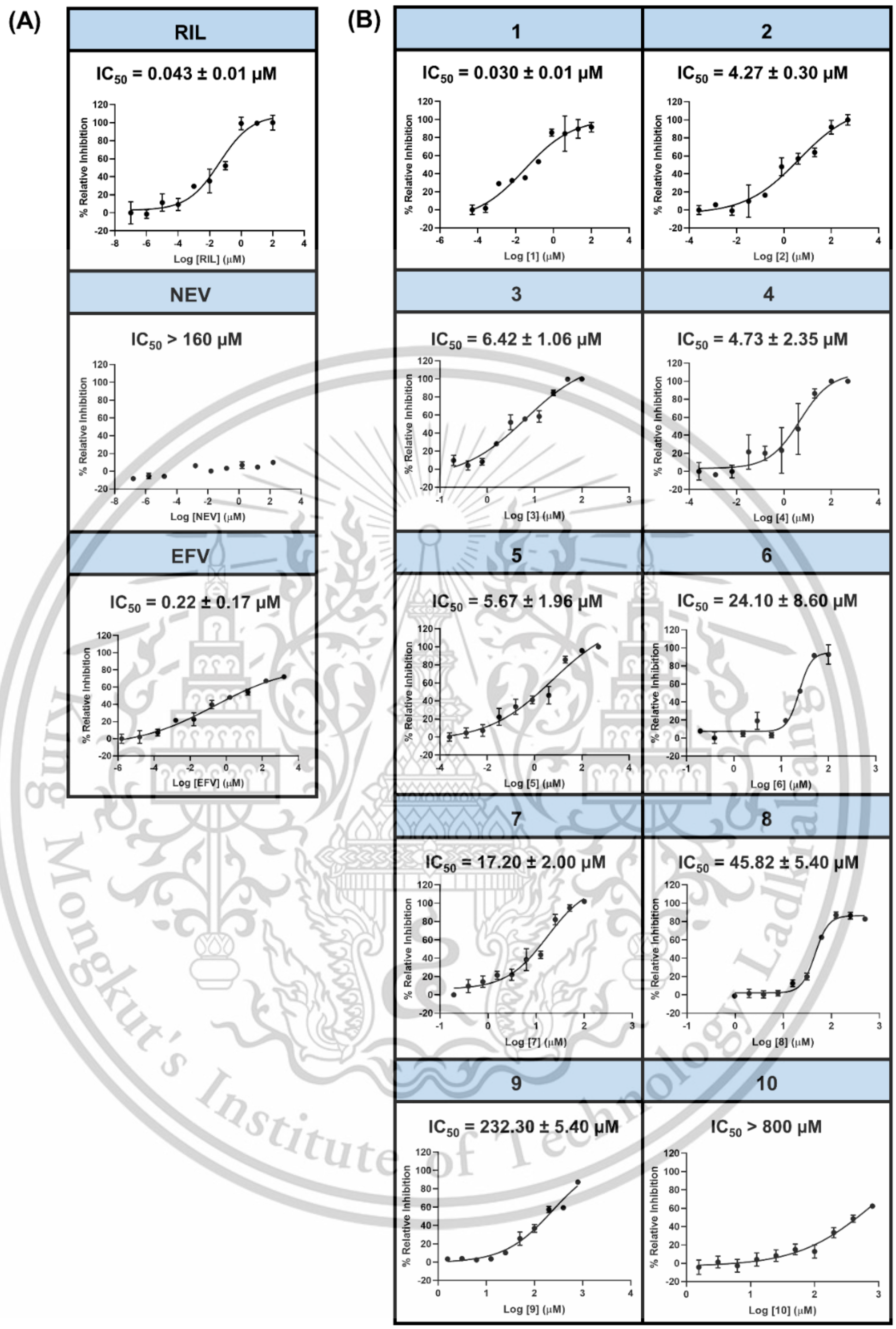

Dose response curves for (A) drug standards, (B) compounds **1-10** against FIV. Data are represented as means ± SD from triplicate independent experiment.

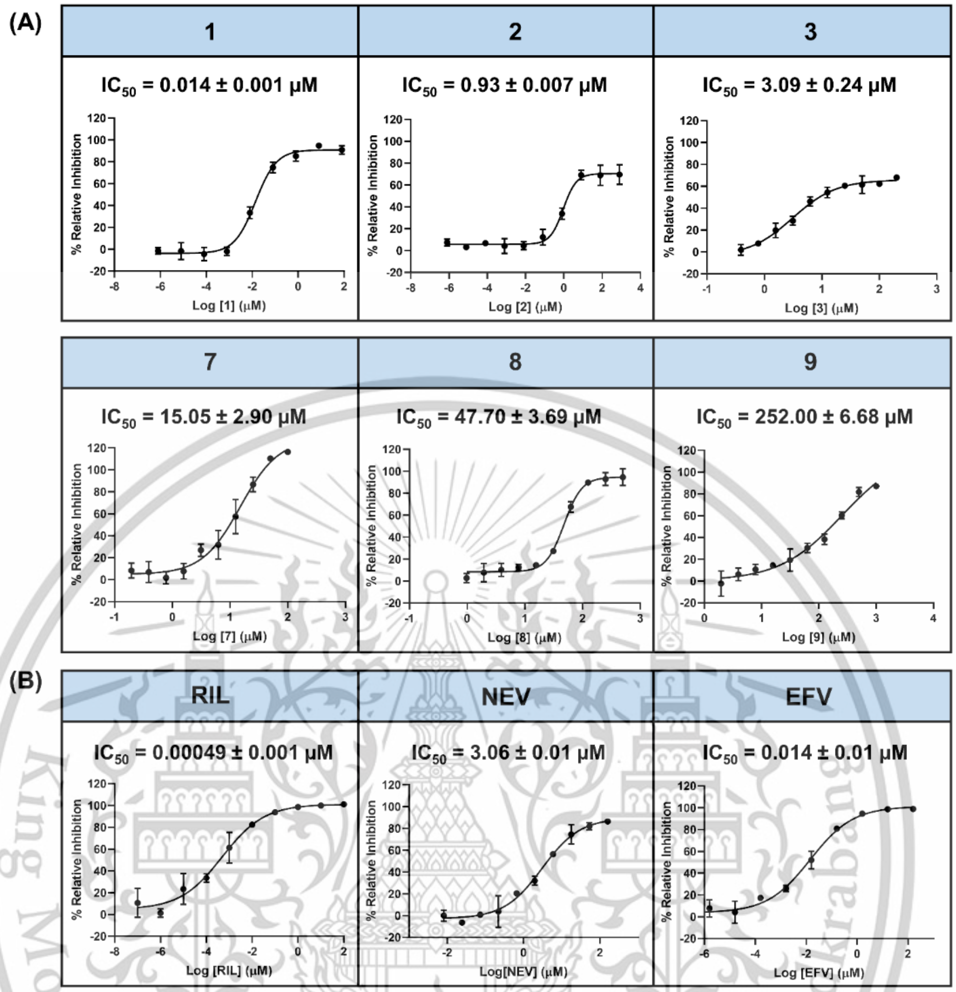

Dose response curves for (A) compounds **1, 2, 3, 7, 8** and **9**, (B) drug standards against wild-type HIV-1 RT. Data are represented as means ± SD from triplicate independent experiment.

Appendix B

Study 2: Chemical Characterization Data & Spectra for Representative Compound 19, 27, 31, 32 and 39

Chemical characterization Data

N[4]-[(2-methoxyphenyl)methyl]-N[2]-(5-methyl-1H-pyrazol-3-yl)pyrimidine-2,4-diamine (19)

Compound **11** and 5-methyl-1*H*-pyrazol-3-amine, following the general procedure F to give compound **19**, 6% yield. ^{1}H NMR (400 MHz, DMSO-d_6) δ 12.42 (s, 1H), 9.14 (s, 1H), 7.86 (d, *J* = 5.5 Hz, 1H), 7.27 (t, *J* = 6.2 Hz, 1H), 7.23 (d, *J* = 5.8 Hz, 1H), 7.01 (d, *J* = 6.3 Hz, 1H), 6.90 (td, *J* = 6.0, 0.6 Hz, 1H), 6.32 (d, *J* = 5.8 Hz, 1H), 5.81 (s, 1H), 4.55 (d, *J* = 4.5 Hz, 2H), 3.79 (s, 3H), 2.20 (s, 3H). ^{13}C NMR (101 MHz, DMSO-d_6) δ 162.77, 157.40, 152.02, 147.22, 130.11, 129.33, 128.83, 125.24, 120.73, 111.19, 100.20, 94.87, 55.88, 11.02. MS-ESI for $C_{16}H_{18}N_6O$ [M+H], Calcd:, 310.3, found: 311.1. MP = 178°C. HPLC analysis: H_2O-ACN (99:1), RT = 3.500 min, 99.5% purity.

N[4]-[(3-methoxyphenyl)methyl]-N[2]-(5-methyl-1H-pyrazol-3-yl)pyrimidine-2,4-diamine (20)

Compound **12** and 5-methyl-1H-pyrazol-3-amine, following the general procedure F to give compound **20**, 14% yield. ^{1}H NMR (500 MHz, DMSO-d6) δ 12.51 (s, 1H), 11.15 (s, 1H), 9.44 (t, J = 5.0 Hz, 1H), 7.92 (d, J = 7.2 Hz, 1H), 7.29 (t, J = 8.1 Hz, 1H), 6.95 – 6.91 (m, 2H), 6.87 (d, J = 7.1 Hz, 1H), 6.35 (d, J = 7.2 Hz, 1H), 5.90 (s, 1H), 4.62 (d, J = 5.7 Hz, 2H), 3.75 (s, 3H), 2.24 (s, 3H). ^{13}C NMR (125 MHz, DMSO-d6) δ 162.68, 159.90, 158.46, 151.81, 139.56, 130.16, 120.18, 113.85, 113.11, 55.52, 44.25, 10.96. MS-ESI for $C_{16}H_{18}N_6O$ [M+H], Calcd:, 310.3, found: 311.1. MP = 164°C. HPLC analysis: H2O-ACN (99:1), RT = 3.413 min, 97.3% purity.

N^4-[(4-methoxyphenyl)methyl]-N^2-(5-methyl-1H-pyrazol-3-yl)pyrimidine-2,4-diamine (21)

Compound **13** and 5-methyl-1H-pyrazol-3-amine, following the general procedure F to give compound **21**, 9% yield. ^{1}H NMR (500 MHz, DMSO-*d$_6$*) **δ** 12.42 (s, 1H), 9.23 (s, 1H), 7.85 (d, *J* = 5.6 Hz, 1H), 7.26 (d, *J* = 6.8 Hz, 2H), 6.89 (d, *J* = 6.9 Hz, 2H), 6.25 (d, *J* = 5.7 Hz, 1H), 5.84 (s, 1H), 4.52 (d, *J* = 4.5 Hz, 2H), 3.70 (s, 3H), 2.21 (s, 3H). ^{13}C NMR (125 MHz, DMSO-*d$_6$*) **δ** 162.44, 159.15, 151.83, 129.81, 129.62, 114.43, 55.60, 43.84, 11.00. MS-ESI for $C_{16}H_{18}N_6O$ $[M+H]^+$, Calcd:, 310.3, found: 311.1. MP = 176°C. HPLC analysis: H_2O-ACN (99:1), RT = 3.440 min, 98.5% purity.

3,5-dimethyl-4-((2-[(5-methyl-1*H*-pyrazol-3-yl)amino]pyrimidin-4-yl)oxy)benzonitrile (22)

Compound **14** and 5-methyl-1H-pyrazol-3-amine, following the general procedure F to give compound **22**, 9% yield. ^{1}HNMR (500 MHz, DMSO-*d$_6$*) **δ** 11.71, 9.68, 8.29 (d, *J* = 3.2 Hz), 7.72, 6.47 (d, *J* = 3.2 Hz), 2.05, 1.98. ^{13}C NMR (125 MHz, DMSO-*d$_6$*) **δ** 161.08, 158.33, 133.03, 132.74, 126.13, 120.23, 101.40, 21.92, 16.77, 16.29, 16.23. LCQTOF for $C_{17}H_{16}N_6O$ $[M+H]^+$, Calcd:, 320.3, found: 321.1462. MP = 110°C. HPLC analysis: H_2O-ACN (99:1), RT = 2.806 min, 95.2% purity.

N^4-[(2-methoxyphenyl)methyl]-N^2-(1-methyl-1H-pyrazol-3-yl)pyrimidine-2,4-diamine (23)

Compound **11** and 1-methyl-1*H*-pyrazol-4-amine, following the general procedure F to give compound **23** as a white solid, 27% yield. ^{1}H NMR (400 MHz, DMSO-*d$_6$*) **δ** 10.37 (s, 1H), 9.21 (s, 1H), 7.72 (s, 1H), 7.63 (s, 1H), 7.45 (s, 1H), 7.27 (td, *J* = 6.5, 1.3 Hz, 1H), 7.17 (d, *J* = 4.3 Hz, 1H), 7.03 (d, *J* = 6.5 Hz, 1H), 6.89 (t, *J* = 6.0 Hz, 1H), 6.21 (d, *J* = 5.8 Hz, 1H), 4.55 (d, *J* = 4.4 Hz, 2H), 3.80 (s, 3H), 3.73 (s, 3H). ^{13}C NMR (101 MHz, DMSO-*d$_6$*) **δ** 163.13, 159.79, 159.47, 157.40, 142.78, 129.28, 128.74, 125.30, 120.78, 111.28, 55.93. HRMS (ESI) for $C_{16}H_{18}N_6O$ $[M+H]^+$, Calcd: 311.1615, found: 311.1645. MP = 90°C. HPLC analysis: H_2O-ACN (99:1), RT = 3.293 min, 97.8% purity.

N^4-[(3-methoxyphenyl)methyl]-N^2-(1-methyl-1H-pyrazol-3-yl)pyrimidine-2,4-diamine (24)

Compound **12** and 1-methyl-1H-pyrazol-4-amine, following the general procedure F to give compound **24**, 65% yield. ^{1}H NMR (400 MHz, DMSO-d_6) δ 10.63 (s, 1H), 9.32 (s, 1H), 7.76 (s, 1H), 7.65 (s, 1H), 7.43 (s, 1H), 7.24 (t, J = 6.4 Hz, 1H), 6.88 (s, 1H), 6.87 (s, 1H), 6.82 (dd, J = 7.1, 1.4 Hz, 1H), 6.17 (d, J = 5.6 Hz, 1H), 4.58 (d, J = 2.9 Hz, 2H), 3.73 (s, 3H), 3.68 (s, 3H). ^{13}C NMR (101 MHz, DMSO-d_6) δ 163.13, 159.89, 159.41, 159.09, 143.30, 139.82, 130.17, 119.85, 113.56, 112.99, 55.47. HRMS (ESI) for $C_{16}H_{18}N_6O$ [M+Na]$^+$, Calcd: 333.1434, found: 333.1434. MP = 190°C. HPLC analysis: H_2O-ACN (99:1), RT = 3.247 min, 98.9% purity.

N^4-[(4-methoxyphenyl)methyl]-N^2-(1-methyl-1H-pyrazol-3-yl)pyrimidine-2,4-diamine (25)

Compound **13** and 1-methyl-1*H*-pyrazol-4-amine, following the general procedure F to give compound **25**, 14% yield. ^{1}H NMR (500 MHz, DMSO-d_6) δ 11.80 (s, 1H), 10.25 (s, 1H), 9.26 (s, 1H), 7.73 (s, 1H), 7.47 (s, 1H), 7.23 (d, J = 6.8 Hz, 2H), 6.89 (d, J = 6.9 Hz, 2H), 6.16 (d, J = 5.6 Hz, 1H), 4.52 (d, J = 3.3 Hz, 2H), 3.76 (s, 3H), 3.69 (s, 3H). ^{13}C NMR (125 MHz, DMSO-d_6) δ 158.88, 129.09, 114.32, 55.56. HRMS (ESI) for $C_{16}H_{18}N_6O$ [M+H]$^+$, Calcd: 311.1615, found: 311.1633. MP = 148°C. HPLC analysis: H_2O-ACN (99:1), RT = 3.293 min, 99.4% purity.

3,5-dimethyl-4-((2-[(1-methyl-1*H*-pyrazol-4-yl)amino]pyrimidin-4-yl)oxy)benzonitrile (26)

Compound **14** and 1-methyl-1*H*-pyrazol-4-amine, following the general procedure F to give compound **26**, 30% yield. ^{1}H NMR (500 MHz, DMSO-d_6) δ 9.68, 8.31 (d, J = 3.4 Hz), 7.78, 6.98, 6.51 (d, J = 22.2 Hz), 2.07. ^{13}C NMR (125 MHz, DMSO-d_6) δ 169.03, 160.30, 159.06, 158.77, 154.21, 133.53, 133.16, 129.40, 123.19, 119.67, 119.07, 117.06, 114.76, 109.03, 96.24, 16.30. LCQTOF for $C_{17}H_{16}N_6O$ [M+H]$^+$, Calcd:, 320.3, found: 321.1457. MP = 180°C. HPLC analysis: H_2O-ACN (99:1), RT = 2.920 min, 99.3% purity.

N^2-(N-(3-aminophenyl)-N'-phenylurea)-N^4-[(2-methoxyphenyl)methyl]pyrimidine-2,4-diamine (27)

Compound **11** and *N*-(3-aminophenyl)-*N'*-phenylurea, following the general procedure F to give compound **27**, 30% yield. ^{1}H NMR (400 MHz, DMSO-d_6) δ 9.39 (s, 1H), 8.91 (d, J = 17.0 Hz, 1H), 7.82 (d, J = 10.6 Hz, 2H), 7.42 (d, J = 7.8 Hz, 2H), 7.25 (q, J = 7.7 Hz, 4H), 7.09 (d, J = 7.1 Hz, 1H), 7.01 (d, J = 8.0 Hz, 1H), 6.94 (t, J = 7.4 Hz, 1H), 6.89 (t, J = 7.5 Hz, 1H), 6.13 (s, 1H), 4.57 (d, J = 5.6 Hz, 2H), 3.82 (s, 3H). ^{13}C NMR (101 MHz, DMSO-d_6) δ 152.97, 140.39, 140.30, 129.20, 129.09, 128.82, 126.77, 122.08, 120.62, 118.40, 113.69, 112.30, 111.05, 109.78, 100.69, 99.49, 55.81, 45.98. HRMS (ESI) for $C_{25}H_{25}N_6O_2$ $[M+H]^+$, Calcd: 441.2034, found 441.2060. MP = 196°C. HPLC analysis: H_2O-ACN (99:1), RT = 2.927 min, 97.5% purity.

N2-(N-(3-aminophenyl)-N'-phenylurea)-N4-[(3-methoxyphenyl)methyl]pyrimidine-2,4-diamine (28)

Compound **12** and *N*-(3-aminophenyl)-*N'*-phenylurea, following the general procedure F to give compound **28**, 72% yield. ^{1}H NMR (500 MHz, DMSO-d_6) δ 10.29 (s), 9.38 (s), 8.75 (s), 8.65 (s), 8.06 (s), 7.77 (d, J = 5.7 Hz), 7.43 – 7.35 (m), 7.26 – 7.21 (m), 6.95 – 6.90 (m), 6.83 – 6.79 (m), 6.24 (d, J = 5.8 Hz), 4.65 (d, J = 4.5 Hz), 3.64 (s). ^{13}C NMR (125 MHz, DMSO-d_6) δ 162.81, 159.87, 153.05, 152.26, 141.07, 140.75, 140.32, 140.22, 139.66, 130.12, 129.73, 129.31, 129.28, 122.24, 120.53, 118.55, 118.48, 114.00, 113.38, 112.10, 108.17, 99.19, 55.47, 44.93. MP = 200°C. HPLC analysis: H_2O-ACN (99:1), RT = 3.787 min, 98.9% purity.

N^2-(N-(3-aminophenyl)-N'-phenylurea)-N^4-[(4-methoxyphenyl)methyl]pyrimidine-2,4-diamine (29)

Compound **13** and *N*-(3-aminophenyl)-*N'*-phenylurea, following the general procedure F to give compound **29**, 46% yield. NMR (500 MHz, DMSO-d_6) δ 8.84 (s), 8.74 (s), 8.69 (s), 8.59 (s), 7.74 (d, J = 5.7 Hz), 7.42 (d, J = 0.7 Hz), 7.40 (d, J = 0.7 Hz), 7.36 (d, J = 6.3 Hz), 7.25 (d, J = 1.5 Hz), 7.24 (s), 7.22 (s), 6.95 – 6.91 (m), 6.84 (d, J = 6.8 Hz), 6.20 (d,

J = 5.5 Hz), 4.57 (d, J = 4.1 Hz), 3.67 (s). ^{13}C NMR (125 MHz, DMSO-d_6) δ 162.59, 159.14, 153.04, 152.41, 142.33, 141.04, 140.74, 140.31, 140.20, 137.92, 129.92, 129.77, 129.60, 129.31, 129.28, 122.26, 118.57, 118.52, 114.39, 112.12, 108.20, 99.18, 55.61, 44.45. MP = 210°C. HPLC analysis: H_2O-ACN (99:1), RT = 3.820 min, 98.4% purity.

N-(3-[(4-([(3,5-dimethyl-4-cyanophenyl)oxy]pyrimidin-2-yl}amino)phenyl]carbamoyl)aniline (30)

Compound **14** and *N*-(3-aminophenyl)-*N'*-phenylurea, following the general procedure F to give compound **30**, 9% yield. NMR (500 MHz, DMSO-d_6) δ 11.47, 9.04, 8.87, 8.12, 7.92, 7.51 – 7.48 (m), 7.19 (t, J = 4.5 Hz), 2.33, 1.44. ^{13}C NMR (125 MHz, DMSO-d_6) δ 168.37, 161.00, 160.16, 154.05, 153.08, 140.37, 139.60, 135.04, 134.19, 133.30, 133.05, 129.29, 122.15, 119.51, 119.16, 119.00, 118.58, 108.87, 97.36, 16.37. LCQTOF for $C_{26}H_{22}N_6O_2$ $[M+H]^+$, Calcd:, 450.5, found: 451.1879. MP = 190°C. HPLC analysis: H_2O-ACN (99:1), RT = 3.213 min, 98.4% purity.

N^2-(N-(4-aminophenyl)-N'-phenylurea)-N^4-[(2-methoxyphenyl)methyl]pyrimidine-2,4-diamine (31)

Compound **11** and *N*-(4-aminophenyl)-*N'*-phenylurea, following the general procedure F to give compound **31**, 26% yield. ^{1}H NMR (400 MHz, DMSO-d_6) δ 10.35 (s, 1H), 9.35 (s, 1H), 9.27 (s, 1H), 9.15 (s, 1H), 7.77 (d, J = 7.0 Hz, 1H), 7.45 (t, J = 7.6 Hz, 5H), 7.33-7.25 (m, 6H), 7.17 (d, J = 7.1 Hz, 1H), 7.06 (d, J = 8.1 Hz, 1H), 6.96 (t, J = 7.4 Hz, 1H), 6.91 (t, J = 7.5 Hz, 1H), 6.30 (d, J = 7.3 Hz, 1H), 4.55 (d, J = 5.6 Hz, 2H), 3.85 (s, 3H). ^{13}C NMR (101 MHz, DMSO-d_6) δ 162.86, 157.43, 153.13, 141.88, 140.28, 129.24, 128.78, 125.26, 122.17, 120.68, 118.75, 118.54, 118.47, 111.21, 100.69, 98.94, 55.92. HRMS (ESI) for $C_{25}H_{25}N_6O_2$ $[M+H]^+$, Calcd: 441.2034, found 441.2056. MP= =220°C. HPLC analysis: H_2O-ACN (99:1), RT = 2.887 min, 97.8% purity.

N^2-(N-(4-aminophenyl)-N'-phenylurea)-N^4-[(3-methoxyphenyl)methyl]pyrimidine-2,4-diamine (32)

Compound **12** and *N*-(4-aminophenyl)-*N'*-phenylurea, following the general procedure F to give compound **32**, 70% yield. ^{1}H NMR (400 MHz, DMSO-d_6) δ 10.04 (s), 9.09 (d, *J* = 48.4 Hz), 8.80 (s), 8.77 (s), 7.72 (d, *J* = 4.4 Hz), 7.45 – 7.37 (m), 7.37 – 7.30 (m), 7.25 – 7.22 (m), 6.95 – 6.90 (m), 6.87 – 6.80 (m), 6.17 (d, *J* = 5.6 Hz), 4.52 (d, *J* = 3.8 Hz), 3.68 (s). ^{13}C NMR (125 MHz, DMSO-d_6) δ 162.91, 159.93, 159.75, 159.50, 153.15, 140.39, 139.97, 130.15, 129.28, 122.25, 120.14, 119.11, 118.76, 118.67, 113.65, 113.20, 98.91, 55.54, 44.48, 31.82, 29.54, 29.23, 22.63, 14.48. MP = 184°C. HPLC analysis: H_2O-ACN (99:1), RT = 3.787 min, 97.8% purity.

N^2-(N-(4-aminophenyl)-N'-phenylurea)-N^4-[(4-methoxyphenyl)methyl]pyrimidine-2,4-diamine (33)

Compound **13** and *N*-(4-aminophenyl)-*N'*-phenylurea, following the general procedure F to give compound **33**, 18% yield. ^{1}H NMR (400 MHz, DMSO-d_6) δ 10.41 (s, 1H), 9.48 (t, *J* = 4.8 Hz, 1H), 9.28 (s, 1H), 9.17 (s, 1H), 7.77 (d, *J* = 6.9 Hz, 1H), 7.53-7.43 (m, 5H), 7.37 (d, *J* = 8.8 Hz, 2H), 7.31-7.21 (m, 5H), 6.96 (t, *J* = 7.4 Hz, 1H), 6.92 (d, *J* = 8.6 Hz, 2H), 6.25 (d, *J* = 7.3 Hz, 1H), 4.51 (d, *J* = 5.6 Hz, 2H), 3.74 (s, 3H). ^{13}C NMR (101 MHz, DMSO-d_6) δ 162.61, 159.06, 153.15, 153.13, 152.48, 141.85, 140.29, 129.87, 129.49, 129.23, 123.54, 122.46, 122.17, 118.90, 118.62, 118.48, 114.59, 114.48, 114.37, 114.32, 98.92, 55.58. HRMS (ESI) for $C_{25}H_{25}N_6O_2$ $[M+H]^+$, Calcd: 441.2034, found 441.2055. MP = 168°C. HPLC analysis: H_2O-ACN (99:1), RT = 2.815 min, 96.8% purity.

N-(4-[(4-([(3,5-dimethyl-4-cyanophenyl)oxy]pyrimidin-2-yl}amino)phenyl]carbamoyl)aniline (34)

Compound **14** and *N*-(4-aminophenyl)-*N'*-phenylurea, following the general procedure F to give compound **34**, 18% yield. ^{1}H NMR (400 MHz, DMSO-d_6) δ 9.48, 8.53, 8.42, 8.34 (d, *J* = 3.4 Hz), 7.72, 7.39 (d, *J* = 4.6 Hz), 7.23 (t, *J* = 4.7 Hz), 7.09 (d, *J* = 5.1 Hz), 6.91 (t, *J* = 4.5 Hz), 6.48 (d, *J* = 3.4 Hz), 2.09. ^{13}C NMR (125 MHz, DMSO-d_6) δ 168.37, 161.00, 160.16, 154.05, 153.08, 140.37, 139.60, 135.04, 134.19, 133.30, 133.05, 129.29, 122.15, 119.51, 119.16, 119.00, 118.58, 108.87, 97.36, 16.37. LCQTOF for $C_{26}H_{22}N_6O_2$ $[M+H]^+$, Calcd:, 450.5, found: 451.1877. MP = 185°C. HPLC analysis: H_2O-ACN (99:1), RT = 3.193 min, 96.9% purity.

4-[(4-([(2-methoxyphenyl)methyl]amino}pyrimidin-2-yl)amino]benzonitrile (35)

Compound **11** and 4-aminobenzonitrile, following the general procedure F to give compound **35**, 35% yield. ^{1}H NMR (400 MHz, DMSO-d_6) δ 7.84 (d, J = 4.1 Hz), 7.72 – 7.63 (m), 7.28 – 7.23 (m), 7.17 (d, J = 5.7 Hz), 7.03 (d, J = 4.8 Hz), 6.88 (t, J = 4.5 Hz), 6.27 (d, J = 3.9 Hz), 4.52 (d, J = 3.4 Hz), 3.80. ^{13}C NMR (125 MHz, DMSO-d_6) δ 157.51, 133.53, 129.29, 128.79, 125.67, 120.81, 120.45, 111.31, 100.01, 55.97, 29.55. LCQTOF for $C_{19}H_{17}N_5O$ $[M+H]^+$, Calcd:, 331.4, found: 332.1474. MP = 168°C. HPLC analysis: H_2O-ACN (99:1), RT = 2.887 min, 97.3% purity.

4-[(4-([(3-methoxyphenyl)methyl]amino}pyrimidin-2-yl)amino]benzonitrile (36)

Compound **12** and 4-aminobenzonitrile, following the general procedure F to give compound **36**, 40% yield. ^{1}H NMR (400 MHz, DMSO-d_6) δ 7.85 (d, J = 4.1 Hz), 7.71, 7.66 (d, J = 5.3 Hz), 7.25 (t, J = 4.7 Hz), 6.88 (d, J = 3.9 Hz), 6.81 (dd, J = 5.0, 1.8 Hz), 6.24 (d, J = 3.9 Hz), 4.53, 3.68. ^{13}C NMR (125 MHz, DMSO-d_6) δ 162.90, 159.93, 154.09, 145.98, 143.28, 140.14, 133.59, 130.18, 120.37, 119.98, 119.65, 113.61, 113.02, 104.94, 99.95, 55.54, 44.68, 29.54. LCQTOF for $C_{19}H_{17}N_5O$ $[M+H]^+$, Calcd:, 331.4, found: 332.1474. MP = 162°C. HPLC analysis: H_2O-ACN (99:1), RT = 2.887 min, 96.4% purity.

4-[(4-([(4-methoxyphenyl)methyl]amino}pyrimidin-2-yl)amino]benzonitrile (37)

Compound **13** and 4-aminobenzonitrile, following the general procedure F to give compound **37**, 27% yield. ^{1}H NMR (400 MHz, DMSO-d_6) δ 10.30, 7.85, 7.75, 7.70 (d, J = 5.3 Hz), 7.24 (d, J = 5.3 Hz), 6.89 (d, J = 5.3 Hz), 6.21 (d, J = 4.1 Hz), 4.48, 3.69. ^{13}C NMR (125

MHz, DMSO-d_6) δ 159.03, 133.57, 129.22, 120.20, 114.45, 55.64, 29.54. LCQTOF for $C_{19}H_{17}N_5O$ $[M+H]^+$, Calcd:, 331.4, found: 332.1472. MP = 182°C. HPLC analysis: H_2O-ACN (99:1), RT = 2.853 min, 98.9% purity.

2-chloro-N-([4-(methanesulfonyl)benzyl]piperazin-1-ylmethyl)-4-(2-methoxybenzylamino)pyrimidine (38)

Compound **11** and compound **18**, following the general procedure G to give compound **38**, 15% yield. ^1H NMR (400 MHz, DMSO-d_6) δ 7.83 (d, J = 4.8 Hz), 7.52 (d, J = 5.0 Hz), 7.15 (dd, J = 10.9, 4.5 Hz), 6.92 (d, J = 4.8 Hz), 6.82 (t, J = 4.5 Hz), 6.19, 5.72, 4.36, 3.76, 3.50, 3.16, 2.67 (d, J = 7.1 Hz), 1.94 (t, J = 7.0 Hz), 1.63 (d, J = 7.8 Hz). ^{13}C NMR (125 MHz, DMSO-d_6) δ 161.96, 157.23, 145.72, 139.81, 129.88, 129.83, 128.29, 127.44, 120.51, 110.83, 62.03, 61.94, 55.78, 52.96, 52.48, 48.69, 44.12, 35.28, 32.68, 32.56, 32.30, 20.57, 14.48. LCQTOF for $C_{25}H_{31}N_5O_3S$ $[M+H]^+$, Calcd:, 481.6, found: 482.2187. MP = 104°C. HPLC analysis: H_2O-ACN (99:1), RT = 2.670 min, 97.6% purity.

3-chloro-N-([4-(methanesulfonyl)benzyl]piperazin-1-ylmethyl)-4-(3-methoxybenzylamino)pyrimidine (39)

Compound **12** and compound **18**, following the general procedure G to give compound **39**, 16% yield. ^1H NMR (400 MHz, DMSO-d_6) δ 7.84 (d, J = 5.0 Hz), 7.59 (d, J = 3.4 Hz), 7.53 (d, J = 5.0 Hz), 7.17 (t, J = 4.8 Hz), 6.83 – 6.72 (m), 5.72, 4.37, 3.67, 3.52, 3.16, 2.70 (d, J = 7.1 Hz), 1.98 (t, J = 6.7 Hz), 1.72, 1.38. ^{13}C NMR (125 MHz, DMSO-d_6) δ 159.77, 139.83, 129.95, 129.80, 127.45, 119.87, 113.50, 112.28, 61.96, 55.46, 52.87, 44.10, 32.18. LCQTOF for $C_{25}H_{31}N_5O_3S$ $[M+H]^+$, Calcd:, 481.6, found: 482.2220. MP = 100°C. HPLC analysis: H_2O-ACN (99:1), RT = 2.653 min, 98.9% purity.

3-chloro-N-([4-(methanesulfonyl)benzyl]piperazin-1-ylmethyl)-4-(4-methoxybenzylamino)pyrimidine (40)

Compound **13** and compound **18**, following the general procedure G to give compound **40**, 18% yield. ^1H NMR (400 MHz, DMSO-d_6) δ 7.85 (dd, J = 5.0, 1.4 Hz), 7.54 (d, J = 4.8 Hz), 7.17 (dd, J = 5.1, 1.9 Hz), 6.80 (dd, J = 11.0, 5.3 Hz), 5.76 – 5.67 (m), 4.38 – 4.23

(m), 3.69 – 3.54 (m), 3.17, 2.72 (d, *J* = 7.1 Hz), 2.03, 1.74 (d, *J* = 8.0 Hz), 1.45 – 1.34 (m). ^{13}C NMR (125 MHz, DMSO-d_6) δ 158.42, 145.34, 139.90, 129.99, 129.09, 128.92, 127.47, 114.15, 113.95, 61.88, 55.57, 55.51, 52.87, 52.58, 44.09, 32.11. LCQTOF for $C_{25}H_{31}N_5O_3S$ $[M+H]^+$, Calcd:, 481.6, found: 482.2196. MP = 80°C. HPLC analysis: H_2O-ACN (99:1), RT = 2.607 min, 99.0% purity.

Spectra for Representative Compound 19, 27, 31, 32 and 39

A representative sample of H-NMR, C-NMR, HPLC-UV and HRMS spectra are reported for compounds **19**, **27**, **31**, **32** and **39**.

***N*^{4}-[(2-methoxyphenyl)methyl]-*N*^{2}-(5-methyl-1*H*-pyrazol-3-yl)pyrimidine-2,4-diamine (19)**

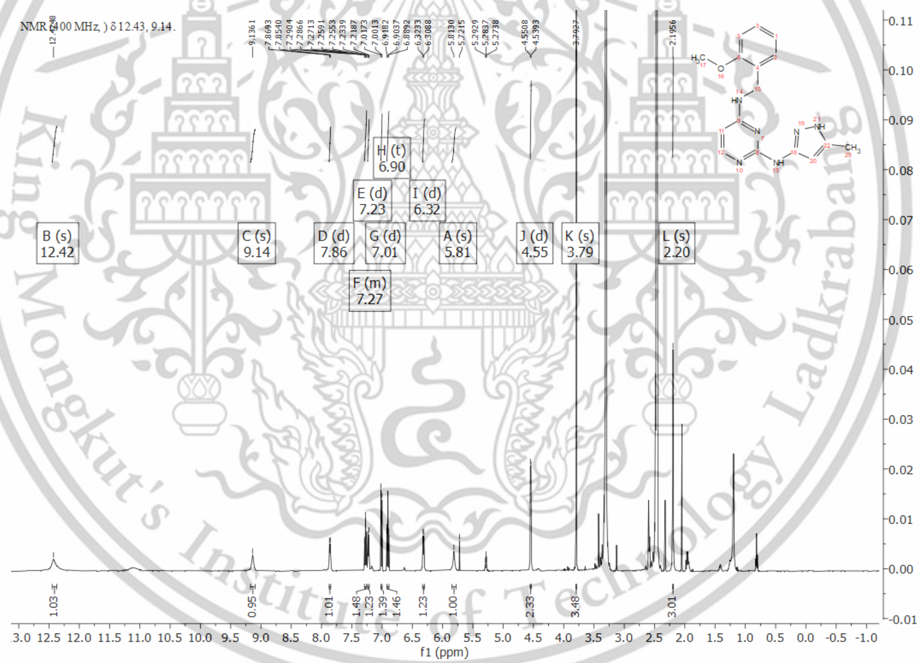

^{1}H-NMR spectra of **19**

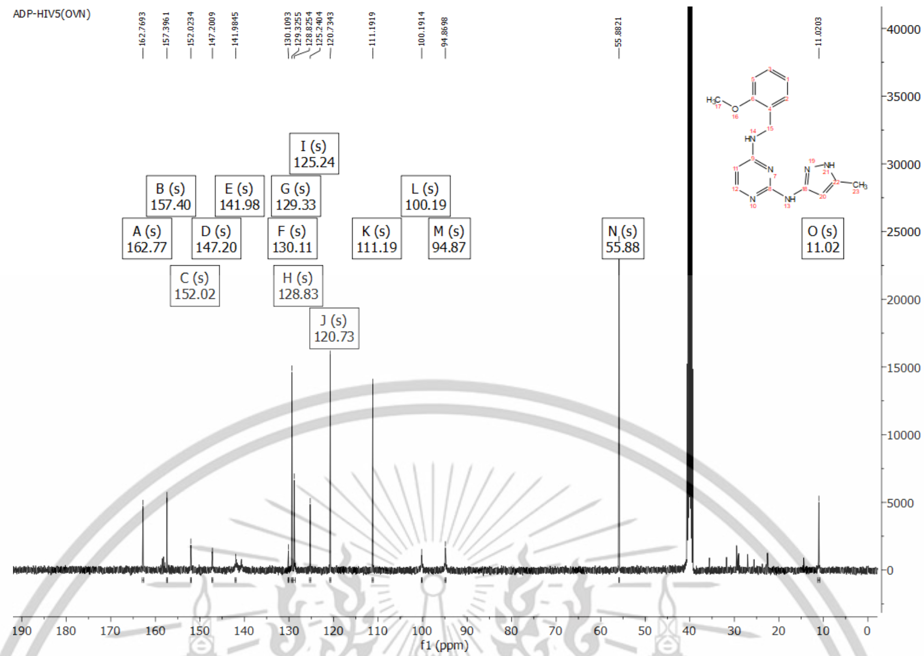

^{13}C-NMR spectra of **19**

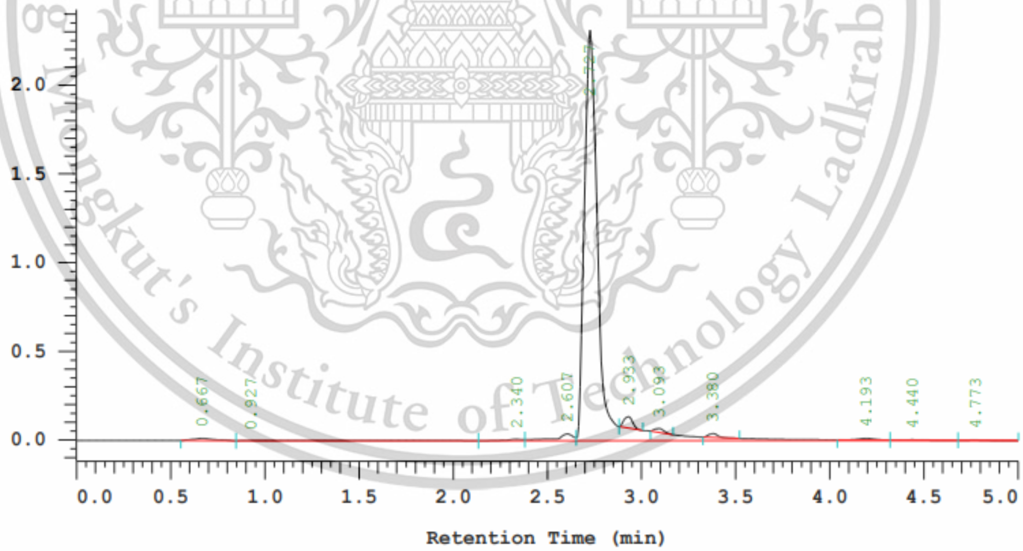

HPLC spectra of **19**

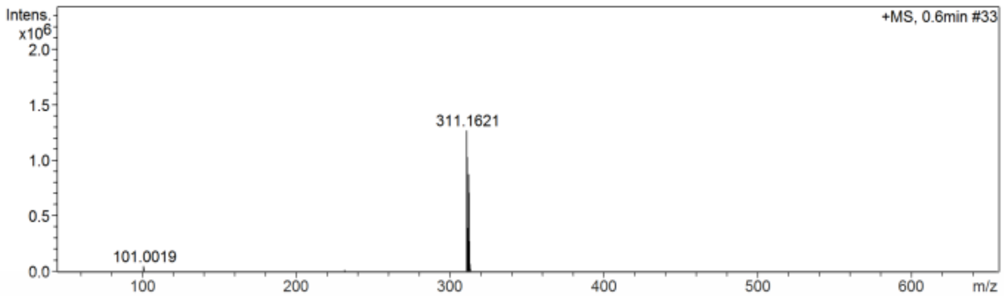

Meas. m/z	#	Ion Formula	m/z	err [mDa]	mSigma	# Sigma	Score	rdb	e¯ Conf	N-Rule
311.1621	1	C16H19N6O	311.1615	0.7	287.0	1	100.00	10.5	even	ok

HRMS spectra of **19**

***N*^2-(N-(3-aminophenyl)-N'-phenylurea)-*N*^4-[(2-methoxyphenyl)methyl]pyrimidine-2,4-diamine (27)**

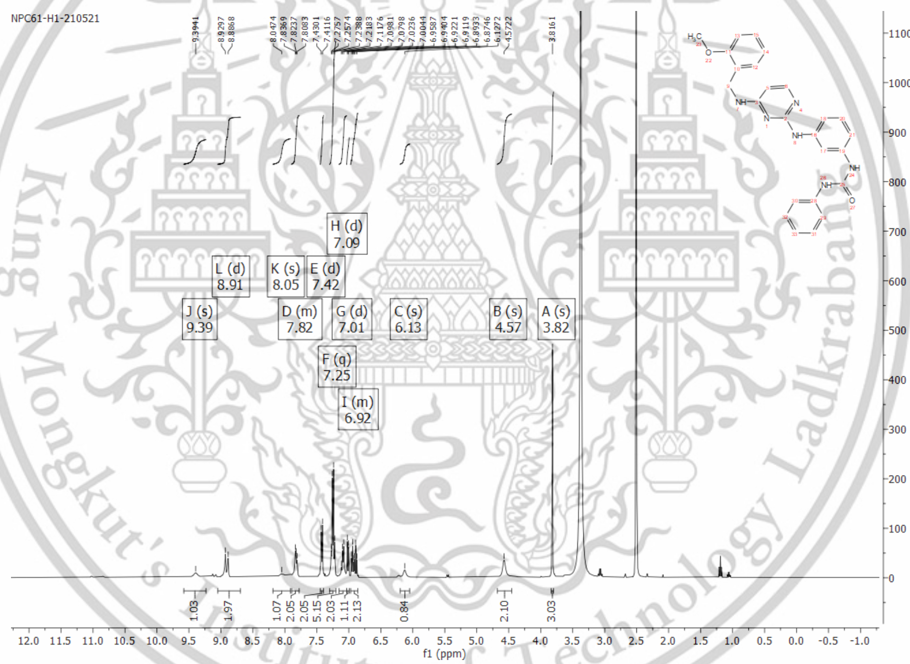

^{1}H-NMR spectra of **27**

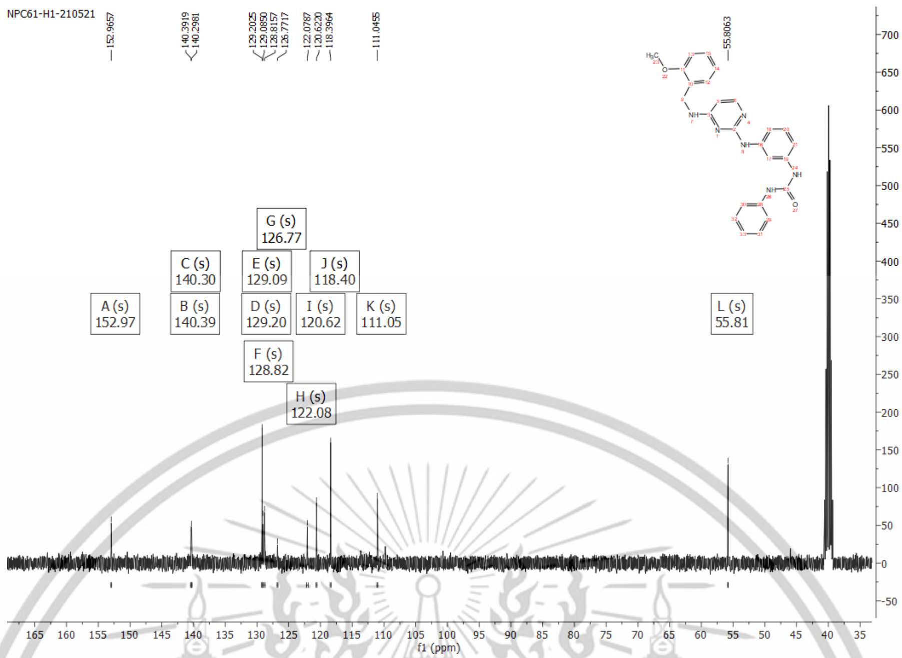

^{13}C-NMR spectra of **27**

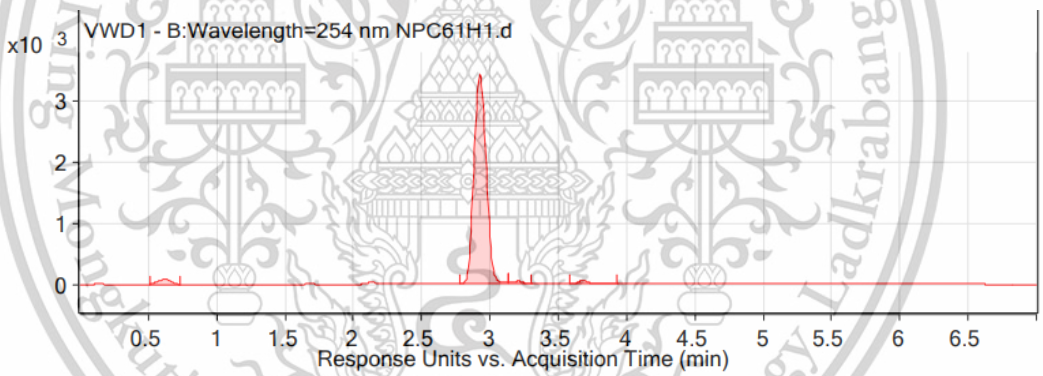

HPLC spectra of **27**

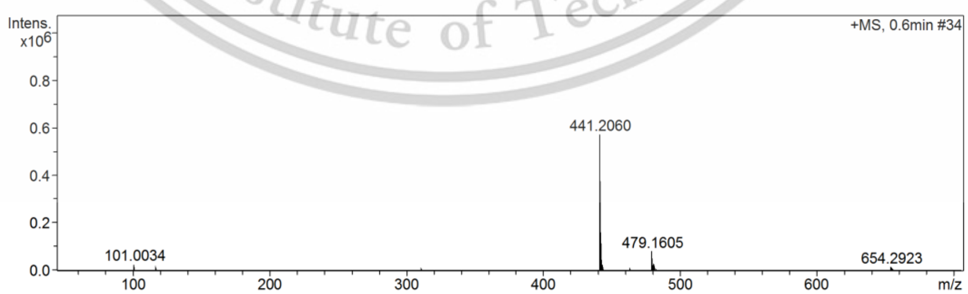

Meas. m/z	#	Ion Formula	m/z	err [mDa]	mSigma	# Sigma	Score	rdb	e⁻ Conf	N-Rule
441.2060	1	C25H25N6O2	441.2034	2.7	6.9	1	100.00	16.5	even	ok

HRMS spectra of **27**

***N*^{2}-(N-(4-aminophenyl)-N'-phenylurea)-*N*^{4}-[(2-methoxyphenyl)methyl]pyrimidine-2,4-diamine (31)**

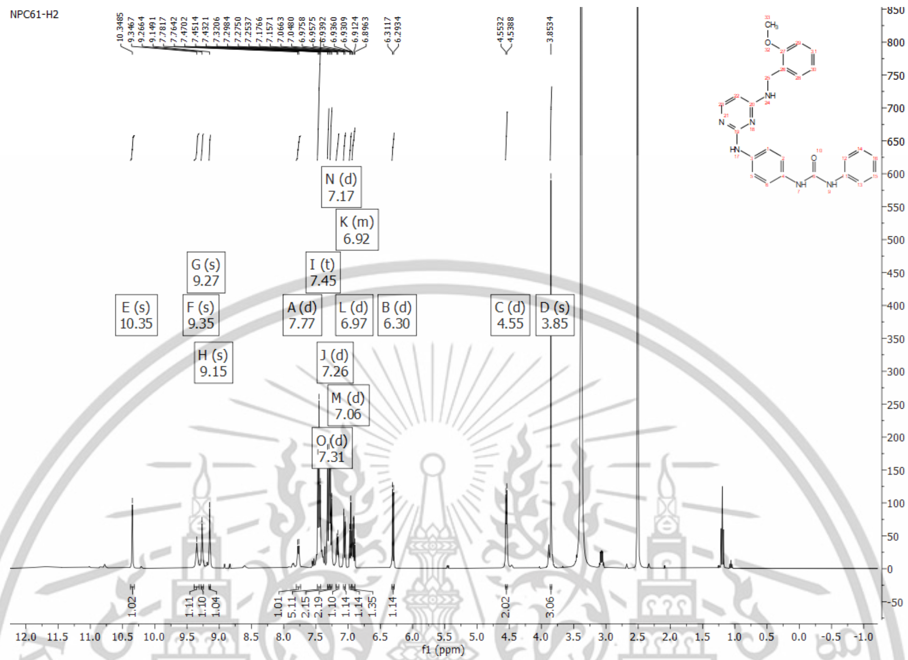

^{1}H-NMR spectra of **31**

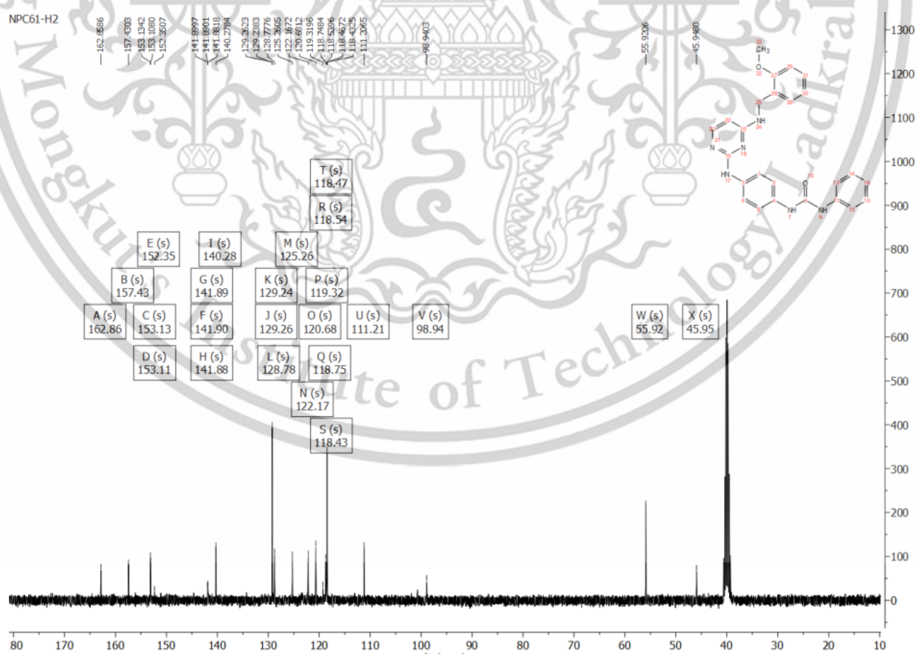

^{13}C-NMR spectra of **31**

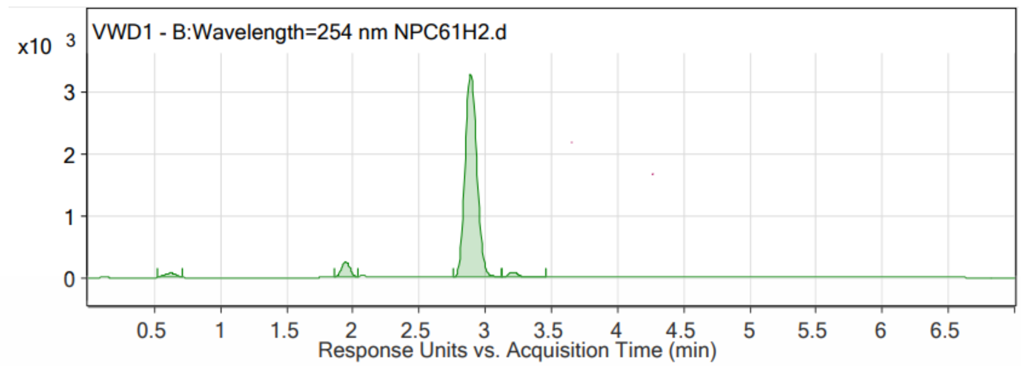

HPLC spectra of **31**

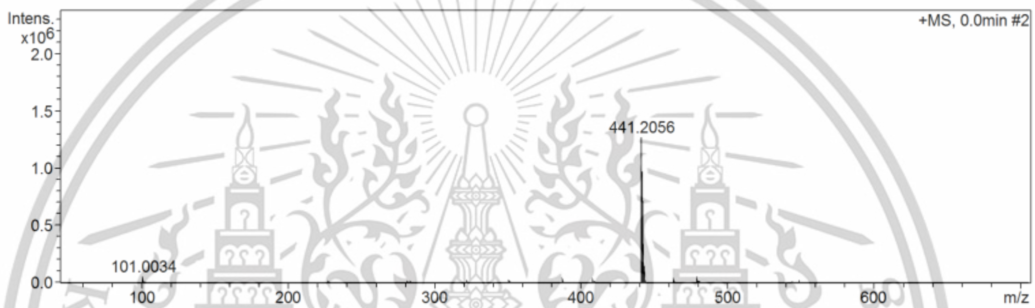

Meas. m/z	#	Ion Formula	m/z	err [mDa]	mSigma	# Sigma	Score	rdb	e⁻ Conf	N-Rule
441.2056	1	C25H25N6O2	441.2034	2.3	234.8	1	100.00	16.5	even	ok

HRMS spectra of **31**

N^2-(N-(4-aminophenyl)-N'-phenylurea)-N^4-[(3-methoxyphenyl)methyl]pyrimidine-2,4-diamine (32)

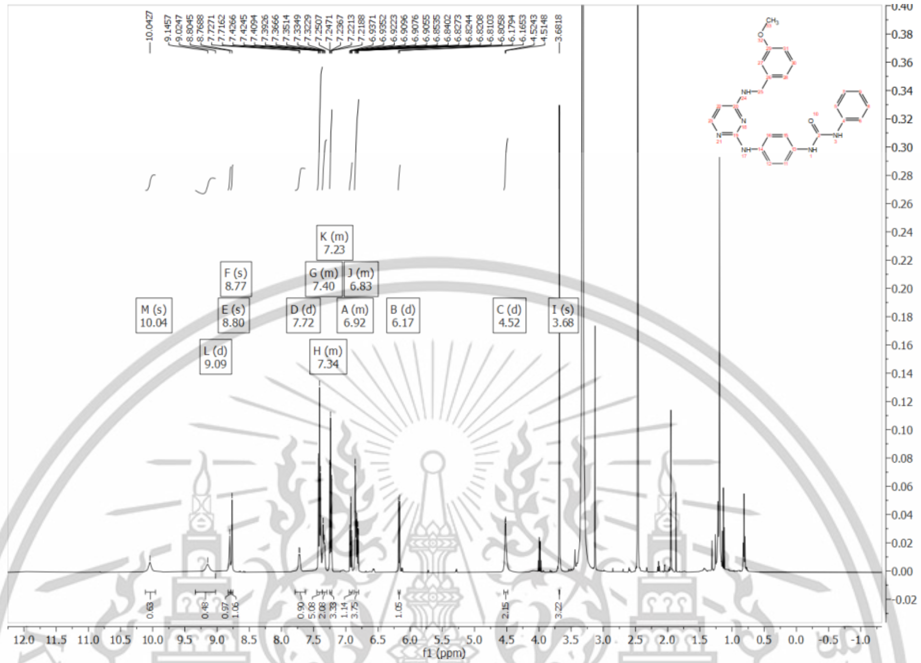

^{1}H-NMR spectra of **32**

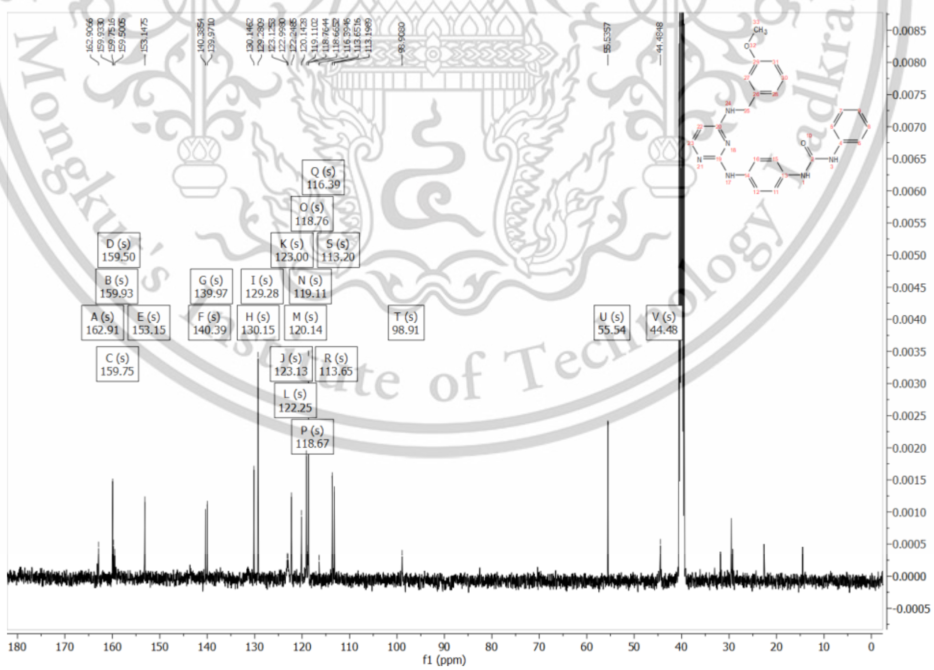

^{13}C-NMR spectra of **32**

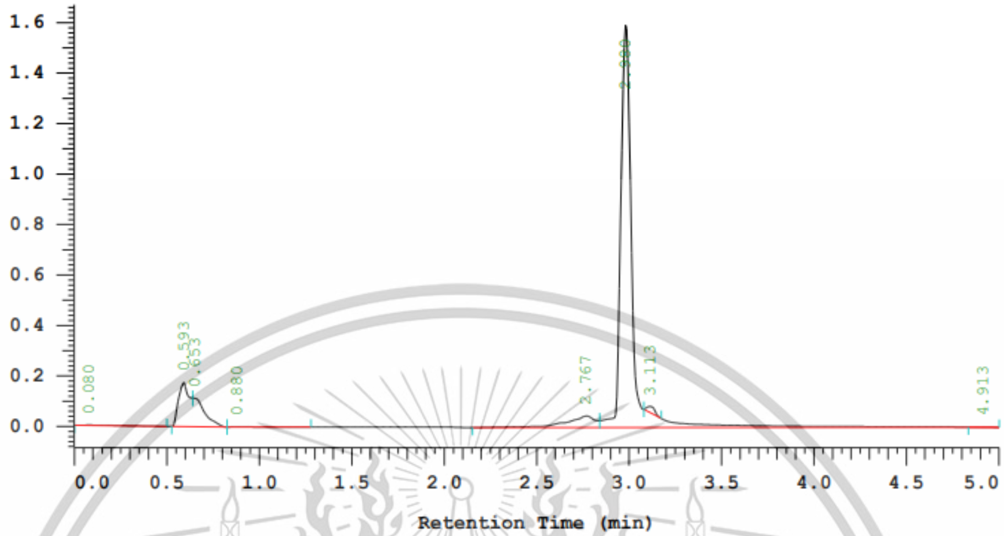

HPLC spectra of **32**

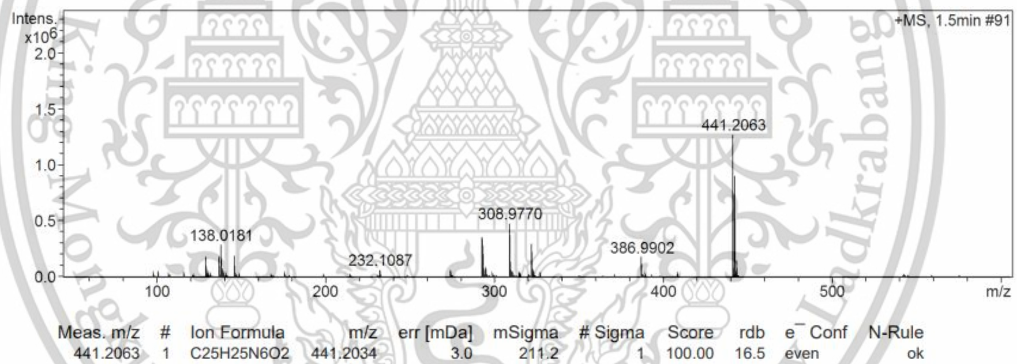

HRMS spectra of **32**

3-chloro-N-([4-(methanesulfonyl)benzyl]piperazin-1-ylmethyl)-4-(3-methoxybenzylamino)pyrimidine (39)

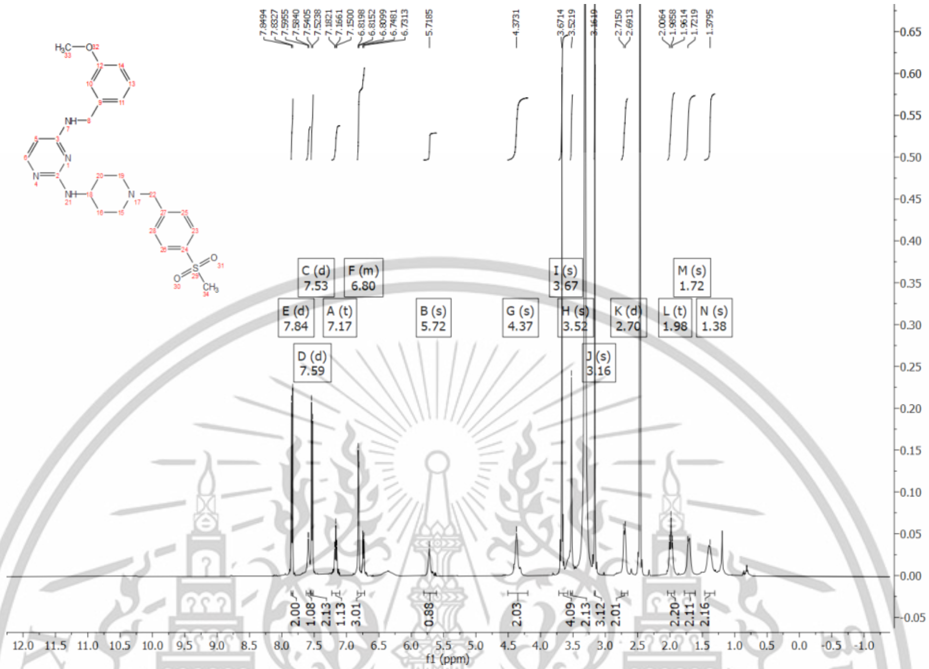

^{1}H-NMR spectra of **39**

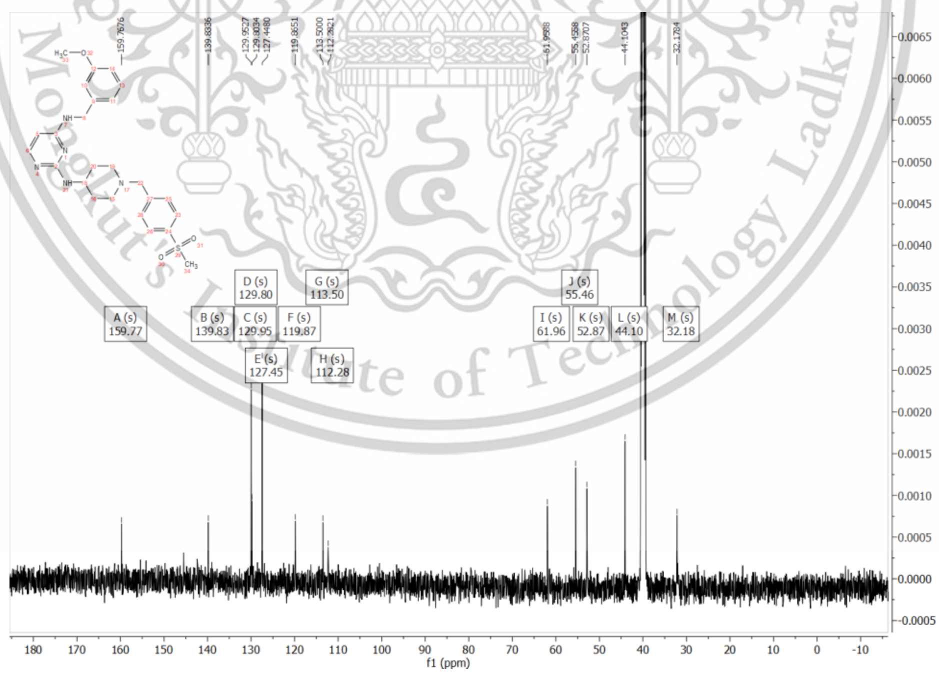

^{13}C-NMR spectra of **39**

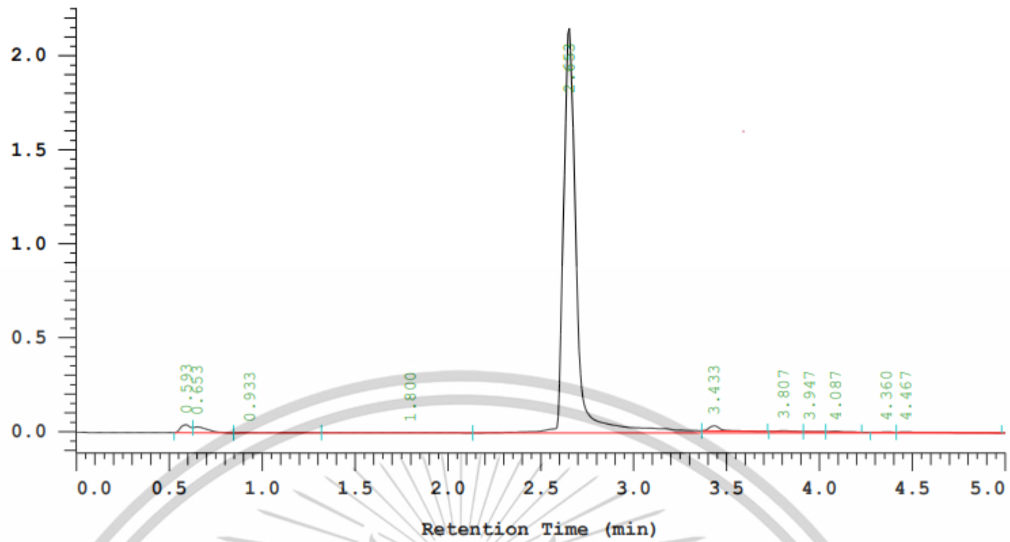

HPLC spectra of **39**

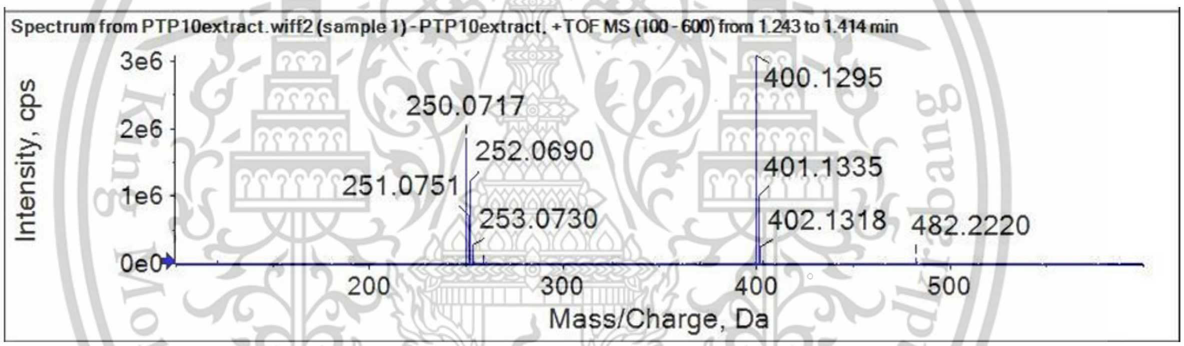

LCQTOF spectra of **39**